ΕΘΝΙΚΟ ΜΕΤΣΟΒΙΟ ΠΟΛΥΤΕΧΝΕΙΟ
ΣΧΟΛΗ ΕΦΑΡΜΟΣΜΕΝΩΝ ΜΑΘΗΜΑΤΙΚΩΝ ΚΑΙ ΦΥΣΙΚΩΝ ΕΠΙΣΤΗΜΩΝ

ΤΟΜΕΑΣ ΦΥΣΙΚΗΣ

Analysis of black hole scalarization in modified theories of gravity: holographic and thermodynamic aspects

Μελέτη του φαινομένου scalarization μελανών οπών σε τροποποιημένες θεωρίες βαρύτητας: ολογραφική και θερμοδυναμική μελέτη

ΔΙΔΑΚΤΟΡΙΚΗ ΔΙΑΤΡΙΒΗ

Στέλλα Κιορπελίδη

Επιβλέπων: Ελευθέριος Παπαντωνόπουλος, Ομότιμος Καθηγητής ΕΜΠ

Αθήνα, Ιούνιος 2024

Επταμελής Εξεταστική Επιτροπή:

- Ελευθέριος Παπαντωνόπουλος (Επιβλέπων) - Ομότιμος Καθηγητής, Τομέας Φυσικής, Εθνικό Μετσόβιο Πολυτεχνείο, Αθήνα, Ελλάδα.
- Νικόλαος Ήργες - Καθηγητής, Τομέας Φυσικής, Εθνικό Μετσόβιο Πολυτεχνείο, Αθήνα, Ελλάδα.
- Γεώργιος Κουτσούμπας - Ομότιμος Καθηγητής,Τομέας Φυσικής, Εθνικό Μετσόβιο Πολυτεχνείο, Αθήνα, Ελλάδα.
- Κωνσταντίνος Αναγνωστόπουλος - Καθηγητής, Τομέας Φυσικής, Εθνικό Μετσόβιο Πολυτεχνείο, Αθήνα, Ελλάδα.
- Αλέξανδρος Κεχαγιάς - Καθηγητής, Τομέας Φυσικής, Εθνικό Μετσόβιο Πολυτεχνείο, Αθήνα, Ελλάδα.
- Εμμανουήλ Σαριδάκης - Ερευνητής, Ινστιτούτο Αστρονομίας, Αστροφυσικής, Διαστημικών Εφαρμογών & Τηλεπισκόπησης, Εθνικό Αστεροσκοπείο Αθηνών, Αθήνα, Ελλάδα.
- Cristian Rodrigo Erices Osorio - Καθηγητής, Πανεπιστήμιο Central της Χιλής, Σαντιάγο, Χιλή.

NATIONAL TECHNICAL UNIVERSITY OF ATHENS
SCHOOL OF APPLIED MATHEMATICAL AND PHYSICAL SCIENCES

DEPARTMENT OF PHYSICS

Analysis of black hole scalarization in modified theories of gravity: holographic and thermodynamic aspects

PH.D. THESIS

Stella Kiorpelidi

Advisor: Eleftherios Papantonopoulos, Emeritus Professor NTUA

Athens, June 2024

Seven-Member PhD examination committee:

- Eleftherios Papantonopoulos (PhD advisor) - Emeritus Professor, Physics Department, National Technical University of Athens, Greece.
- Nikolaos Irges - Professor, Physics Department, National Technical University of Athens, Greece.
- George Koutsoumbas - Emeritus Professor, Physics Department, National Technical University of Athens, Greece.
- Konstantinos Anagnostopoulos - Professor, National Technical University of Athens, Greece.
- Alexandros Kehagias - Professor, Physics Department, National Technical University of Athens.
- Emmanuel Saridakis - Researcher, Institute for Astronomy, Astrophysics, Space Applications and Remote Sensing, National Observatory of Athens, Greece.
- Cristian Rodrigo Erices Osorio - Professor, Central University of Chile, Chile.

.....

Στέλλα Κιορπελίδη
Διδάκτωρ Εφαρμοσμένων Μαθηματικών και Φυσικών Επιστημών

Αφιερώνεται στη μητέρα μου

Ευχαριστίες

Η παρούσα διδακτορική διατριβή εκπονήθηκε στον Τομέα Φυσικής της Σχολής Εφαρμοσμένων Μαθηματικών και Φυσικών Επιστημών του Εθνικού Μετσοβίου Πολυτεχνείου υπό την επίβλεψη του Ομότιμου Καθηγητή κ. Ελευθέριου Παπαντωνόπουλου, τον οποίο ευχαριστώ θερμά για την εμπιστοσύνη που μου έδειξε, την υπομονή του, την καθοδήγηση του και την συνεργασία του. Ευχαριστώ με την σειρά τους τα υπόλοιπα μέλη της τριμελούς επιτροπής, τον κ. Γεώργιο Κουτσούμπα και τον κ. Νικόλαο Ήργε για τη στήριξή τους και τις επισυμάνσεις τους όλα αυτά τα χρόνια. Επιπλέον, ευχαριστώ τα υπόλοιπα μέλη της επταμελούς εξεταστικής επιτροπής για τον χρόνο που διέθεσαν στην αξιολόγηση της παρούσας διατριβής και τα πολύτιμα σχόλιά τους.

Θα ήθελα να ευχαριστήσω όλους τους συνεργάτες μου και ιδιαιτέρως τους Αθανάσιο Καρακάση, διδακτορικό φοιτητή του Τομέα Φυσικής της Σχολής Εφαρμοσμένων Μαθηματικών και Φυσικών Επιστημών του Εθνικού Μετσοβίου Πολυτεχνείου και κ. Cristian Erices, καθηγητή του Πανεπιστημίου Central της Χιλής, για τις πολύτιμες και πολύωρες συζητήσεις και την ηθική συμπαράσταση που μου προσέφεραν.

Εκφράζω τις εγκάρδιες ευχαριστίες μου στην οικογένειά μου και τους φίλους μου για την ηθική και οικονομική υποστήριξη που μου παρείχαν καθόλη τη διάρκεια της εκπόνησης της διδακτορικής μου διατριβής.

Contents

Publications List

The present Ph.D. dissertation is based on three publications, which are listed below:

1. **"Charged Gauss-Bonnet black holes with curvature induced scalarization in the extended scalar-tensor theories"**, Daniela D. Doneva, Stella Kiorpelidi, Petya G. Nedkova, Eleftherios Papantonopoulos, and Stoytcho S. Yazadjiev [1].

2. **"Spontaneous Holographic Scalarization of Black Holes in Einstein-Scalar-Gauss-Bonnet Theories"**, Hong Guo, Stella Kiorpelidi, Xiao-Mei Kuang, Eleftherios Papantonopoulos, Bin Wang and Jian-Pin Wu [2].

3. **"Scalarization of the Reissner-Nordström black hole with higher derivative gauge field corrections"**, Stella Kiorpelidi, Thanasis Karakasis, George Koutsoumbas and Eleftherios Papantonopoulos [3].

During my Ph.D. I also published the following papers, which are not part of this thesis.

4. **"Topological Black Holes with curvature induced scalarization in the extended scalar-tensor theories"**, Stella Kiorpelidi, George Koutsoumbas, Andri Machattou, and Eleftherios Papantonopoulos [4].

5. **"Cosmological perturbations in modified teleparallel gravity models: Boundary term extension"**, Sebastian Bahamonde, Viktor Gakis, Stella Kiorpelidi, Tomi Koivisto, Jackson Levi Said, and Emmanuel N. Saridakis [5].

Περίληψη

Στην παρούσα διδακτορική διατριβή, ερευνούμε το φαινόμενο της βαθμοτοποίησης μελανών οπών σε βαθμοτανυστικές τροποποιημένες θεωρίες βαρύτητας. Αρχικά, μελετάμε φορτισμένες βαθμοτοποιημένες μελανές οπές στα πλαίσια της θεωρίας βαρύτητας Einstein-scalar-Gauss-Bonnet (EsGB). Τα αποτελέσματα της μελέτης αποκαλύπτουν την ύπαρξη σημείων διακλάδωσης, όπου φορτισμένοι βαθμοτοποιημένοι κλάδοι λύσεων μελανών οπών διακλαδώνονται από τον κλάδο λύσεων της Γενικής Θεωρίας Σχετικότητας (ΓΘΣ) του Einstein, που περιγράφει την μελανή οπή Reissner-Nordström, παρέχοντας ενδιαφέρουσες πληροφορίες ως προς τις αποκλίσεις των δύο θεωριών και ως προς την συμπεριφορά των νέων λύσεων. Συγκρίνουμε την εντροπία που περιγράφει τις βαθμοτοποιημένες λύσεις μελανών οπών, αποδεικνύοντας ότι ο θεμελιώδης κλάδος μη τετριμμένων λύσεων είναι θερμοδυναμικά προτιμητέος σε σχέση με τον κλάδο λύσεων της Reissner-Nordström και τους άλλους βαθμοτοποιημένους κλάδους. Στη συνέχεια, μελετάμε το φαινόμενο της βαθμοτοποίησης της μελανής οπής Reissner-Nordström στα πλαίσια της θεωρίας βαρύτητας Einstein-Maxwell-scalar (EMs) συμπεριλαμβανομένων μη γραμμικών όρων ηλεκτρομαγνητισμού. Οι κλάδοι των βαθμοτοποιημένων μελανών οπών διακλαδώνονται από τον κλάδο λύσεων της μελανής οπής RN, τερματίζοντας με μια βαρυτική ιδιομορφία. Οι βαθμοτοποιημένες λύσεις μπορούν να χαρακτηριστούν υπερφορτισμένες, με την έννοια ότι μπορούν να φέρουν μεγαλύτερο ηλεκτρικό φορτίο σε σχέση με τη μάζα τους. Επιπλέον, εμφανίζουν μεγαλύτερη εντροπία σε σχέση με τη μελανή οπή RN και άλλες βαθμοτοποιημένες μελανές οπές γραμμικών θεωριών ηλεκτρομαγνητισμού, προτείνοντας τη θερμοδυναμική τους προτίμηση. Τέλος, εξετάζουμε το φαινόμενο της βαθμοτοποίησης ολογραφικά στα πλαίσια της θεωρίας EsGB, με την παρουσία αρνητικής κοσμολογικής σταθεράς. Σε αυτό το σημείο, αποδεικνύουμε την υπάρξη σύνδεσης μεταξύ του μηχανισμού της βαθμοτοποίησης μελανών οπών της ΓΘΣ και μιας μετάβασης φάσης της ύλης σε μια σύμμορφη θεωρία πεδίου. Εφαρμόζοντας την ολογραφική αρχή, συσχετίζουμε το φαινόμενο της βαθμοτοποίησης που λαμβάνει χώρα εντός συνόρου με τη δημιουργία συμπυκνώματος ύλης στο σύνορο, χωρίς το σπάσιμο κάποιας συμμετρίας, και υπολογίζουμε την σχετιζόμενη ολογραφική εντροπία εμπλοκής. Επιπλέον, εξετάζουμε το φαινόμενο της βαθμοτοποίησης ολογραφικά παρουσιά ενός ηλεκτρομαγνητικού πεδίου, και ερευνούμε βαθμοτοποιημένες μελανές οπές. Υπολογίζουμε το βαθμωτό συμπύκνωμα, την αγωγιμότητα και την υπέρρευστη πυκνότητα υπεραγώγιμου υλικού μέσω της αντιστοιχίας AdS/CFT και περιγράφουμε το φαινόμενο της βαθμοτοποίησης ως μια μετάβαση φάσης ενός υλικού από μια κανονική σε μια υπεραγώγιμη κατάσταση, σε μια κρίσιμη θερμοκρασία.

Abstract

In this Ph.D. dissertation, we investigate the phenomenon of black hole scalarization in Modified Theories of Gravity. Initially, we study charged scalarized black hole solutions within the Einstein-scalar-Gauss-Bonnet (EsGB) gravity framework. Our findings reveal the presence of bifurcation points, where charged scalarized branches bifurcate from the Reissner-Nordström solution, providing insights into their behavior and deviations from General Relativity (GR). We compute the entropy of the scalarized black hole solutions, demonstrating that the fundamental branch is thermodynamically favorable over the Reissner-Nordström solution and other branches. Subsequently, we discuss spontaneous scalarization of the Reissner-Nordström black hole in Einstein-Maxwell-scalar (EMs) gravity in the presence of higher derivative gauge field corrections. Scalarized black hole branches of solutions bifurcate from the Reissner-Nordström branch of solutions, terminating with a curvature singularity. The black holes can be overcharged in the sense that they may carry a larger electric charge in comparison to their mass. Additionally, they exhibit greater entropy than the Reissner-Nordström black hole and other scalarized black holes in EMs theory without higher-order derivative gauge field terms, suggesting their thermodynamic preference. Finally, we explore scalarization within EsGB gravity with a negative cosmological constant. Here, we establish a connection between instability in Schwarzschild-AdS black hole with the planar horizon and holographic scalarization. By applying the holographic principle, we correlate bulk scalarization with a boundary description of the scalar hair condensation without breaking any symmetry, and we compute the associated holographic entanglement entropy. Moreover, we explore the holographic scalarization in the presence of an electromagnetic field and investigate the phase transition to a holographic superconductor. We compute the scalar condensation, the optical conductivity, and the superfluid density, describing scalarization as a mechanism for the holographic superconducting phase transition.

Εκτενής Περίληψη στα Ελληνικά

Τον τελευταίο αιώνα, πολυάριθμα πειραματικά και παρατηρησιακά δεδομένα έχουν καθιερώσει τη *Γενική Θεωρία Σχετικότητας* (ΓΘΣ) ως την πιο επιτυχημένη θεωρία της Φυσικής για την περιγραφή της βαρυτικής αλληλεπίδρασης. Η ΓΘΣ είναι μια γεωμετρική θεωρία που περιγράφει βαρυτικές αλληλεπιδράσεις μέσω της καμπυλότητας του χωροχρόνου. Οι δύο ακρογωνιαίοι λίθοι της ΓΘΣ είναι η αρχή του Mach και η αρχή της ισοδυναμίας. Η τροχιά οποιουδήποτε μικρού δοκιμαστικού σωματιδίου σε ένα βαρυτικό πεδίο είναι ανεξάρτητη από τη σύσταση και τη μάζα του σωματιδίου. Αυτό σημαίνει ότι όλα τα αντικείμενα, ανεξαρτήτως της μάζας ή της σύνθεσής τους, θα επιταχυνθούν με τον ίδιο ρυθμό όταν υποβάλλονται σε βαρυτική δύναμη. Η αρχή αυτή ήταν καθοριστική στην ανάπτυξη της ΓΘΣ, καθώς οδήγησε στην ιδέα ότι η βαρύτητα μπορεί να θεωρηθεί ως καμπύλωση του χωροχρόνου.

Για την θεμελίωση της ΓΘΣ, ο Einstein έκανε τη βασική υπόθεση ότι ο χωροχρόνος αναπαρίσταται από μια τετραδιάστατη, ομαλή, συνεχή, Λορεντζιανή τετραδιάστατη πολλαπλότητα. Οι διαστάσεις αυτές: τρεις χωρικές και μια χρονική, συνδυάζονται σε μια ενιαία οντότητα που ονομάζεται χωρόχρονος. Τις αποστάσεις και τις γωνίες στο χωρόχρονο τις περιγράφει μια μαθηματική οντότητα, γνωστή ως μετρικός τανυστής. Η παρουσία μάζας και ενέργειας προκαλεί την καμπύλωση του χωροχρόνου, την οποία περιγράφει ο τανυστής καμπυλότητας του Riemann, που προκύπτει από τον μετρικό τανυστή. Ο βαθμός και η μορφή της καμπυλότητας εξαρτάται από την κατανομή της μάζας και της ενέργειας στο σύμπαν. Το θεμελιώδες σύνολο εξισώσεων στη ΓΘΣ, που συνδέει τη γεωμετρία του χωροχρόνου (μέσω του μετρικού τανυστή και των παραγώγων του) με την κατανομή της ύλης και της ενέργειας, είναι οι εξισώσεις πεδίου του Einstein.

Οι κυριότερες επιτυχίες της ΓΘΣ περιλαμβάνουν την καμπύλωση του φωτός το 1919 από τον Arthur Eddington κατά τη διάρκεια μιας έκλειψης ηλίου. Οι παρατηρήσεις έδειξαν ότι το φως των αστέρων που περνούσε κοντά από τον ήλιο καμπυλωνόταν με το προβλεπόμενο από τη θεωρία ποσό. Η ΓΘΣ εξήγησε την ανωμαλία στην τροχιά του Ερμή, η οποία δεν μπορούσε να εξηγηθεί πλήρως από την κλασική μηχανική του Νεύτωνα. Η θεωρία προέβλεψε σωστά την επιπρόσθετη προχώρηση του περιηλίου του Ερμή, που είναι περίπου 43 δευτερόλεπτα της μοίρας ανά αιώνα. Επιπλέον, η ΓΘΣ προβλέπει το φαινόμενο Lense-Thirring, όπου όταν ένα μαζικό σώμα, όπως ένας πλανήτης ή ένα αστέρι, περιστρέφεται, η περιστροφή του επηρεάζει τον χωροχρόνο γύρω του. Το φαινόμενο αυτό έχει επιβεβαιωθεί πειραματικά με μετρήσεις από δορυφόρους όπως το Gravity Probe B. Η ΓΘΣ προβλέπει ότι το φως που διαφεύγει από ένα ισχυρό βαρυτικό πεδίο θα ερυθρομετατοπιστεί, δηλαδή θα χάσει ενέργεια και η συχνότητά του θα μειωθεί. Αυτό το φαινόμενο έχει επιβεβαιωθεί σε διάφορα πειράματα και παρατηρήσεις, όπως αυτά με τη βοήθεια του δορυφόρου Gravity Probe A. Το 2015, η ανακάλυψη των βαρυτικών κυμάτων από τη συνεργασία LIGO επισφράγισε μια άλλη σημαντική πρόβλεψη της ΓΘΣ. Αυτά τα κύματα είναι διαταραχές στον χωροχρόνο που προκαλούνται από επιταχυνόμενες μάζες, όπως η συγχώνευση μελανών οπών ή αστέρων νετρονίων. Η ΓΘΣ προβλέπει την ύπαρξη μελανών οπών, αντικείμενα με τόσο ισχυρό βαρυτικό πεδίο που ούτε το φως δεν μπορεί να διαφύγει. Οι παρατηρήσεις των αστροφυσικών φαινομένων, όπως τα φαινόμενα της ακτινοβολίας X από τα άκρα των μελανών οπών, και η πρόσφατη απευθείας εικόνα μιας μελανής οπής από το Event Horizon Telescope το 2019, επιβεβαιώνουν αυτές τις προβλέψεις. Αυτές οι επιτυχίες καταδεικνύουν τη δύναμη και την ακρίβεια της ΓΘΣ στην περιγραφή των βαρυτικών φαινομένων, καθιστώντας την μία από τις πιο επιτυχημένες θεωρίες

στην ιστορία της φυσικής.

Η ΓΘΣ έχει επιβεβαιωθεί κυρίως σε πολλαπλές περιπτώσεις όπου τα βαρυτικά πεδία είναι σχετικά ασθενή, όπως στο ηλιακό μας σύστημα. Ωστόσο, η ίδια δεν έχει ελεγχθεί επαρκώς σε συνθήκες ισχυρού βαρυτικού πεδίου, όπως αυτές που επικρατούν κοντά σε μελανές οπές ή αστέρες νετρονίων. Αυτό το ανεξερεύνητο καθεστώς αφήνει περιθώριο για πιθανές νέες φυσικές θεωρίες που θα μπορούσαν να συμπληρώσουν ή να επεκτείνουν τη ΓΘΣ.

Σε κοσμολογική κλίμακα, η ΓΘΣ ατνιμετωπίζει επίσης σημαντικές προκλήσεις και ερωτήματα όπως το πρόβλημα της κοσμολογικής σταθεράς, η ένταση της σταθεράς Hubble, καθώς η φύση της σκοτεινής ύλης και σκοτεινής ενέργειας. Αυτά τα αναπάντητα ερωτήματα δείχνουν ότι η κατανόησή μας για τη βαρύτητα και το σύμπαν είναι ακόμα ατελής. Υπάρχει η ανάγκη για νέες θεωρίες που θα μπορούσαν να επεκτείνουν τη ΓΘΣ και να προσφέρουν εξηγήσεις για αυτά τα φαινόμενα. Οι *τροποποιημένες θεωρίες βαρύτητας* (ΤΘΒ) και άλλες προσεγγίσεις στην κβαντική βαρύτητα συνεχίζουν να ερευνούν αυτούς τους τομείς με στόχο να γεφυρώσουν τα υπάρχοντα κενά στη γνώση μας. Παρόλο που έχουν προταθεί πολλές θεωρίες κβαντικής βαρύτητας, όλες παραμένουν ατελείς, καθώς αντιμετωπίζουν σημαντικά εννοιολογικά προβλήματα που καθιστούν την πλήρη ανάπτυξη και αποδοχή τους δύσκολη. Οι προτεινόμενες θεωρίες απαιτούν νέες φυσικές διαστάσεις και δομές που δεν έχουν παρατηρηθεί μέχρι στιγμής. Επιπλέον, τα πειράματα που θα μπορούσαν να τις επαληθεύσουν απαιτούν ενέργειες που είναι απρόσιτες με την τρέχουσα τεχνολογία. Ενώ, οι μαθηματικές δομές των θεωριών αυτών είναι εξαιρετικά πολύπλοκες και πολλές φορές οδηγούν σε απροσδιόριστα ή μη φυσικά αποτελέσματα, όπως άπειρες τιμές για φυσικές ποσότητες.

Γενικά, οι ΤΘΒ μπορούν να θεωρηθούν ως μια αποτελεσματική θεωρία πεδίου μιας υποκείμενης θεμελιώδους θεωρίας. Έτσι, αυτές οι θεωρίες προτείνουν οτι η ΓΘΣ αποκτά επιπλέον βαθμούς ελευθερίας πέρα από αυτούς της μετρικής. Ειδικότερα, οι *βαθμοτανυστικές θεωρίες*, ως η πιο απλή κατηγορία ΤΘΒ, επεκτείνουν τη ΓΘΣ μέσω της εισαγωγής επιπλέον βαθμωτών πεδίων. Αυτές έχουν προσελκύσει το ενδιαφέρον της επιστημονικής κοινότητας λόγω των εφαρμογών τους στην κοσμολογία για να εξηγήσουν τη σκοτεινή ενέργεια και την επιτάχυνση της διαστολής του σύμπαντος. Το βαθμωτό πεδίο μπορεί να προσφέρει μια δυναμική εξήγηση για την κοσμολογική σταθερά. Παράλληλα, η επικείμενη αστρονομία βαρυτικών κυμάτων καθιστά τα συμπαγή αντικείμενα, όπως οι μελανές οπές και οι αστέρες νετρονίων, ως τα ιδανικά συστήματα για την μελέτη των βαθμοτανυστικών θεωριών σε καθεστώτα ισχυρού βαρυτικού πεδίου.

Η γενικότερη μορφή βαθμοτανυστικών θεωριών είναι οι θεωρίες Horndeski. Οι θεωρίες Horndeski μπορούν να περιγραφούν από μια δράση που περιλαμβάνει έναν μετρικό τανυστή και ένα βαθμωτό πεδίο, και έχουν ως στόχο να διασφαλίσουν ότι οι εξισώσεις κίνησης είναι δευτέρας τάξεως, ώστε να αποφευχθούν αστάθειες Ostrogradsky και ανεπιθύμητα φαινόμενα, όπως παρουσία φαντασμάτων. Οι θεωρίες Horndeski είναι εξαιρετικά γενικές και περιλαμβάνουν πολλές άλλες θεωρίες ως ειδικές περιπτώσεις, όπως τη θεωρία Brans-Dicke, τη θεωρία Gauss-Bonnet και τις θεωρίες Galileon. Μετά την παρατήρηση των βαρυτικών κυμάτων από τα πειράματα LIGO και Virgo, υπήρξε ανανεωμένο ενδιαφέρον για τις θεωρίες Horndeski. Οι παρατηρήσεις των βαρυτικών κυμάτων μπορούν να θέσουν αυστηρούς περιορισμούς σε αυτές τις θεωρίες, ειδικά σχετικά με την ταχύτητα των βαρυτικών κυμάτων, η οποία σύμφωνα με τη ΓΘΣ πρέπει να είναι ίση με την ταχύτητα του φωτός.

Οι μελανές οπές ως λύσεις της ΓΘΣ συνοδεύονται από θεωρήματα μοναδικότητας και το θεώρημα εξάληψης ιχνών, το οποίο δεν είναι τίποτα άλλο από μια σειρά αποτελεσμάτων, τα οποία διατυπώνουν ότι οι μελανές οπές καθορίζονται πλήρως από μερικές βασικές παραμέτρους όπως η μάζα M, το ηλεκτρικό φορτίο Q και η στροφορμή J. Οι λύσεις μπορούν να επεκταθούν για να περιλάβουν και μαγνητικό φορτίο. Συνεπώς, οι μελανές οπές δε διαθέτουν άλλα "ίχνη" ή "μαλλιά", απλοποιώντας την περιγραφή τους και επιτρέποντας την κατηγοριοποίηση τους ως:

- Μελανή οπή Schwarzschild: Μη περιστρεφόμενη και χωρίς φορτίο ($J = 0, Q = 0$).
- Μελανή οπή Reissner-Nordström: Μη περιστρεφόμενη αλλά φορτισμένη ($J = 0, Q \neq 0$).

- Μελανή οπή Kerr: Περιστρεφόμενη και χωρίς φορτίο ($J \neq 0, Q = 0$).
- Μελανή οπή Kerr-Newman: Περιστρεφόμενη και φορτισμένη ($J \neq 0, Q \neq 0$).

Οι μελανές οπές μπορούν να σχηματιστούν μέσω διαφόρων διαδικασιών, όπως μέσω βαρυτικής κατάρρευσης μεγάλου αστέρα νετρονίων ή όπως μέσω συγχώνευσης δύο αστέρων νετρονίων ή δύο μικρότερων μελανών οπών, όπως έχει παρατηρηθεί μέσω βαρυτικών κυμάτων. Οι ΤΘΒ και οι βαθμοτανυστικές θεωρίες εξετάζουν και αποδεικνύουν τη δυνατότητα ύπαρξης μελανών οπών με επιπλέον "μαλλιά", παραβιάζοντας το θεώρημα εξάλειψης ιχνών. Μια νέα παράμετρος εμφανίζεται να περιγράφει μια μελανή οπή, εκτός της μάζας, του ηλεκτρικού φορτίου και της στροφορμης. Στις βαθμοτανυστικές θεωρίες, η νέα αυτή παράμετρος σχετίζεται με το βαθμωτό πεδίο, επομένως, καλείται *βαθμωτό φορτίο* D. Το βαθμωτό φορτίο χαρακτηρίζεται ως πρωτεύον ή δευτερεύον, αν, αντίστοιχα, δεν σχετίζεται με τις προαναφερθείσες βασικές παραμέτρους ή αν σχετίζεται με αυτές.

Σε αυτό το πλαίσιο, έχει πρόσφατα αποδειχθεί ότι οι βαθμοτανυστικές θεωρίες μπορούν να προβλέψουν τη δυνατότητα ύπαρξης μη τετριμμένων μελανών οπών μέσω ενός μηχανισμού που περιγράφει μια μεταβάση φάσης μιας τετριμμένης μελανής οπής σε μια μη-τετριμμένη, γνωστού ως *αυθόρμητη βαθμοτοποίηση*. Οι νέες λύσεις εμφανίζουν μεγάλες διαφορές σε σχέση με αυτές της ΓΘΣ σε περιοχές υψηλής καμπυλότητας του χωροχρόνου, ενώ οι διαφορές αυτές παραμένουν σχεδόν δυσδιάκριτες σε περιοχές ασθενούς βαρύτητας.

Το φαινόμενο της βαθμοτοποίησης μπορεί να λαβεί χώρα όταν το βαθμωτό πεδίο είναι μη-ελάχιστα και "κατάλληλα" συζευγμένο με την καμπύλωση του χωροχρόνου. Αυτό το οποίο καθιστά το φαινόμενο της βαθμοτοποίησης τόσο ενδιαφέρον και ιδιαίτερο βρίσκεται στη λέξη "κατάλληλα". Πίσω από αυτήν την λέξη βρίσκεται κρυμμένος ο μηχανισμός μιας δυναμικής μετάβασης φάσης μιας τετριμμένης μελανής οπής σε μια μη-τετριμμένη. Ο μηχανισμός αυτός διακρίνει το φαινόμενο της βαθμοτοποίησης από άλλα μοντέλα, τα οποία περιγράφουν τη δημιουργία μη τετριμμένων μελανών οπών. Γι'αυτόν τον λόγο, ο όρος *"βαθμοτοποιημένη μελανή οπή"* χρησιμοποιείται για να περιγράψει "μαλλιαρές" μελανές οπές, που έχουν σχηματιστεί μέσω του μηχανισμού της βαθμοτοποίησης.

Η παρούσα διδακτορική έρευνα συμβάλει στην ανάλυση του φαινομένου της βαθμοτοποίησης μελανών οπών σε βαθμοτανυστικές θεωρίες βαρύτητας, εστιάζοντας ιδιαίτερα στο ρόλο του ηλεκτρομαγνητικού πεδίου και στην εξερεύνηση ολογραφικών πτυχών. Στο *κεφάλαιο 1*, γίνεται μια εισαγωγή στη ΓΘΣ και τις λύσεις μελανών οπών που περιγράφει. Δίνονται τα κίνητρα για την τροποποίησή της, καθώς και κάποια παραδείγματα μη τετριμμένων λύσεων μελανών οπών σε βαθμοτανυστικές θεωρίες που παραβιάζουν τα θεωρήματα εξάλειψης ιχνών. Στο τέλος του κεφαλαίου εισαγάγεται το φαινόμενο της βαθμοτοποίησης μελανών οπών.

Η πρώτη μελέτη βαθμοτοποιημένων λύσεων μελανών οπών έγινε στην θεωρία Einstein-scalar-Gauss-Bonnet (EsGB), της οικογένειας των θεωριών Horndeski. Η θεωρία EsGB περιλαμβάνει, επιπλέον, ένα βαθμωτό πεδίο μ' έναν κανονικό κινητικό όρο και έναν όρο μη-ελάχιστης σύζευξης του βαθμωτού πεδίου με τον αναλλοίωτο όρο της βαρύτητας Gauss-Bonnet. Η θεωρία αυτή δέχεται ως λύση την τετριμμένη μελανή οπή Schwarzschild της ΓΘΣ, μ' ένα τετριμμένο πεδίο. Η λύση αυτή καλείται ως *λύση του κενού της θεωρίας*. Το μη-ελάχιστα συζευγμένο βαθμωτό πεδίο με τον αναλλοίωτο όρο της βαρύτητας Gauss-Bonnet καθίσταται ταχυονικό πέρα από ένα κατώφλι μάζας στις περιοχές ισχυρής καμπυλότητας. Τότε, η λύση του κενού της θεωρίας υποφέρει από ταχυονικές αστάθειες, οι οποίες περιγράφονται από την παρουσία ένος αρνητικού δυναμικού με την μορφή πηγαδιού εξώ από τον ορίζοντα γεγονότων της μελανής οπής.

Η παρουσία ταχυονικών ασταθειών ερμηνεύεται ως ένα σημάδι ύπαρξης μη τετριμμένων λύσεων μελανών οπών. Όταν το αρνητικό πηγάδι δυναμικού γίνει αρκετά βαθύ και μπορεί να υποστηρίξει μια δέσμια κατάσταση, τότε ένα *σημείο διακλάδωσης* εμφανίζεται στον κλάδο των τετριμμένων λύσεων της ΓΘΣ. Όσο η αλληλεπίδραση του βαθμωτού πεδίου με τη βαρύτητα γίνεται όλο και πιο ισχυρή, το αρνητικό πηγάδι δυναμικού ολοένα και βαθαίνει και ο αριθμός των δέσμιων καταστάσεων που μπορεί να υποστηρίζει αυξάνεται. Για κάθε μια δέσμια κατάσταση που προστίθενται στο φάσμα, ένα νέο σημείο διακλάδωσης εμφανίζεται.

Κάθε σημείο διακλάδωσης ορίζει έναν ολόκληρο νέο κλάδο μη τετριμμένων λύσεων μελανών οπών, συνοδευόμενο με ένα μη τετριμμένο βαθμωτό φορτίο D. Ο πρώτος κλάδος λύσεων καλείται *θεμελιώδης*, διότι περιγράφεται από την πρώτη θεμελιώδη δέσμια κατάσταση του τετριμμένου βαθμωτού πεδίου. Ο θεμελιώδης κλάδος λύσεων περιγράφεται από βαθμωτά πεδία τα οποία είναι ομαλά κοντά στον ορίζοντα γεγονότων και ασυμπτωτικα τετριμμένα σε μεγάλες αποστάσεις χωρίς τοπικά ακρότατα. Ο δεύτερος κλάδος λύσεων περιγράφεται από βαθμωτά πεδία με ένα ακρότατο, ο τρίτος κλάδος από πεδία με δύο ακρότατα κ.ο.κ.. Σημειώνουμε ότι μελέτες της δυναμικής ευστάθειας βαθμοτοποιημένων λύσεων αποδεικνύει την ευστάθεια μόνο των λύσεων του θεμελιώδους κλάδου, ενώ οι υπόλοιποι κλάδοι χαρακτηρίζονται ως ασταθείς κάτω από γραμμικές διαταραχές.

Συνεπώς, το φαινόμενο της βαθμοτοποίησης περιγράφει μια δυναμική μετάβαση φάσης που πραγματοποιείται σε μια κατάλληλη βαθμοτανυστική θεωρία, με αποτέλεσμα μια τετριμμένη μελανή οπή να "ντύνεται" με ένα βαθμωτό πεδίο. Η νέα μη τετριμμένη βαθμοτοποιημένη λύση περιγράφεται από την μάζα M και το βαθμωτό φορτίο D. Η νέα παράμετρος D χαρακτηρίζεται ως δευτερεύον "μαλλί", εφόσον εξαρτάται από την μάζα M της μελανής οπής. Οι νέες βαθμοτοποιημένες λύσεις αποκαλύπτουν νέα φυσική πέραν της ΓΘΣ και ενδέχεται να οδηγήσουν σε νέες ανακαλύψεις σχετικά με τη φύση της βαρύτητας και τη δομή του χωροχρόνου.

Στο *κεφάλαιο 2*, επεκτείνουμε την αρχική μελέτη βαθμοτοποίησης μελανών οπών, εισαγάγοντας ένα ηλεκτρομαγνητικό πεδίο, επομένως μελετάμε το φαινόμενο της βαθμοτοποίησης της Reissner-Nordström επαγόμενο από την αλληλεπίδραση ενός βαθμωτού πεδίου με τον αναλλοίωτο όρο βαρύτητας Gauss-Bonnet. Ο αναλλοίωτος όρος της βαρύτητας Gauss-Bonnet, πέραν του ότι εμφανίζεται στη γενικευμένη θεωρία Horndeski, αναπαριστά πρώτης τάξης διορθώσεις του R^2, στη δράση του Einstein στη δεκαδιάστατη ετεροτική θεωρία χορδών. Μια αλληλεπίδραση ενός βαθμωτού πεδίου με τον όρο Gauss-Bonnet περιγράφει καταστάσεις στις οποίες τα βαρυτικά φαινόμενα ενισχύονται σε εκείνες τις περιοχές ισχυρής βαρύτητας.

Η δράση που περιγράφει τη θεωρία EsGB με την παρουσία ενός ηλεκτρομαγνητικού πεδίου είναι:

$$\mathcal{S} = \frac{1}{16\pi} \int d^4x\sqrt{-g}\left[R - 2\nabla_\mu\phi\nabla^\mu\phi + \lambda^2 f(\phi)\mathcal{R}^2_{GB} + F_{\mu\nu}F^{\mu\nu}\right], \tag{1}$$

όπου ϕ είναι το βαθμωτό πεδίο που εισαγάγουμε, και είναι μη-ελάχιστα συζευγμένο με τον αναλλοίωτο όρο Gauss-Bonnet $\mathcal{R}^2_{GB} = R^2 - 4R_{\mu\nu}R^{\mu\nu} + R_{\mu\nu\rho\sigma}R^{\mu\nu\rho\sigma}$, μέσω μιας συνάρτησης σύζευξης $f(\phi)$ και μιας σταθεράς σύζευξης λ. Το ηλεκτρομαγνητικό πεδίο A^μ ορίζεται μέσω του τανυστή Faraday ως $F^{\mu\nu} = \nabla^\mu A^\nu - \nabla^\nu A^\mu$.

Η λύση του κενού της θεωρίας αυτής είναι η μελανή οπή Reissner-Nordström της ΓΘΣ, για συναρτήσεις σύζευξης οι οποίες ικανοποιούν την σχέση $f'(\phi)|_{\phi=0} = 0$, όταν το βαθμωτό πεδίο είναι τετριμμένο. Η λύση αυτή εμφανίζει ταχυονικές αστάθειες κάτω από μικρές διαταραχές. Στην παρούσα θεωρία, οι διαταραχές περιγράφονται από την εξίσωση των βαθμωτών διαταραχών:

$$\left(\Box + \frac{1}{4}\lambda^2 f''(\phi)\mathcal{R}^2_{GB}\right)|_{\phi=0}\delta\phi = 0, \tag{2}$$

όπου ο όρος μάζας της βαθμωτής διαταραχής $\mu^2_{eff} = -\frac{1}{4}\lambda^2 f''(\phi)\mathcal{R}^2_{GB}|_{\phi=0}$, είναι αρνητικός για συναρτήσεις σύζευξης οι οποίες ικανοποιούν την επιπλέον σχέση $f''(\phi)|_{\phi=0} > 0$. Σε αυτήν την περίπτωση, ένα αρνητικό πηγάδι δυναμικού εξώ από τον ορίζοντα της Reissner-Nordström είναι δυνατό να υποστηρίξει δέσμιες καταστάσεις, με αποτέλεσμα την εμφάνιση διακλαδώσεων στον τετριμμένο κλάδο των λύσεων του κενού της θεωρίας μας. Εφόσον, η δυναμική ανάλυση της ευστάθειας των βαθμοτοποιημένων λύσεων της Schwarzschild προτείνει ότι μόνο ο θεμελιώδης κλάδος των μη τετριμμένων λύσεων είναι ευσταθής, στην εργασία αυτή, ενδιαφερόμαστε για την εμφάνιση του πρώτου σημείου διακλάδωσης του κλάδου της Reissner-Nordström. Μια εξαιρετικά χρήσιμη συνθήκη για την εύρεση αυτού, που περιγράφει ενά αρνητικό πηγάδι δυναμικού το οποίο

μπορεί να υποστηρίξει τουλάχιστον μια δέσμια κατάσταση δίνεται ακολούθως:

$$\int_{-\infty}^{+\infty} U(r_*)dr_* = \int_{r_H}^{+\infty} \frac{U(r)}{f(r)}dr < 0, \tag{3}$$

όπου r_* είναι η συντεταγμένη "χελώνας" και $U(r)$ είναι το δυναμικό. Η συνθήκη αυτή δίνει το ελάχιστο όριο της τιμής που μπορεί να λάβει η σταθερά σύζευξης λ, εξασφαλίζοντας την εμφάνιση της πρώτης θεμελιώδους δέσμιας κατάστασης. Για τιμές κάτω αυτού του ελαχίστου ορίου, η μελανή οπή Reissner-Nordström είναι ευσταθής κάτω από μικρές βαθμωτές διαταραχές. Για τιμές ανώ αυτού του ορίου, το βαθμωτό πεδίο γίνεται ταχυονικό, η Reissner-Nordström παρουσιάζει ταχυονικές αστάθειες και "μεταβαίνει" σε μια νέα βαθμοτοποιημένη μη τετριμμένη φορτισμένη μελανή οπή.

Ο μηχανισμός της βαθμοτοποίησης λαμβάνει χώρα όταν ικανοποιούνται οι συνθήκες $f'(\phi)|_{\phi=0} = 0$, $f''(\phi)|_{\phi=0} > 0$. Στην παρούσα εργασία επιλέγονται τρεις διαφορετικές συναρτήσεις περιγράφοντας τρεις διαφορετικές περιπτώσεις βαθμοτοποίησης της Reissner-Nordström, με σκοπό να μελετηθεί η ευαισθησία του μηχανισμού.

Λύνουμε αριθμητικά τις διαφορικές εξισώσεις πεδίου σ'έναν στατικά και σφαιρικά συμμετρικό χωροχρόνο:

$$ds^2 = -e^{2\Phi(r)}dt^2 + e^{2\Lambda(r)}dr^2 + r^2(d\theta^2 + \sin^2\theta d\varphi^2). \tag{4}$$

Το πρόβλημα αρχικών τιμών που προκύπτει επιλύνεται με τη μέθοδο της βολής. Οι συνοριακές συνθήκες που περιγράφουν το πρόβλημα οριακών τιμών καθορίζονται από την απαίτηση ότι οι βαθμοτοποιημένες λύσεις θα πρέπει να είναι ασυμπτωτικά επίπεδες σε άπειρα μακρινές αποστάσεις από τη βαρυτική πηγή, προσεγγίζοντας τον επίπεδο χωροχρόνο Minkowski. Επιπλέον, κοντά στον ορίζοντα γεγονότων οι βαθμοτοποιημένες λύσεις θα πρέπει να είναι ομαλές, υποθέτοντας την ύπαρξη του ορίζοντα γεγονότων. Η συνθήκη για ομαλότητα της πρώτης παραγώγου της συνάρτησης του βαθμωτού πεδίου δίνει έναν περιορισμό για την εύρεση των βαθμοτοποιημένων λύσεων:

$$f_1^2(\phi)\left(r_H^6 - 4Q^2 f_1^2(\phi)\right) < \frac{r_H^7\left(Q^2 + \Phi_1 r_H^3\right)^2}{8\Phi_1\left(2Q^2 + 3\Phi_1 r_H^3\right)}, \tag{5}$$

όπου ο δείκτης 1 δηλώνει παραγώγιση ως προς την ακτινική συνιστώσα και υπολογισμό πάνω στον ορίζοντα γεγονότων. Ο περιορισμός αυτός εννοιολογικά εξασφαλίζει στο σύστημα την ελάχιστη ενέργεια που θα πρέπει να έχει, προκειμένου να πραγματοποιήσει μια δυναμική μετάβαση φάσης.

Η επιλογή της συνάρτησης σύζευξης φαίνεται να μην επηρεάζει την θέση των θεμελιωδών σημείων διακλάδωσης της Reissner-Nordström. Οι νέες μη τετριμμένες βαθμοτοποιημένες λύσεις φορτισμένω μελανών όπων για κάθε επιλογή της συνάρτησης σύζευξης ακολουθούν την ίδια ποιοτική συμπεριφορά, και διαφέρουν μόνο ως προς την απόκλιση από τη ΓΘΣ. Αυτή η διαφορά όμως, περιγράφεται επαρκώς από την σταθερά σύζευξης λ της θεωρίας μας. Συνεπώς, αποφαινόμαστε ότι το φαινόμενο της βαθμοτοποίησης δεν παρουσιάζει κάποια ιδιαίτερη ευαισθησία ως προς την επιλογή της συνάρτησης σύζευξης, εφόσον η τελευταία ικανοποιεί τις συνθήκες που ορίζει ο μηχανισμός της βαθμοτοποίησης.

Από την άλλη μεριά, η παρουσία του ηλεκτρομαγνητικού πεδίου στη θεωρία φαίνεται να επηρεάζει τους βαθμοτοποιημένους κλάδους λύσεων ποιοτικά αλλά και ποσοτικά. Παρατηρούμε ότι όσο το ηλεκτρικό φορτίο Q αυξάνεται, τα σήμεια διακλάδωσης του τετριμμένου κλάδου λύσεων μετατοπίζονται ολοένα και σε μεγαλύτερες μάζες M. Επίσης, οι βαθμοτοποιημένοι κλάδοι γίνονται στενότεροι με την αύξηση του ηλεκτρικού φορτίου Q, τερματίζοντας είτε σε μια μη-ακραία φορτισμένη βαθμοτοποιημένη λύση μελανής οπής, είτε σε μια τετριμμένη λύση μελανής οπής Reissner-Nordström, προτείνοντας έναν μηχανισμό απο-βαθμοτοποίησης. Επιπλέον, η αύξηση του ηλεκτρικού φορτίου φαίνεται να οδηγεί σε μικρότερες αποκλίσεις από τη ΓΘΣ, εφόσον το πλάτος των βαθμοτοποιημένων λύσεων μικραίνει.

Το μέγεθος που περιγράφει τις αποκλίσεις της θεωρίας μας από τη ΓΘΣ είναι το βαθμωτό φορτίο D. Παράλληλα, η σταθερά σύζευξης αποτελεί το μέγεθος που περιγράφει το πόσο ισχυρή

είναι η αλληλεπίδρασης του βαθμωτού πεδίου με τον αναλλοίωτο όρο βαρύτητας, συνεπώς το πόσο ισχυρό είναι το βαρύτικο πεδίο στον χωροχρόνο. Στις περιοχές που το πεδίο είναι ισχυρό οι αποκλίσεις της θεωρίας μας από τη ΓΘΣ είναι σαφείς, ενώ στις περιοχές ασθενούς βαρύτητας η θεωρία μας είναι σχεδόν δυσδιάκριτη από τη ΓΘΣ.

Τέλος, γνωρίζοντας ότι οι μελανές οπές μπορούν να θεωρηθούν ως θερμοδυναμικά σώματα, μελετάμε τις θερμοδυναμικές ιδιότητες των βαθμοτοποιημένων κλάδων της θεωρίας μας, όπως η θερμοκρασία και η εντροπία. Η θερμοκρασία της σφαιρικά συμμετρικής βαθμοτοποιημένης μελανής οπής περιγράφεται από την επιφανειακή βαρύτητα πάνω στον ορίζοντα γεγονότων ως ακολούθως:

$$T = \frac{k_H}{2\pi} = \frac{1}{4\pi}\left(\frac{1}{\sqrt{|g_{tt}g_{rr}|}}\left|\frac{dg_{tt}}{dr}\right|\right)_{r_H} . \tag{6}$$

Έλεγχος πολλών βαθμοτοποιημένων κλάδων λύσεων επιβεβαίωνει την αδυναμία της θεωρίας μας να δεχτεί λύσεις ακραίων βαθμοτοποιημένων ηλεκτρικά φορτισμένων μελανών οπών, σε αντίθεση με τον κλάδο λύσεων της ΓΘΣ, όπου η Reissner-Nordström μπορεί να είναι ακραία, με την έννοια ότι μπορεί να έχει ηλεκτρικό φορτίο ίσο με την μάζα της.

Η εντροπία σε ΤΘΒ, οι οποίες περιλαμβάνουν όρους υψηλότερης τάξης στην καμπυλότητα του χωροχρόνου, δεν ακολουθεί τον νόμο επιφάνειας σύμφωνα με τον 2ο θερμοδυναμικό νόμο, αλλά περιγράφεται από επιπρόσθετες διορθώσεις. Σύμφωνα με τον τύπο του Wald η εντροπία των βαθμοτοποιημένω κλάδων των λύσεων της θεωρίας μας υπολογίζεται ως ακολούθως:

$$S_H = \frac{1}{4}A_H + 4\pi\lambda^2 f(\phi_H). \tag{7}$$

Είναι αξιοσημείωτο ότι όλες οι βαθμοτοποιημένες λύσεις φορτισμένων μελανών οπών εμφανίζουν μεγαλύτερη εντροπία από τις αντίστοιχες λύσεις της ΓΘΣ. Αυτό υποδηλώνει θερμοδυναμική ευστάθεια έναντι θερμικών διακυμάνσεων, καθιστώντας τις νέες λύσεις θερμοδυναμικά προτιμηταίες από αυτές της ΓΘΣ.

Στο *κεφάλαιο 3*, μελετάμε το φαινόμενο της βαθμοτοποίησης συμπεριλαμβάνοντας την εισαγωγή ενός μη-ελάχιστα συζευγμένου βαθμωτού πεδίου με ένα πεδίο ύλης. Αυτού του είδους η σύζευξη περιγράφει καταστάσεις στις οποίες μια τετριμμένη μελανή οπή αλληλεπιδρά με την περιβάλλουσα ύλη της και μέσω του μηχανισμού της βαθμοτοποίησης μεταβαίνει σε μια μη τετριμμένη μελανή οπή.

Θεωρούμε τη βαρυτική θεωρία μη γραμμικού ηλεκτρομαγνητισμού, η οποία περιγράφεται από την εξής δράση:

$$S = \frac{1}{8\pi}\int d^4x\,\sqrt{-g}\left[\frac{R}{2} - \frac{1}{2}\nabla^\mu\phi\nabla_\mu\phi - \frac{1}{2}\mathcal{P} - f(\phi)\left(\mathcal{P} - \alpha\mathcal{P}^2\right)\right] , \tag{8}$$

όπου η ποσότητα $\mathcal{P}$ συμβολίζει τον αναλλοίωτο όρο Maxwell και η θετική ποσότητα $\alpha > 0$ συμβολίζει μια σταθερά σύζευξης, η οποία σχετίζεται με την σταθερά λεπτής υφής.

Η λύση του κενού αυτής της θεωρίας αποτελεί και πάλι η Reissner-Nordström:

$$ds^2 = -N(r)dt^2 + \frac{1}{N(r)}dr^2 + r^2d\theta^2 + r^2\sin^2\theta d\varphi^2,\ N(r) \equiv 1 - \frac{2M}{r} + \frac{Q^2}{r^2} , \tag{9}$$

με ένα τετριμμένο βαθμωτό πεδίο και τη συνάρτηση σύζευξης να ικανοποιεί την συνθήκη $\dot{f}(\phi = 0) = 0$. Μικρές διαταραχές της λύσης αυτής περιγράφονται από την εξίσωση των βαθμωτών διαταραχών:

$$\left(\Box - \mu^2_{\text{eff}}\right)\big|_{\phi=0}\delta\phi = 0 , \tag{10}$$

όπου ο όρος μάζας δίνεται από την σχέση:

$$\mu^2_{\text{eff}} = \ddot{f}(\phi)\left(\mathcal{P} - \alpha\mathcal{P}^2\right)\Big|_{\phi=0} . \tag{11}$$

Θεωρώντας ηλεκτρικά πεδία, ο όρος αυτός της μάζας μπορεί να γίνει αρκετά αρνητικός όταν η συνάρτηση σύζευξης ικανοποιεί την συνθήκη $\ddot{f}(\phi = 0) > 0$, με αποτέλεσμα να προκαλέσει ταχυονικές αστάθειες στην λύση της τετριμμένης μελανής οπής. Επιλέγουμε την τετραγωνική συνάρτηση $f(\phi) = \beta^2\phi^2$. Ένα αρκετά βαθύ αρνητικό πηγάδι δυναμικού εμφανίζεται εξώ από τον ορίζοντα γεγονότων της Reissner-Nordström με αποτέλεσμα να φιλοξενεί δέσμιες καταστάσεις, για κάθε μια από τις οποίες ένα νέο σημείο διακλάδωσης να εμφανίζεται στον τετριμμένο κλάδο λύσεων.

Οι ακτινικές εξισώσεις των βαθμωτών διαταραχών περιγράφονται ως εξής:

$$\left(r^2 N(r) u'(r)\right)' - \left(l(l+1) - \frac{2Q^2\left(2\alpha Q^2 + r^4\right) f''(0)}{r^6}\right) u(r) = 0 \ . \tag{12}$$

Η εξίσωση αυτή είναι δύσκολο να ληθεί με κοινές μεθόδους, επομένως αναζητούμε τις δέσμιες καταστάσεις οι οποίες σέβονται την σφαιρική συμμετρία του χωρόχρονου, είναι ομαλές κοντά στον ορίζοντα γεγονότων της Reissner-Nordström και είναι ασυμπτωτικά επίπεδες σε μακρινές αποστάσεις από την πηγή βαρύτητας. Για κάθε δεδομένη τιμή των σταθερών της θεωρίας μας, αναζητώντας δέσμιες καταστάσεις, συλλέγουμε ένα διακριτό σύνολο από τετριμμένες μελανές οπές που χαρακτηρίζονται από έναν καθορισμένο λόγο του ηλεκτρικού φορτίου προς την μάζα της τους. Αυτός ο λόγος ορίζει τα σημεία διακλάδωσης στον παραμετρικό χώρο της θεωρίας μας. Το πρώτο σύνολο λύσεων περιγράφει τις θεμελιώδεις δέσμιες καταστάσεις της βαθμωτής διαταραχής και άρα, χαρακτηρίζει το πρώτο σημείο διακλάδωσης του τετριμμένου θεμελιώδους κλάδου βαθμοτοποιημένων λύσεων μελανών οπών, κ.ο.κ.. Εξετάζοντας διάφορες τιμές των παραμέτρων όλοι οι λόγοι ηλεκτρικού φορτίου ως προς τη μάζα παραμένουν μικρότεροι της μονάδας, σεβόμενοι τη μη-ακραία συνθήκη της Reissner-Nordström.

Στην συνέχεια, στον παραμετρικό χώρο όπου η Reissner-Nordström παρουσιάζει ταχυονικές αστάθειες, ερευνούμε για νέες βαθμοτοποιημένες λύσεις μελανών οπών. Το διαφορικό σύστημα των εξισώσεων πεδίου περιγράφεται από ένα πρόβλημα αρχικών τιμών, το οποίο λύνουμε με την μέθοδο της βολής. Με δεδομένη την ομαλότητα των λύσεων κοντά στον ορίζοντα γεγονότων, αναζητούμε λύσεις με ασυμπτωτικά επίπεδη συμπεριφορά στο άπειρο, σ'ένα στατικά και σφαιρικά συμμετρικά χωρόχρονο:

$$ds^2 = -e^{-2\delta(r)} N(r) dt^2 + \frac{dr^2}{N(r)} + r^2 d\theta^2 + r^2 \sin^2\theta d\varphi^2, \ N(r) \equiv 1 - \frac{2m(r)}{r} \ . \tag{13}$$

Οι νέες βαθμοτοποιημένες λύσεις φορτισμένων μελανών οπών σχηματίζουν κλάδους που διακλαδώνονται από τον κλάδο της Reissner-Nordström και εκτείνονται σε λύσεις "υπερφορτισμένων" μελανών οπών, με την έννοια ότι οι λύσεις ικανοποιούνται για τιμές του λόγου του ηλεκτρικού φορτίου ως προς τη μάζα μεγαλύτερες της μονάδας, παραβιάζοντας την μη-ακραία συνθήκη. Πλέον, οι φορτισμένες βαθμοτοποιημένες μελανές οπές μπορούν να "κουβαλήσουν" περισσότερο ηλεκτρικό φορτίο σε σχέση με την μάζα τους.

Οι βαθμοτοποιημένοι κλάδοι λύσεων τερματίζουν σε μια γυμνή ιδιομορφία. Αυτό επιβεβαιώνεται από τον απειρισμό της βαθμωτής ποσότητας της βαρύτητας Kretschmann κοντά στον ορίζοντα γεγονότων, που σημαίνει ότι η παρουσία του ορίζοντα γεγονότων που υποθέσαμε λύνοντας το πρόβλημα αρχικών τιμών δεν υπάρχει πλέον, και η γυμνή ιδιομορφία εμφανίζεται. Αυτό το αποτέλεσμα επιβεβαιώνεται με την μελέτη των θερμοδυναμικών ιδιοτήτων των βαθμοτοποιημένων μελανών οπών. Το εμβαδόν της επιφάνειας του ορίζοντα γεγονών μηδενίζεται για όλους τους βαθμοτοποιημένους κλάδους, στο ισχυρό καθώς και, στο ασθενές βαρυτικό πεδίο.

Η εντροπία εμφανίζεται αυξημένη στις περιπτώσεις των βαθμοτοποιημένων μελανών οπών σε σχέση με αυτήν της Reissner-Nordström, σύμφωνα με τον επιφανειακό νόμο, καθιστώντας τις νέες λύσεις θερμοδυναμικά προτιμηταίες. Η θερμοκρασία των βαθμοτοποιημένων μελανών οπών είναι σταθερά υψηλότερη σε σχέση με τις αντίστοιχες τετριμμένες μελανές οπές, στον παραμετρικό χώρο μη μοναδικότητας των λύσεων, κάτι που τις χαρακτηρίζει ως θερμότερες.

Στο τέλος, πραγματοποιούμε έναν έλεγχο των ενεργειακών συνθηκών, επιβεβαιώνοντας ότι ο χωρόχρονος της θεωρίας μας υπακούει σε αυτές.

Στο *κεφάλαιο 4*, εξετάζουμε το φαινόμενο της βαθμοτοποίησης ολογραφικά. Σύμφωνα με την ολογραφική αρχή και την αντιστοιχία του Maldacena, μια σύμμορφη θεωρία πεδίου ισοδυναμεί με μια AdS βαρυτική θεωρία πεδίου. Τότε, μια μελανή οπή είναι ολογραφικά ισοδύναμη με μια καθορισμένη κατάσταση ύλης. Επομένως, μπορούμε να θεωρήσουμε ότι μια τετριμμένη και μια μη-τετριμμένη μελανή οπή ισοδυναμεί σε μια κανονική καταστάση και μια αγώγιμη ή ακόμα και, υπεραγώγιμη κατάσταση της ύλης. Στο κεφάλαιο αυτό, ερευνούμε τι είδους καταστάσεις ύλης περιγράφουν οι βαθμοτοποιημένες μελανές οπές. Για την επίτευξη αυτού, υποθέτουμε δύο διαφορετικές περιπτώσεις, τη βαθμοτανυστική θεωρία AdS EsGB με και χωρίς την παρουσία ηλεκτρομαγνητικού πεδίου.

Στην πρώτη περίπτωση, θεωρούμε ότι η δράση της θεωρίας μας περιγράφεται ως εξής:

$$\mathcal{S} = \frac{1}{16\pi G_N}\int d^4x\sqrt{-g}\left(R + \frac{6}{L^2} - \nabla_\mu\phi\nabla^\mu\phi - m^2\phi^2 + f(\phi)\mathcal{R}^2_{GB}\right), \tag{14}$$

όπου ο όρος μάζας του βαθμωτού πεδίου εισαγάγεται ώστε, κοντά στην συνοριακή επιφάνεια του χωρόχρονου της μελανής οπής, το βαθμωτό πεδίο να πέφτει ως δύναμη της ακτινικής συνεταγμένης.

Σύμφωνα με την συνθήκη $f'(0) = 0$, η επίπεδη μελανή οπή Schwarzschild-AdS αποτελεί λύση των πεδιακών μας εξισώσεων για ένα τετριμμένο βαθμωτό πεδίο:

$$\begin{aligned} ds^2 =& -g(r)dt^2 + \frac{1}{g(r)}dr^2 + r^2(dx^2 + dy^2) \\ g(r) =& \frac{r^2}{L^2} - \frac{M}{r}. \end{aligned} \tag{15}$$

Η λύση του κενού της θεωρίας μας, όταν η συνάρτηση σύζευξης ικανοποιεί την επιπρόσθετη συνθήκη $f''(0) > 0$, παρουσιάζει ταχυονικές αστάθειες, όπως φαίνεται από την εξίσωση των βαθμωτών διαταραχών ακολούθως:

$$\left(\Box - \left(m^2 - \frac{1}{2}f''(\phi)\mathcal{R}^2_{GB}\right)\right)\Big|_{\phi=0}\delta\phi = 0. \tag{16}$$

Προσεγγίζοντας αριθμητικά τη λύση της εξίσωσης των βαθμωτών διαταραχών, βρίσκουμε ότι πέρα από μια κρίσιμη τιμή της σταθεράς σύζευξης, αρνητικά πηγάδια ενεργού δυναμικού εμφανίζονται εξώ από τον ορίζοντα γεγονότων της τετριμμένης μελανής οπής. Πέρα από την ίδια κρίσιμη τιμή, οι βαθμωτές ακτινικές διαταραχές μεγαλώνουν με την πάροδο του χρόνου, καθιστώντας το χωρόχρονο της Schwarzschild-AdS ασταθή.

Λύνοντας αριθμητικά το σύστημα των εξισώσεων πεδίου της θεωρίας μας βρίσκουμε λύσεις βαθμωτοποιημένων μελανών οπών που σε ασυμπτωτικά μεγάλες αποστάσεις από την πηγή της βαρύτητας, προσεγγίζουν τον χωρόχρονο Schwarzschild-AdS ενώ, σε κοντινές αποστάσεις εμφανίζονται σαφείς αποκλίσεις από αυτόν. Στη βαρυτική θεωρία AdS, η παρουσία μη-τετριμμένων βαθμωτών πεδίων περιγράφει τις βαθμοτοποιημένες λύσεις μελανών οπών. Στην σύμμορφή θεωρία πεδίου, παρατηρείται ραγδαία αύξηση της προσδοκώμενης τιμής του τελεστή πέρα από ένα κατώφλι της σταθεράς σύζευξης. Αυτό το αποτέλεσμα δηλώνει, την εμφάνιση συμπύκνωσης της ύλης σε ένα υλικό, με έναν μηχανισμό παρόμοιο με αυτόν της βαθμοτοποίησης, όπου έχουμε την εμφάνιση "μαλλιών" σε μια τετριμμένη μελανή οπή. Επομένως, η βαθμοτοποίηση σε μια σύμμορφη θεωρία πεδίου περιγράφει μια διακριτή μετάβαση φάσης ενός υλικού, από μια κανονική κατάσταση ύλης με τετριμμένη προσδοκώμενη τιμή του τελεστή, σε μια διαφορετική κατάσταση συμπυκνωμένης ύλης με μια μη-τετριμμένη προσδοκώμενη τιμή. Σημειώνουμε ότι, η απουσία σπάσιμου συμμετρίας $U(1)$ στη βαρυτική θεωρία, υποδηλώνει μια κβαντικού τύπου μετάβασης φάσης σε μια καθορισμένη θερμοκρασία.

Επιπλέον, σε αυτήν την περίπτωση μελετάμε την ολογραφική εντροπία εμπλοκής, η οποία αποτελεί μια από τις πιο σημαντικές χαρακτηριστικές ποσότητες στην σύμμορφη θεωρία βαθμίδας. Η ποσότητα αυτή λειτουργεί ως μέτρο των βαθμών ελευθερίας ενός συστήματος. Η εισαγωγή του βαθμωτού πεδίου αυξάνει τους βαθμούς ελευθερίας επομένως, η εντροπία, παρατηρούμε να αυξάνεται μετά το φαινόμενο της βαθμοτοποίησης. Αυτή η συμπεριφόρα έρχεται σε πλήρη αντίθεση με αυτήν που παρατηρείται σε ολογραφικές καταστάσεις υπεραγωγών. Τυπικά, μια υπεραγώγιμη κατάσταση ύλης έχει χαμηλότερη εντροπία σε σχέση με την κανονική της κατάσταση. Η θεωρία των Bardeen-Cooper-Schrieffer περιγράφη την ακαριαία δημιουργία ζευγαριών Cooper στην υπεραγώγιμη κατάσταση, η οποία ελλατώνει τους βαθμούς ελευθερίας του συστήματος. Επομένως, μπορούμε να αποφανθούμε ότι το φαινόμενο της βαθμοτοποίησης δεν μπορεί να περιγράψει μια ολογραφική μετάβαση φάσης σε μια υπεραγώγιμη κατάσταση ύλης.

Στη δεύτερη περίπτωση, εισάγουμε ένα ηλεκτρομαγνητικό πεδίο $A_\mu = (A_t(r), 0, 0, 0)$ στην θεωρία EsGB ενώ, το βαθμωτό πεδίο είναι φορτισμένο πλέον. Η δράση που περιγράφει το θεωρητικό μοντέλο είναι:

$$\mathcal{S} = \frac{1}{16\pi G_N}\int dx^2\sqrt{-g}\left(R + \frac{6}{L^2} - \frac{1}{4}F_{\mu\nu}F^{\mu\nu} - D_\mu\phi(D^\mu\phi)^* - m^2|\phi|^2 + f(\phi)\mathcal{R}^2_{GB}\right), \quad (17)$$

όπου η ποσότητα $D_\mu = \nabla_\mu - iqA_\mu$ αποτελεί την συναλλοίωτη παράγωγο βαθμίδας. Και σε αυτήν την περίπτωση οι δύο συνθήκες για την συνάρτηση σύζευξης $f'(0) = 0$ και $f''(0) = 0$ καθιστούν την λύση του κενού της θεωρίας μας ασταθή. Η εξίσωση των βαθμωτών διαταραχών υποδεικνύει την παρουσία μιας ενεργού μάζας που μπορεί να δεχτεί ικανοποιητικά αρνητικές τιμές, περιγράφοντας ένα αρνητικό βαθύ πηγάδι δυναμικού με την παρουσία δέσμιων καταστάσεων, όπως φαίνεται ακολούθως:

$$\left(\Box - \left(m^2 + q^2A_\mu A^\mu\right) + \frac{1}{2}f''(\phi)\mathcal{R}^2_{GB}\right)\delta\phi = 0,\ m^2_{eff} = m^2 - \frac{q^2A_t(r)^2}{g(r)} - \frac{\lambda^2}{2}\mathcal{R}^2_{GB}. \quad (18)$$

Πέρα απ'το κατώφλι, απ' το οποίο η μελανή οπή Reissner-Nordström-AdS γίνεται ασταθής λόγω της ύπαρξης του ηλεκτρομαγνητικού πεδίου και της αλληλεπίδρασης του βαθμωτού πεδίου με τον αναλλοίωτο όρο βαρύτητας Gauss-Bonnet, λύνουμε αριθμητικά και ασυμπτωτικά το πλήρες σύστημα των πεδιακών εξισώσεων θεωρώντας την ύπαρξη ενός ορίζοντα γεγονότων. Το σύστημα ανάγεται σε πρόβλημα αρχικών τιμών με λύσεις που ικανοποιούν εκείνες τις συνοριακές συνθήκες, έτσι ώστε να περιγράφονται από ομαλές συναρτήσεις κοντά στον ορίζοντα γεγονότων, και ο χωρόχρονος που θα περιγράφεται από τις νέες βαθμοτοποιημένες μελανές οπές να τείνει ασυμπτωτικά στον χωρόχρονο AdS σε μακρινές αποστάσεις.

Οι νέες βαθμοτοποιημένες λύσεις μελανών οπών παρουσιάζουν ένα συμπύκνωμα του βαθμωτού πεδίου σε μια κρίσιμη θερμοκρασία. Καθώς η τιμή της σταθεράς σύζευξης λ αυξάνεται, παρατηρούμε μια αμυδρή αύξηση της κρίσιμης θερμοκρασίας. Όταν η σταθερά λάβει μια κρίσιμη τιμή, τότε η κρίσιμη θερμοκρασία εμφάνισης του συμπυκνώματος απειρίζεται ραγδαία. Πέρα απ'αυτό το κατώφλι, θεωρούμε ότι η βαρυτική αλληλεπίδραση είναι τόσο ισχυρή, ωστέ μια μετάβαση φάσης από μια τετριμμένη μελανή οπή σε μια μη-τετριμμένη είναι αδύνατη.

Στην περίπτωση αυτή, για μικρότερες τιμές της κρίσιμης σταθεράς σύζευξης, παρατηρούμε τον σχηματισμό συμπυκνώματος, ο οποίος ελαττώνεται όσο η βαρυτική αλληλεπίδραση του βαθμωτού πεδίου γίνεται ολοένα και πιο ισχυρή. Με βάση την αντιστοιχία AdS/CFT, θεωρούμε το παραπάνω αποτέλεσμα ισοδύναμο με μια μετάβαση φάσης σε μια υπεραγώγιμη κατάσταση ύλης, με το βαθμωτό συμπύκνωμα του βαθμωτού πεδίου να ισοδυναμεί με την προσδοκώμενη τιμή ενός τελεστή καταστροφής ζευγών Cooper.

Στη συνέχεια, υπολογίζουμε την αγωγιμότητα της ύλης στην θεωρία πεδίου, ως συνάρτηση της συχνότητας του αρμονικού κύματος που περιγράφει την λύσης της εξίσωσης Maxwell. Καθώς, η σταθερά σύζευξης αυξάνεται, η αγωγιμότητα γίνεται ασθενέστερη και το σύστημα τείνει να ισοδυναμεί με ένα μέταλλο σε καθορισμένη θερμοκρασία. Τέλος, υπολογίζουμε την υπερρεύστη πυκνότητα του υπεραγώγιμου υλικού, η οποία φαίνεται να μηδενίζεται γραμμικώς, όσο

η θερμοκρασία τείνει στην κρίσιμη θερμοκρασία. Η μείωση αυτή της υπέρρευστης πυκνότητας ευθυγραμμίζεται με την μείωση της παρουσίας συμπυκνώματος, όσο η βαρυτική αλληλεπίδραση γίνεται ισχυρότερη. Συνεπώς, το φαινόμενο της βαθμοτοποίησης παρουσία ηλεκτρομαγνητικού φορτίου, μπορεί να ερμηνευτεί ολογραφικά, ως μια μετάβαση φάσης ενός υλικού από μια κανονική σε μια υπεραγώγιμη κατάσταση, σε μια κρίσιμη θερμοκρασία.

Στο *κεφάλαιο 5*, παρουσιάζουμε τα αποτελέσματα της παρούσας διδακτορικής έρευνας, η μελέτη της οποίας αναδεικνύει τον ρόλο της μη-ελάχιστης αλληλεπίδρασης μεταξύ βαθμωτών πεδίων, ηλεκτρομαγνητικών πεδίων και βαρυτικών διορθώσεων στη δημιουργία νέων μη-τετριμμένων λύσεων μελανών οπών, αποκαλύπτοντας νέα φυσικά φαινόμενα πέρα από αυτά που περιγράφονται στη ΓΘΣ. Τα αποτελέσματα αυτά ενισχύουν την κατανόησή μας όσον αφορά το φαινόμενο της βαθμοτοποίησης, παρέχοντας πολύτιμες γνώσεις για μελλοντική έρευνα σε ΤΘΒ και στην ανάπτυξη θεωρητικών μοντέλων για την περιγραφή των μελανών οπών που πράγματι "ταξιδεύουν" στο σύμπαν.

Chapter 1

Introduction

1.1 General Theory of Relativity

1.1.1 Gravity as Geometry

Einstein's General Theory of Relativity (GR) has established itself as an extraordinarily successful geometrical theory that describes gravitational interactions through the curvature of spacetime [6]. The two cornerstones of GR are Mach's and the Equivalence principles. The Austrian physicist and philosopher Ernst Mach stated in 1883 [7] that "mass there influences inertial here," suggesting that an object's inertial is influenced not only by its mass but also by the gravitational influence of all other matter in the universe. "Inertial" describes the trajectories of unaccelerated particles (freely falling). In 1907, the German physicist Albert Einstein demonstrated the Equivalence Principle [8], which states that "locally a free-falling observer and an inertial observer are indistinguishable," meaning that inertial mass and gravitational mass are equal to each other. The second law of Newton expresses the force $\vec{F}$ acting on an object as the mass m_i of that object multiplied by its acceleration $\vec{a}$:

$$\vec{F} = m_i \cdot \vec{a}. \tag{1.1}$$

On the other hand, Newton's law of gravitation expresses the gravitational force $\vec{F}_G$ exerted on an object as the gravitational mass m_G multiplied by the gravitational potential $\nabla\Phi$:

$$\vec{F}_G = -m_G \nabla\Phi. \tag{1.2}$$

The Equivalence principle states the equality $m_i = m_G$, implying that the acceleration due to gravity $\vec{a}$ equals the strength of the gravitational field $-\nabla\Phi$ itself.

$$\vec{a} = -\nabla\Phi. \tag{1.3}$$

In the case of the electric force, the result is different. Einstein realized there was something special about the gravitational force, linking it with a strange property arising from Hamilton's principle of stationary action in classical mechanics. The action is the integral of the Lagrangian with respect to time. Hamilton's principle asserts that the trajectory that a particle will follow makes its action stationary. This principle provides a powerful framework for deriving the equations of motion of physical systems, such as the famous Euler-Lagrange equations, which describe how the system evolves over time. Einstein noticed that when solving the Euler-Lagrange equations for a free particle, under the influence of no external forces, which is bound to a surface by the corresponding constraint forces, the trajectory that makes action stationary coincides exactly with a geodesic of that surface. The intriguing observation that mass can be eliminated from the Euler-Lagrangian equations without affecting the particle's trajectory

inspired Einstein to propose the idea that 'there exists a geometry of space in which the motion of a free particle is indistinguishable from the motion of a particle under the influence of gravity. In 1915, Einstein developed how energy and momentum distort spacetime, and particles in the vicinity move along trajectories determined by spacetime geometry.

1.1.2 The Geometrical Framework

To establish the geometrical framework of GR, Einstein made the foundational assumption that spacetime is represented by a four-dimensional, smooth, connected, Lorentzian manifold $(\mathcal{M}^4, g_{\mu\nu})$, where $\mathcal{M}^4$ denotes the manifold's dimensionality and $g_{\mu\nu}$ denotes the metric tensor.

Each event is characterized by a point p on a coordinate basis of spacetime, $x^\mu = (ct, \vec{x})$, where c represents the speed of light and $t, \vec{x}$ represents the time and the spatial coordinates. It's important to note that GR is a coordinate-independent theory, meaning that the physical laws it describes remain invariant under infinitesimal changes in coordinates. Mathematically, this means that an infinitesimal change of coordinates:

$$x^\mu \to x'^\mu = x^\mu + \xi^\mu, \tag{1.4}$$

preserves the fundamental structure of spacetime.

Lorentzian manifold is assumed to be smooth and connected, meaning it is possible to travel smoothly and continuously from any point to any other point within the manifold without encountering any gaps, boundaries, or abrupt changes. Given that there is always a possibility to zoom into a curved space to the point where the space is flat. Afterward, at each point p of the manifold $\mathcal{M}$, the tangent space $T_p\mathcal{M}$ is defined as the vector space of all tangent vectors at that point. A tangent vector at p represents the direction and the rate of change of curves passing through p on the manifold. The basis vectors of the tangent space are defined as $\partial_\mu = \partial/\partial x^\mu$. Similarly, a cotangent space $T_p^*\mathcal{M}$ is defined as the dual vector space to the tangent space with the basis $\partial^\mu = dx^\mu$. With the basis elements of $T_p\mathcal{M}$ and $T_p^*\mathcal{M}$, any tensor field with arbitrary covariant and contravariant indices can be defined.

The geometry of the manifold is constructed through a three-step process. Firstly, the metric tensor $g_{\mu\nu}$ is defined for the spacetime, enabling the measurement of distances, [9]. This tensor assigns a scalar product to each point in the tangent space, allowing us to quantify the length between two infinitesimally separated points in space and the rates at which time flows within a region of space. It is described by the scalar invariant "measure" in four-dimensional spacetime, known as the infinitesimal line element:

$$ds^2 = g_{\mu\nu} dx^\mu dx^\nu \tag{1.5}$$

where dx^μ is an infinitesimal spacetime interval, a vector whose components are infinitesimal time and distances, respectively. Metric signature $(-,+,+,+)$ is used, reflecting the fact that the spatial components have the opposite sign compared to the time component, which is responsible for phenomena like time dilation. The metric is non-degenerate, mathematically, meaning that the determinant $g = |g_{\mu\nu}|$ doesn't vanish, allowing the definition of the inverse metric $g^{\mu\nu}$:

$$g^{\mu\nu} g_{\nu\sigma} = g_{\lambda\sigma} g^{\lambda\mu} = \delta^\mu_\sigma \tag{1.6}$$

where δ^μ_ν is the Kronecker delta symbol.

Secondly, the connection of the manifold is defined to ensure that the transported vectors remain parallel to itself with respect to the manifold's curvature. For each Lorentzian manifold, there exists a unique Levi-Civita connection ∇ (covariant derivative), characterized by the Christoffel symbols $\Gamma^\lambda_{\mu\nu}$. This connection allows for the differentiation of vector fields along curves on the manifold. Hence, the term 'connection' describes a unique relationship between vectors in tangent spaces. Levi-Civita connection ∇ satisfies l linearity, the Leibniz Rule,

commutativity with contractions, torsion-freeness, and metric compatibility. The Christoffel symbols $\Gamma^{\lambda}_{\mu\nu}$ encapsulate the curvature of the manifold and are defined by:

$$\Gamma^{\lambda}_{\mu\nu} = \frac{1}{2} g^{\lambda\sigma} \left(\partial_\mu g_{\nu\sigma} + \partial_\nu g_{\sigma\mu} - \partial_\sigma g_{\mu\nu} \right). \tag{1.7}$$

Therefore, the covariant derivative of a vector field A^ν is defined as:

$$\nabla_\mu A^\nu \equiv \partial_\mu A^\nu + \Gamma^{\nu}_{\mu\lambda} A^\lambda, \tag{1.8}$$

$$\nabla_\mu A_\nu \equiv \partial_\mu A_\nu - \Gamma^{\lambda}_{\mu\nu} A_\lambda. \tag{1.9}$$

Similarly, the covariant derivative of a second rank tensor field $A^{\mu\nu}$ is given by:

$$\nabla_\lambda A^{\mu\nu} = \partial_\lambda A^{\mu\nu} + \Gamma^{\mu}_{\alpha\lambda} A^{\alpha\nu} + \Gamma^{\nu}_{\alpha\lambda} A^{\mu\alpha}, \tag{1.10}$$

$$\nabla_\lambda A_{\mu\nu} = \partial_\lambda A_{\mu\nu} - \Gamma^{\alpha}_{\mu\lambda} A_{\alpha\nu} - \Gamma^{\alpha}_{\nu\lambda} A_{\mu\alpha}, \tag{1.11}$$

and it can be generalized for tensors with more indices $A^{\mu_1 \cdots \mu_r}{}_{\nu_1 \ldots \nu_s}$ as follows:

$$\begin{aligned} \nabla_\lambda A^{\mu_1 \cdots \mu_r}{}_{\nu_1 \ldots \nu_s} =& \partial_\lambda A^{\mu_1 \cdots \mu_r}{}_{\nu_1 \ldots \nu_s} \\ &+ \Gamma^{\mu_1}_{\alpha\lambda} A^{\alpha \mu_2 \ldots \mu_r}{}_{\nu_1 \ldots \nu_s} + \cdots + \Gamma^{\mu_r}_{\alpha\lambda} A^{\mu_1 \ldots \mu_{r-1} \alpha}{}_{\nu_1 \ldots \nu_s} \\ &- \Gamma^{\alpha}_{\nu_1 \lambda} A^{\mu_1 \ldots \mu_r}{}_{\alpha \nu_2 \ldots \nu_s} - \cdots - \Gamma^{\alpha}_{\nu_s \lambda} A^{\mu_1 \ldots \mu_r}{}_{\nu_1 \ldots \nu_{s-1} \alpha}. \end{aligned} \tag{1.12}$$

Once the covariant derivative is defined, then a geodesic can be determined. Given a manifold equipped with a metric connection, the geodesic equation can be derived from the condition that the tangent vector to a path, $dx^\mu/d\lambda$, remains parallel transported to the connection, mathematically, meaning the following condition:

$$\frac{dx^\mu}{d\lambda} \nabla_\mu \frac{dx^\mu}{d\lambda} = 0. \tag{1.13}$$

This leads to a second-order differential equation known as the geodesic equation:

$$\frac{d^2 x^\mu}{d\lambda^2} + \Gamma^{\mu}_{\rho\sigma} \frac{dx^\rho}{d\lambda} \frac{dx^\sigma}{d\lambda} = 0. \tag{1.14}$$

Finally, the Riemannian curvature tensor $R^{\rho}{}_{\sigma\mu\nu}$ is determined through the parallel vector transport concept. This tensor provides valuable insights into how the components of a vector change when it is parallel transported along a small closed curve. Specifically, it reveals how the directional derivative of a vector field fails to commute, indicating the curvature in the space. As Sean Carroll notes, "Everything we want to know about the curvature of a manifold is given to us by the Riemann tensor; it will vanish if and only if the metric is perfectly flat." [10], which is given by:

$$R^{\rho}{}_{\sigma\mu\nu} = \partial_\mu \Gamma^{\rho}_{\nu\sigma} - \partial_\nu \Gamma^{\rho}_{\mu\sigma} + \Gamma^{\rho}_{\mu\lambda} \Gamma^{\lambda}_{\nu\sigma} - \Gamma^{\rho}_{\nu\lambda} \Gamma^{\lambda}_{\mu\sigma} \tag{1.15}$$

The components of the Riemann tensor are defined in terms of the Christoffel symbols $\Gamma^{\lambda}_{\mu\nu}$. For the Christoffel connection, the only independent contraction of the Riemann tensor forms the Ricci tensor:

$$R_{\mu\nu} = R^{\lambda}{}_{\mu\lambda\nu} \tag{1.16}$$

The trace of the Ricci tensor is the Ricci scalar or curvature scalar:

$$R = R^{\mu}_{\ \mu} = g^{\mu\nu} R_{\mu\nu} \tag{1.17}$$

In GR, two essential properties concern the specific connection, described by the Christoffel symbol (1.7), of a manifold: metric compatibility and torsion-free. A metric-compatible connection ensures that the notion of distance and angle defined by the metric tensor remains

consistent under parallel transport, mathematically this implies that the covariant derivative of the metric tensor vanishes: $\nabla_\lambda g_{\mu\nu} = 0$ and $\nabla^\lambda g_{\mu\nu} = 0$. A torsion-free connection ensures the consistency of parallel transport of vectors in curved spacetime; mathematically, this implies that the Christoffel symbols are symmetric under the change of the two lower indices: $\Gamma^\lambda_{\mu\nu} = \Gamma^\lambda_{\nu\mu}$. Therefore, the symmetries of the Riemann tensor that arise are: it is antisymmetric in its first two indices and its two last indices, and it is invariant under the interchange of the first pair of indices with the second:

$$R_{\rho\sigma\mu\nu} = -R_{\sigma\rho\mu\nu}, \;\; R_{\rho\sigma\mu\nu} = -R_{\rho\sigma\nu\mu}, \;\; R_{\rho\sigma\mu\nu} = R_{\mu\nu\rho\sigma}. \tag{1.18}$$

Using the aforementioned symmetries, it is straightforward to see that the Ricci tensor is symmetric $R_{\mu\nu} = R_{\nu\mu}$. Moreover, another property of the Riemann tensor is described by the Bianchi identity:

$$\nabla_\lambda R_{\rho\sigma\mu\nu} + \nabla_\rho R_{\sigma\lambda\mu\nu} + \nabla_\sigma R_{\lambda\rho\mu\nu} = 0. \tag{1.19}$$

A very useful form of the Bianchi identity arises from contracting twice on:

$$\begin{aligned} g^{\nu\sigma} g^{\mu\lambda} \left(\nabla_\lambda R_{\rho\sigma\mu\nu} + \nabla_\rho R_{\sigma\lambda\mu\nu} + \nabla_\sigma R_{\lambda\rho\mu\nu}\right) = 0 \Rightarrow \\ \nabla^\mu \left(R_{\mu\nu} - \frac{1}{2} g_{\mu\nu} R\right) = 0 \Rightarrow \\ \nabla^\mu G_{\mu\nu} = 0, \end{aligned} \tag{1.20}$$

where $G_{\mu\nu} \equiv R_{\mu\nu} - \frac{1}{2} g_{\mu\nu} R$ is the Einstein tensor, which describes the geometry of spacetime. Consequently, gravitation is an effect of the curvature of the manifold $\mathcal{M}^4$.

1.1.3 Electrodynamics in General Relativity

In the context of GR, electromagnetism is typically described by the classical theory of electromagnetism within the framework of curved spacetime. Maxwell's equations, which govern classical electromagnetism, describe how electric $\vec{E}$ and magnetic $\vec{B}$ fields are generated and interact with charges ρ, currents $\vec{J}$, and changes of the fields In flat spacetime, these equations take the form:

$$\nabla \cdot \vec{E} = \frac{\rho}{\epsilon_0}, \tag{1.21}$$

$$\nabla \cdot \vec{B} = 0, \tag{1.22}$$

$$\nabla \times \vec{E} = -\frac{\partial \vec{B}}{\partial t}, \tag{1.23}$$

$$\nabla \times \vec{B} = \mu_0 \vec{J} + \mu_0 \epsilon_0 \frac{\partial \vec{E}}{\partial t}, \tag{1.24}$$

where ϵ_0 is the vacuum permittivity and μ_0 is the vacuum permeability, which quantities satisfy the relation:

$$c^2 = \frac{1}{\mu_0 \epsilon_0}. \tag{1.25}$$

A charged particle perceives Lorentz force due to the electromagnetic fields as follows:

$$\vec{F} = q(\vec{E} + \vec{v} \times \vec{B}). \tag{1.26}$$

The conservation of charge can be written as:

$$\frac{\partial \rho}{\partial t} + \nabla \cdot \vec{J} = 0. \tag{1.27}$$

In the vector potential formulation of electromagnetism, the electric $\vec{E}$ and magnetic $\vec{B}$ fields are related to an electric scalar potential Φ and the magnetic vector potential $\vec{A}$ as follows:

$$\vec{E} = -\nabla\Phi - \frac{\partial\vec{A}}{\partial t}, \tag{1.28}$$

$$\vec{B} = \nabla \times \vec{A}. \tag{1.29}$$

Substituting the above equations into the Maxwell equations, one can derive the simple homogeneous formulation as:

$$\nabla^2\Phi + \frac{\partial}{\partial t}(\nabla \cdot \vec{A}) = -\frac{\rho}{\epsilon_0}, \tag{1.30}$$

$$\left(\nabla^2\vec{A} - \frac{1}{c^2}\frac{\partial^2\vec{A}}{\partial t^2}\right) - \nabla\left(\nabla \cdot \vec{A} + \frac{1}{c^2}\frac{\partial\Phi}{\partial t}\right) = -\mu_0\vec{J}. \tag{1.31}$$

The scalar potential Φ and the vector potential $\vec{A}$ are auxiliary quantities introduced to simplify the mathematical description of electromagnetic phenomena. Therefore, Lorentz gauge transformation can be applied to both two potentials, ensuring that they will not affect the electromagnetic fields and they satisfy the following condition:

$$\nabla \cdot \vec{A} + \frac{1}{c^2}\frac{\partial\Phi}{\partial t} = 0. \tag{1.32}$$

Furthermore, introducing the d'Alembertian operator as:

$$\Box \equiv \nabla^2 - \frac{1}{c^2}\frac{\partial^2}{\partial t^2}, \tag{1.33}$$

the Maxwell equations take the simplest form:

$$\Box\Phi = -\frac{\rho}{\epsilon_0}, \tag{1.34}$$

$$\Box\vec{A} = -\mu_0\vec{J}. \tag{1.35}$$

Maxwell's equations within the framework of curved spacetime can be written using tensors and changing all partial derivatives with covariant derivatives. The tensors that are defined are the electromagnetic potential A^μ, the Faraday tensor $F_{\mu\nu}$ and the current j^μ as follows:

$$A^\mu \equiv \left(\frac{\Phi}{c}, \vec{A}\right), \tag{1.36}$$

$$F^{\mu\nu} \equiv \nabla^\mu A^\nu - \nabla^\nu A^\mu, \tag{1.37}$$

$$j^\mu \equiv \left(c\rho, \vec{J}\right). \tag{1.38}$$

The electromagnetic potential A^μ can be defined in a curved spacetime as a vector field whose components transform under Lorentz transformations $\nabla_\mu A^\mu = 0$, and also under general coordinate transformations. The time component represents the electrostatic potential Φ, and the spatial components represent the magnetic vector potential $\vec{A}$. The Faraday tensor $F_{\mu\nu}$ is an antisymmetric tensor that combines both electric and magnetic fields into a single mathematical object, and it provides a covariant description of electromagnetism. The components of the Faraday tensor are given by:

$$F_{\mu\nu} = \begin{pmatrix} 0 & E_1/c & E_2/c & E_3/c \\ -E_1/c & 0 & -B_3 & B_2 \\ -E_2/c & B_3 & 0 & -B_1 \\ -E_3/c & -B_2 & B_1 & 0 \end{pmatrix} \tag{1.39}$$

Therefore, the Maxwell's equations can be written as:

$$\nabla_\nu F^{\mu\nu} = -\mu_0 j^\mu, \tag{1.40}$$

$$\nabla_\lambda F_{\mu\nu} + \nabla_\nu F_{\lambda\mu} + \nabla_\mu F_{\nu\lambda} = 0, \tag{1.41}$$

where the first one corresponds to Eq. (1.21),(1.24) and the second one is equivalent to Eq. (1.22),(1.23). The current j^μ represents the density ρ and the flow of electric charge in space $\vec{J}$. Note that the equation for charge conservation, $\nabla_\mu j^\mu = 0$, is given from the same Eq. (1.27).

1.1.4 Lagrangian Formulation

A mathematical description of the dynamics of gravity of a physical system can be obtained from the Lagrangian formulation of GR. In 1915, Einstein formulated the action as part of his development of the theory of GR, where he realized that the dynamics of gravity could be described in terms of the curvature of spacetime, leading him to propose the Einstein-Hilbert action as the basis for his field equations. Just a few days after Einstein's achievement, David Hilbert, a prominent mathematician, also independently arrived at the same action. The dynamical variable is the metric tensor $g_{\mu\nu}$ and the Einstein-Hilbert action reads as:

$$\mathcal{S}_{\text{EH}} = \int dx^4 \sqrt{-g} R, \tag{1.42}$$

where $dx^4\sqrt{-g}$ represents the element of 4-volume, and Ricci scalar R is the only independent scalar that can be constructed from the Riemann curvature tensor, involving second derivatives of the metric. Therefore, based on the action principle [11], the vacuum Einstein field equations can be derived by the variation of the action with respect to the metric as follows:

$$\delta S_{\text{EH}} = \frac{\delta S_{\text{EH}}}{\delta g^{\mu\nu}} \delta g^{\mu\nu} = \int dx^4 \sqrt{-g} \left(R_{\mu\nu} - \frac{1}{2} g_{\mu\nu} R \right) \delta g^{\mu\nu}. \tag{1.43}$$

Extremizing the action leads to the following vacuum field equations:

$$R_{\mu\nu} - \frac{1}{2} g_{\mu\nu} R = 0, \tag{1.44}$$

where the Einstein tensor $G_{\mu\nu}$ is recovered. The non-vacuum field equations arise by adding terms for matter fields in Lagrangian density. A matter field is described by a kinetic term, a potential, and terms of possible interactions. Hence, the action reads as:

$$\mathcal{S} = \frac{1}{2\kappa^2} \mathcal{S}_{\text{EH}} + \mathcal{S}_{\text{M}}, \tag{1.45}$$

where $\mathcal{S}_{\text{M}}$ is the matter term and $\kappa^2 = 8\pi G/c^4$. The full Einstein field equations are:

$$G_{\mu\nu} = \kappa^2 T_{\mu\nu}, \tag{1.46}$$

where $T_{\mu\nu}$ represents the energy-momentum tensor of the minimally coupled matter field, defined as:

$$T_{\mu\nu} = -\frac{2}{\sqrt{-g}} \frac{\delta \mathcal{S}_{\text{M}}}{\delta g^{\mu\nu}}. \tag{1.47}$$

The divergence-free nature of the Einstein tensor, $\nabla^\mu G_{\mu\nu} = 0$, implies that the energy-momentum tensor is also divergence free, $\nabla^\mu T_{\mu\nu} = 0$. This property is necessary for geodesic motion, and it guarantees the validity of the weak equivalence principle [12], [13].

1.1.5 Black Hole Solutions

The Schwarzschild Solution

The Schwarzschild solution is a fundamental solution to Einstein's field equations in GR that describes the spacetime geometry outside a static, spherically symmetric, non-rotating, and uncharged massive object such as black holes, stars, and planets. It was first discovered by Karl Schwarzschild in 1916, only a few weeks after Einstein formulated his theory of GR [14]. The Schwarzschild solution can be derived by solving Einstein's field equations, applying the Lagrangian formulation of GR, and neglecting the presence of matter. This solution arises from the Einstein-Hilbert action (1.42). In polar coordinates $\{t, r, \theta, \varphi\}$, the line element ds^2 of a static and spherically symmetric spacetime is given by:

$$ds^2 = -e^{2A(r)}dt^2 + e^{2B(r)}dr^2 + e^{2\Gamma(r)}r^2 d\Omega^2, \tag{1.48}$$

where $d\Omega^2$ is the line element on a unit two-sphere $d\Omega^2 = d\theta^2 + \sin^2\theta d\varphi^2$. The choice of the exponential functions ensures the correct signature of the metric. Defining a new coordinate:

$$\bar{r} = e^{\Gamma(r)}r, \quad d\bar{r} = e^{\Gamma(r)}dr + e^{\Gamma(r)}r d\Gamma(r) = \left(1 + r\frac{d\Gamma(r)}{dr}\right)e^{\Gamma(r)}dr, \tag{1.49}$$

then the line element (1.48) becomes:

$$ds^2 = -e^{2A(r)}dt^2 + \left(1 + r\frac{d\Gamma(r)}{dr}\right)^{-2} e^{2B(r)-2\Gamma(r)}d\bar{r}^2 + \bar{r}^2 d\Omega^2. \tag{1.50}$$

Relabeling the following:

$$\bar{r} \to r, \quad \left(1 + r\frac{d\Gamma(r)}{dr}\right)^{-2} e^{2B(r)-2\Gamma(r)} \to e^{2B(r)}, \tag{1.51}$$

the line element takes the simplest form:

$$ds^2 = -e^{2A(r)}dt^2 + e^{2B(r)}dr^2 + r^2 d\Omega^2. \tag{1.52}$$

The two unknown functions $A(r)$ and $B(r)$ are determined by solving the Einstein field equations (1.44). There are three non-trivial independent field equations:

$$-\frac{1}{r^2} + \frac{e^{2B(r)}}{r^2} + \frac{2B'(r)}{r} = 0, \tag{1.53}$$

$$\frac{1}{r^2} - \frac{e^{2B(r)}}{r^2} + \frac{2A'(r)}{r} = 0, \tag{1.54}$$

$$r^2A''(r) - r^2A'(r)B'(r) + r^2A'(r)^2 + rA'(r) - rB'(r) = 0, . \tag{1.55}$$

Adding the first two equations (1.53) and (1.54) results in the equation:

$$A'(r) = -B'(r) \Rightarrow A(r) = -B(r) + c, \tag{1.56}$$

where c denotes an integration constant, which can be absorbed by rescaling the time coordinate, $t \to e^{-c}t$, and setting the constant to zero. Therefore, substituting $B'(r) = -A'(r)$ into the Eq. (1.55) yields the second order differential equation of the unknown function $A(r)$, the analytical solution of which is:

$$A(r) = \frac{1}{2}\log(2 - c_1 r) - \frac{\log(r)}{2} + c_2. \tag{1.57}$$

Here, the constants c_1 and c_2 represent the two integration constants, and they must be related by the equation $c_1 = -e^{-2c_2}$ for the function $A(r)$ to satisfy all the field equations. Hence, the obtained metric function is $g_{00} = -e^{2A(r)} = -\left(1 + \frac{2e^{2c_2}}{r}\right)$. To determine the last constant c_2, it is sufficient to compare this result with the description of the Newtonian limit in GR, $g_{00} = -(1+2\Phi)$, where the gravitational potential is $\Phi = -\frac{GM}{r}$ [10]. Finally, the Schwarzschild solution can be described by the following line element:

$$ds^2 = -\left(1 - \frac{2GM}{r}\right) dt^2 + \left(1 - \frac{2GM}{r}\right)^{-1} dr^2 + r^2 d\Omega^2. \tag{1.58}$$

Note here that the spacetime becomes flat as the Newtonian mass $M \to 0$. Also, the line element is asymptotically flat as $r \to \infty$.

A problematic aspect when describing the behavior of matter and energy using GR is the existence of curvature singularities. Curvature singularities represent breakdowns in the classical description of spacetime and highlight the limitations of GR, especially in extreme conditions where quantum effects may become significant. To check for curvature singularities, it is sufficient to determine if any curvature scalar quantity diverges. The simplest such scalar is the Ricci scalar, while a quadratic scalar is the Kretschmann scalar $K = R^{\mu\nu\rho\sigma} R_{\mu\nu\rho\sigma}$. The Kretschmann for the Schwarzschild solution (1.58) is given by:

$$K = \frac{48G^2M^2}{r^6}. \tag{1.59}$$

This expression ensures that $r = 0$ is a curvature singularity.

Geodesics in the Schwarzschild metric describes the paths that particles, photons, or test masses follow as they move through the spacetime surrounding a spherically symmetric, non-rotating mass (such as a black hole or a massive object). These trajectories can describe phenomena such as the motion of planets around a massive star, with a specific example of Mercury's motion around the Sun, which is known for verifying its perihelion advance.

Beyond the curvature singularity at $r = 0$ in spherical coordinates, a coordinate singularity exists at $r = 2GM$, where the metric component g_{11} diverges. A coordinate singularity indicates an inadequacy in the chosen coordinates to describe the spacetime geometry accurately at that point. However, employing a different coordinate system can overcome this limitation and provide a well-behaved description of the entire spacetime manifold, excluding the curvature singularity. Martin Kruskal and George Szekeres addressed this issue by introducing Kruskal-Szekeres coordinates $\{T, R, \theta, \varphi\}$ [15], which incorporate a new timelike coordinate, T, and a new spacelike coordinate, R. These coordinates comprehensively represent the maximally extended Schwarzschild solution and ensure smooth behavior throughout the spacetime, except at the curvature singularity. For $r \geq 2GM$, Kruskal-Szekeres coordinates read as:

$$\begin{aligned} T &= \left(\frac{r}{2GM} - 1\right)^{1/2} e^{r/4GM} \sinh \frac{t}{4GM}, \\ R &= \left(\frac{r}{2GM} - 1\right)^{1/2} e^{r/4GM} \cosh \frac{t}{4GM}, \end{aligned} \tag{1.60}$$

while for $r \leq 2GM$ they read as:

$$\begin{aligned} T &= \left(1 - \frac{r}{2GM}\right)^{1/2} e^{r/4GM} \sinh \frac{t}{4GM}, \\ R &= \left(1 - \frac{r}{2GM}\right)^{1/2} e^{r/4GM} \cosh \frac{t}{4GM}. \end{aligned} \tag{1.61}$$

Therefore, the Schwarzschild line element becomes:

$$ds^2 = \frac{32G^3M^3}{r} e^{-r/2GM} \left(-dT^2 + dR^2\right) + r^2 d\Omega^2. \tag{1.62}$$

This line element represents a maximally extended spacetime in the sense that any geodesic can be determined everywhere except at the curvature singularity. A Kruskal diagram in Fig. (1.1) is cited from [16], representing the Schwarzschild geometry in the $T - R$ plane.

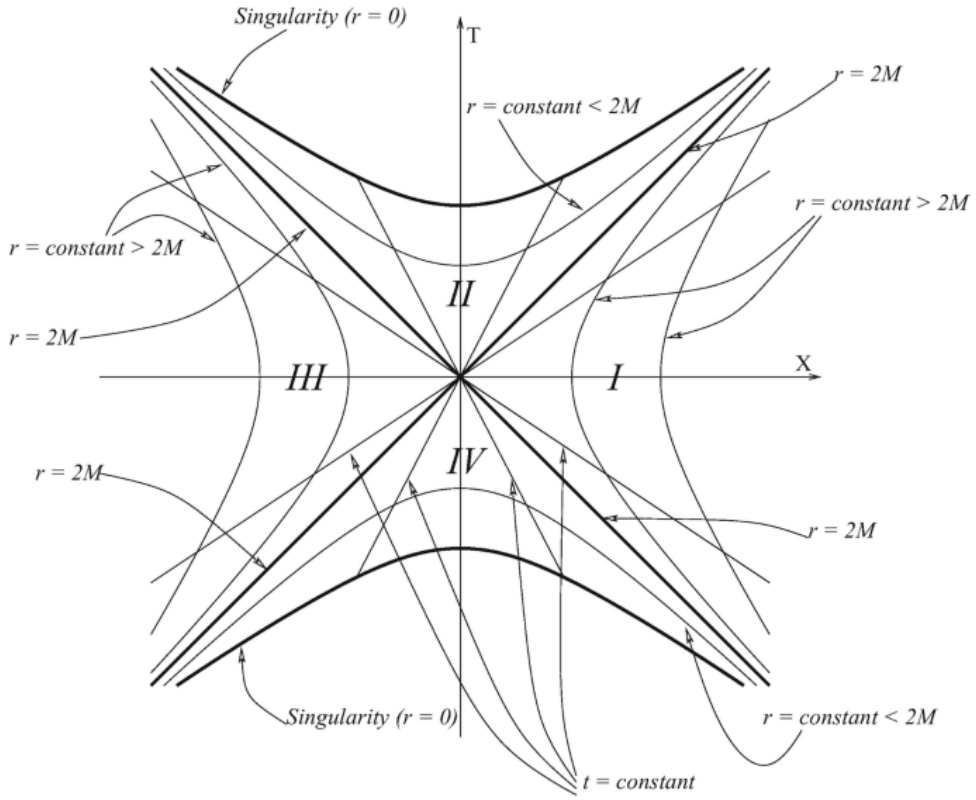

Figure 1.1: The Schwarzschild solution in Kruskal coordinates [**?**].

In Fig. (1.1), the thin lines represent geodesics. Spacelike paths appear as hyperbolas, along which particles travel faster than the speed of light and do not experience time ordering with respect to the event. Timelike paths are depicted as thin, straight lines passing through the origin. Particles following timelike paths move slower than the speed of light and experience time continuously. The two thick lines passing through the origin represent null geodesics, which are trajectories followed by light or other massless particles. The two remaining thick hyperbolas represent curvature singularities.

The Kruskal diagram divides spacetime into four regions, with the Schwarzschild solution depicted in region I. The coordinate singularity at $r = 2GM$ is represented by the thick, straight lines passing through the origin. Consequently, according to the geodesics, once a particle crosses from region I to region II, it can never return. Region II describes a black hole, where the coordinate singularity is defined as the event horizon area where gravity is so strong that nothing, not even light, can escape. Also, particles can traverse from region I to regions III and IV along past-directed null and spacelike geodesics, respectively. Region III represents the time-reverse of the region II, known as a white hole, while region IV is a mirror image of the region I connected by a wormhole.

American physicist George David Birkhoff proved in 1923 that any spherically symmetric vacuum solution of Einstein's field equations—meaning the equations without matter or energy density—must be static and asymptotically flat. In simpler terms, the spacetime geometry of any non-rotating spherically symmetric distribution of mass or energy without matter outside is described by the Schwarzschild metric outside the mass distribution, highlighting the uniqueness of this solution.

The Reissner-Nordström Solution

The Reissner-Nordström solution is an extension of the previous solution of GR that describes the gravitational field outside a charged, non-rotating, spherically symmetric compact object. The solution was independently discovered by Hans Reissner and Gunnar Nordström in 1916 [17], [18]. In the context of the Reissner-Nordström solution, the compact object is charged, leading to both gravitational and electromagnetic fields. Consequently, the action governing the dynamics of this system consists of two terms: the Einstein-Hilbert action, which accounts for the gravitational field via the Ricci curvature, and the electromagnetic action, representing the kinetic energy of the electromagnetic field in the absence of matter. The Einstein-Maxwell action can be expressed as follows:

$$S = \int dx^4 \sqrt{-g} \left(\frac{1}{2\kappa^2} R - \frac{1}{4\mu_0} F_{\mu\nu} F^{\mu\nu} \right), \tag{1.63}$$

and it leads to the Einstein field equations as:

$$R_{\mu\nu} - g_{\mu\nu} R = \frac{\kappa^2}{\mu_0} \left(F_\mu{}^\rho F_{\nu\rho} - \frac{1}{4} g_{\mu\nu} F_{\rho\sigma} F^{\rho\sigma} \right). \tag{1.64}$$

The line element ds^2 of a static and spherically symmetric spacetime is given by the same simplest ansatz as in the Schwarzschild case:

$$ds^2 = -e^{2A(r)} dt^2 + e^{2B(r)} dr^2 + r^2 d\Omega^2. \tag{1.65}$$

Assuming that the object is just electrically charged, the four-potential A^μ admits an ansatz as follows:

$$A^\mu = (\Phi(r), 0, 0, 0), \tag{1.66}$$

which respects the symmetries of staticity and sphericity. Hence, from Eq. (1.64), the independent Einstein field equations read as:

$$-\frac{e^{-2A(r)} \Phi'(r)^2}{4\mu_0} + \frac{B'(r)}{\kappa^2 r} + \frac{e^{2B(r)}}{2\kappa^2 r^2} - \frac{1}{2\kappa^2 r^2} = 0, \tag{1.67}$$

$$\frac{4A'(r)}{\kappa^2 r} + \frac{e^{-2A(r)} \Phi'(r)^2}{\mu_0} - \frac{2e^{2B(r)}}{\kappa^2 r^2} + \frac{2}{\kappa^2 r^2} = 0, \tag{1.68}$$

$$2e^{2A(r)} \left(rA''(r) - rA'(r)B'(r) + rA'(r)^2 + A'(r) - B'(r) \right) - \frac{\kappa^2 r \Phi'(r)^2}{\mu_0} = 0. \tag{1.69}$$

The source-free Maxwell equation follows as:

$$\begin{aligned} \nabla_\mu F^{\mu\nu} &= 0 \Rightarrow \\ rA'(r)V'(r) + rB'(r)V'(r) - rV''(r) - 2\Phi'(r) &= 0. \end{aligned} \tag{1.70}$$

The algebraic combination of (1.67) and (1.68) results in:

$$A'(r) = -B'(r) \Rightarrow A(r) = -B(r) + c, \tag{1.71}$$

where, as in the previous section, the integration constant c is absorbed by the time coordinate rescaling, $t \to e^{-c} t$, and is typically set to zero. Consequently, Maxwell equation (1.70) yields a second-order differential equation of the electric potential $\Phi(r)$, with an analytical solution given by:

$$\Phi(r) = -\frac{c_1}{r} + c_2. \tag{1.72}$$

The integration constants $c_1 = -\frac{Q}{4\pi\epsilon_0}$, and $c_2 = 0$ can be determined by applying Gauss's law. Hence, the electric potential is given by:

$$\Phi(r) = \frac{Q}{4\pi\epsilon_0 r}. \tag{1.73}$$

Substituting Eq. (1.71) and (1.73) into Eq. (1.69), a second-order differential equation for the metric function $A(r)$ emerges:

$$2re^{2A(r)}A''(r) + 4re^{2A(r)}A'(r)^2 + 4e^{2A(r)}A'(r) - \frac{\kappa^2 Q^2}{16\pi^2\mu_0 r^3\epsilon_0^2} = 0. \tag{1.74}$$

Then, the metric tensor component reads as:

$$g_{00} = -e^{2A(r)} = -\left(2c_3 + \frac{2c_4}{r} + \frac{\kappa^2 Q^2}{32\pi^2\mu_0 r^2\epsilon_0^2}\right). \tag{1.75}$$

The last two constants $c_3 = 1/2, c_4 = -GM$ are determined considering the limit to the Schwarzschild metric (1.58), whereas $Q \to 0$ the metric component g_{00} must approach $1 - 2GM/r$. Finally, normalizing the constant $k = \frac{1}{4\pi\epsilon_0} = 1$ and substituting $\mu_0 = \frac{1}{\epsilon_0}$, we end up with the line element of the Reissner-Nordström solution as:

$$ds^2 = -\left(1 - \frac{2GM}{r} + \frac{GQ^2}{r^2}\right)dt^2 + \left(1 - \frac{2GM}{r} + \frac{GQ^2}{r^2}\right)^{-1}dr^2 + r^2 d\Omega^2. \tag{1.76}$$

Note that in this derivation, magnetic monopoles are not included due to the lack of experimental evidence for their existence. However, there are no theoretical arguments supporting their absence. Therefore, a more comprehensive static and spherically symmetric charged solution would involve adding a radial magnetic potential component $B(r)$. This modification can be achieved by replacing Q^2 with $Q^2 + P^2$ in natural units, where P represents the magnetic charge of the solution.

Like the Schwarzschild case, the Reissner-Nordström solution seems to exhibit singularities. Kretschmann scalar determines a curvature singularity at $r = 0$:

$$K = \frac{4\left(12G^2M^2r^2 - 24G^2MQ^2r + 14G^2Q^4\right)}{r^8}. \tag{1.77}$$

The geodesics in the Reissner-Nordstr{om metric exhibit intriguing behaviors due to the curvature of spacetime induced by the presence of mass and electric charge. These geodesics are influenced by both the gravitational attraction stemming from the mass M and the repulsive force arising from the electric charge Q. Specifically, the study of geodesics in the Reissner-Nordström metric is essential for understanding phenomena such as gravitational time dilation and redshift, the behavior of particles falling into the black hole, among others.

The Reissner-Nordström solution also provides a black hole interpretation. As previously mentioned, the event horizon serves as the boundary beyond which events, including light, cannot escape the gravitational pull of the black hole following radial null geodesics. As in the Schwarzschild case, a satisfied condition indicates that horizons will be located at $g^{11} = 0$:

$$\begin{aligned} 1 - \frac{2GM}{r} + \frac{GQ^2}{r^2} = 0 \Rightarrow \\ r_\pm = GM \pm \sqrt{G^2M^2 - GQ^2}. \end{aligned} \tag{1.78}$$

The presence of electric charge modifies the configuration of the event horizons, which depends on the sign of the expression under the square root, $G^2M^2 - GQ^2$.

In cases where $G^2M^2 - GQ^2 < 0$, curvature singularities are absent, and the metric remains entirely regular in the spherical coordinates, except at the point $r = 0$ where a curvature singularity exists. Consequently, in such cases, there are no event horizons; instead, a naked singularity exists. These solutions are generally deemed unphysical due to the cosmic censorship hypothesis [19], which states that nature abhors naked singularities.

In cases where $G^2M^2 - GQ^2 > 0$, the line element exhibits two distinct coordinate singularities at $r_\pm$, which can be remedied through a more suitable choice of coordinates. In the region far away from the black hole to just outside the outer event horizon at large distances $r_+ = GM + \sqrt{G^2M^2 - GQ^2}$, gravitational effects are significant but not overwhelming. Particles and light can still escape the gravitational pull of the black hole with sufficient energy and velocity. Observers in this region can witness the gravitational effects of the black hole, such as gravitational lensing and time dilation, without being pulled into the black hole themselves. However, as particles or light approach this event horizon, their gravitational redshift increases dramatically, making them appear fainter and redder to distant observers. After crossing the outer event horizon, particles or light enter an intermediate region bounded by the outer event horizon r_+ and the inner event horizon $r_- = GM - \sqrt{G^2M^2 - GQ^2}$, where escape is impossible. All massive particles and photons necessarily move towards decreasing r until reaching the region inside the inner event horizon r_-. From there, the object may either proceed towards the curvature singularity at $r = 0$ or move toward increasing r back into the intermediate region.

Lastly, the two horizons coincide in cases where $G^2M^2 - GQ^2 = 0$, resulting in the extremal Reissner-Nordström solution. This solution represents a specific configuration of a charged black hole where the electric charge Q reaches its maximum value while maintaining the black hole's stability. As the black hole approaches the extremal limit, its properties become more exotic. For instance, the area of the event horizon vanishes, and the black hole's characteristics approach those of a naked singularity; therefore, this solution is considered unstable.

The German theoretical physicist Werner Israel, in 1968, stated the uniqueness theorem of the Reissner-Nordström solution [20]. He demonstrated the uniqueness of the Reissner{Nordström solution amongst all asymptotically flat, static electro-vacuum black hole configurations with nondegenerate horizons [21].

The Kerr Solution

Here, we provide a brief overview of the Kerr solution in GR, omitting the derivation process and discussions on maximally extended spacetimes. The Kerr solution was first derived by the New Zealand mathematician Roy Kerr in 1963 [22]. It describes the geometry of empty spacetime around a rotating, uncharged, axially symmetric compact object. Specifically, it rotates about the angular momentum axis, and it is characterized by only two parameters: the mass M and the angular momentum J. The line element that describes the Kerr solution reads in Boyer-Lindquist coordinates $\{t, r, \theta, \varphi\}$ as:

$$ds^2 = \frac{\Sigma}{\Delta}dr^2 - \frac{\Delta}{\Sigma}\left(dt - \alpha \sin^2\theta d\varphi\right)^2 + \Sigma d\theta^2 + \frac{\sin^2\theta}{\Sigma}\left((r^2+\alpha^2)d\varphi - \alpha dt\right)^2, \qquad (1.79)$$

where

$$\alpha = \frac{J}{M},\ \Delta = r^2 - 2GMr + \alpha^2,\ \Sigma = r^2 + \alpha^2 \cos^2\theta. \tag{1.80}$$

The Kerr geometry is asymptotically flat at large distances $r \to \infty$ and reduces to the Schwarzs-child solution when the rotational parameter α vanishes. Two curvature singularities at $r = 0$ and $\theta = \pi/2$ can disappear with a change to a different coordinate system. The event horizon determining the Kerr black hole is located at $g^{11} = \Delta/\Sigma = 0$. Solving $\Delta = 0$ two horizons, one inner and one outer, arise as:

$$r_\pm = GM \pm \sqrt{G^2M^2 - \alpha^2}, \tag{1.81}$$

where the outer horizon represents the physical boundary that nothing can escape. The Kerr metric is essential for understanding the spacetime around rotating black holes and finds numerous astrophysical applications [23]. Kerr black holes, also known as astrophysical black holes, are supported by both theoretical and observational evidence [24] suggesting that black holes in nature possess non-zero angular momentum and thus rotate. A natural extension of the Kerr metric, considering the presence of an electromagnetic field, results in the Kerr-Newman metric [25], which describes the most general spacetime geometry outside a charged, rotating, spherically symmetric mass.

The uniqueness theorems of both the Kerr and Kerr-Newman metrics [26–28] have led to the conjecture known as the No-hair conjecture [29]. This conjecture suggests that black holes are characterized by only three externally observable properties: mass (M), electric charge (Q), and angular momentum (J), with no other physical quantities retained, implying that all other information about the collapsed matter that formed the black hole is lost behind the event horizon.

1.1.6 Black Hole Thermodynamics

Bekenstein [30] and Hawking [31] were among the pioneers who laid the foundation for understanding black holes as thermodynamic objects which can possess thermodynamic parameters such as area A, entropy S, and temperature T. Black hole thermodynamics is the study of black holes using the laws of thermodynamics. The analogy between black holes and thermodynamic systems arises from the observation that black holes have properties that closely resemble thermodynamic quantities. Four laws of black hole mechanics were formulated [32], resembling the thermodynamic laws of a conventional thermodynamic system. This relation is illuminated in the following Table (1.1).

The zeroth law states that the surface gravity κ of a black hole is constant over the

Law	Thermodynamic System	Black Hole Mechanics
Zeroth	T constant throughout body in thermal equilibrium.	κ constant over horizon of a stationary black hole.
First	$dE = TdS + pdV +$ work terms.	$dM = \frac{\kappa}{8\pi G}dA + \Omega_H dJ + \Phi dQ$.
Second	$\delta S \geq 0$.	$\delta A \geq 0$.
Third	Impossible to achieve $T = 0$.	Impossible to achieve $\kappa = 0$.

Table 1.1: Thermodynamic systems and black hole mechanics.

event horizon. Note that surface gravity can be interpreted as the gravitational acceleration needed to keep an object at the event horizon, as measured at infinity. In black hole thermodynamics, the surface gravity is analogous to the temperature of a thermodynamic system in equilibrium. The famous Hawking temperature T_H of a black hole is directly proportional to its surface gravity:

$$T_H = \frac{\kappa}{2\pi}. \tag{1.82}$$

The Hawking temperature is the temperature at which black holes emit radiation due to quantum effects near the event horizon, a phenomenon known as Hawking radiation.

The first law of black hole mechanics relates changes in the mass of the black hole M to changes in the area A, angular momentum J, and electric charge Q, as follows:

$$dM = \frac{\kappa}{8\pi G} dA + \Omega_H dJ + \Phi dQ, \tag{1.83}$$

where Ω_H is the angular velocity and Φ is the electrostatic potential at the event horizon. On the other hand, the first thermodynamic law reads as:

$$dE = TdS + pdV + \text{work terms}, \tag{1.84}$$

where E is the energy, T is the temperature, S is the entropy, p is the pressure, and V is the volume of a thermodynamic system. Therefore, the correspondence of the black hole conserved quantities with the thermodynamic quantities appears to be straightforward:

$$\begin{aligned} E &\longleftrightarrow M, \\ S &\longleftrightarrow \frac{A}{4G}, \\ T &\longleftrightarrow \frac{\kappa}{2\pi}. \end{aligned} \tag{1.85}$$

The terms $\Omega_H dJ$ and ΦdQ represent the thermodynamic work term pdV of the first law.

The second law is described by the area theorem, proposed by Hawking, which states that the total area of the event horizons of black holes can never decrease, analogous to the second law of thermodynamics where the entropy of a closed system never decreases:

$$dA \geq 0, \tag{1.86}$$

The third law states that it is impossible to reduce the surface gravity of a black hole to zero through any physical process. This is similar to the third law of thermodynamics, which states that the entropy of a system approaches a constant minimum as temperature approaches absolute zero.

1.1.7 Testing Einstein's Legacy

GR stood as a self-contained and successful gravitational theory for many decades, explaining experimental and observational results [33].

The Weak Equivalence Principle has been confirmed through experiments demonstrating that all freely falling test particles fall at the same rate, irrespective of their internal composition [34, 35].

Additionally, two predictions concerning the geometry of GR - the Local Lorentz Invariance Principle and the Local Position Invariance Principle - have been confirmed by observations, showing that non-gravitational physical laws are independent of velocity [36, 37] and the spacetime position of the freely falling frame in which they are described [38, 39], respectively.

Moreover, Einstein first predicted the gravitational deflection of light in 1911 using field equations. According to GR, massive objects such as stars and galaxies curve the surrounding spacetime. When light travels through this curved spacetime, its path is bent as if it were following the curved geometry of space. This effect causes the apparent position of a distant object, such as a star, to be shifted when its light passes near a massive object, such as the Sun. This prediction was later confirmed during the solar eclipse of 1919 when astronomers observed stars near the Sun during a total solar eclipse and found that their apparent positions were shifted slightly from their expected positions [40]. Since then, numerous observations of gravitational lensing, where the gravitational fields of foreground objects bend the light from distant objects, have provided further evidence [41], [42].

In Newtonian mechanics, the gravitational force between two objects decreases with distance according to the inverse square law. However, this simple description fails to fully account for the perihelion precession of Mercury, which exhibits a small additional shift beyond what can be explained by the gravitational influence of other planets and known sources of mass in the Solar System. Einstein predicted that the gravitational field of the Sun causes Mercury's orbit to rotate slightly over time, leading to a slow but measurable shift in the position of its perihelion [43]. The predicted rate of precession from GR, approximately 43 arcseconds per century, matched the observed rate, thus providing strong evidence in support of Einstein's revolutionary new theory of gravity [44].

The Lense-Thirring effect is a prediction of GR that describes how the rotation of a massive body can "drag" the surrounding spacetime, affecting the motion of nearby objects and inertial frames. Specifically, the Lense-Thirring effect states that a rotating massive body, such as a planet or a star, will cause the inertial frames of reference around it to undergo a slight precession along the direction of its rotation. This effect arises due to the curvature of spacetime caused by the rotation-induced gravitational field of the massive object. The Lense-Thirring effect has been observed indirectly through experiments such as the Gravity Probe B mission [45], which measured the precession of gyroscopes placed in Earth's orbit. The observed precession of the gyroscopes' spin axes matched the predictions of GR, providing strong evidence for the existence of frame-dragging effects caused by rotating massive bodies.

The gravitational redshift, predicted by GR, describes the phenomenon where light emitted from a massive object, such as a star or a planet, is observed to be redshifted when measured by an observer located at a greater distance from the massive object compared to an observer closer to the object's surface. According to GR, the gravitational field of a massive object causes the curvature of spacetime around it. As a result, light traveling through this curved spacetime experiences a change in frequency, known as gravitational redshift, due to the gravitational potential of the massive object. Specifically, when light travels away from a massive object, it loses energy as it climbs out of the gravitational field. This energy loss corresponds to a decrease in frequency, causing the light to be redshifted when observed by a distant observer. The gravitational redshift effect has been observed and confirmed through various experiments

and astronomical observations [46], [47]. For example, the redshift of light emitted by stars near the center of our galaxy has been measured and found to be consistent with the predictions of GR [48].

According to the theory of GR, mass distributions with time-varying quadrupole moments, such as binary systems of compact objects (e.g., neutron stars or black holes) orbiting each other, will emit gravitational waves as they lose orbital energy. This phenomenon is a prediction of GR, known as the emission of gravitational waves. Gravitational waves are ripples in the curved spacetime caused by the acceleration of massive objects. When two massive objects orbit each other, their motion generates variations in the gravitational fields propagating through spacetime as gravitational waves. The emission of gravitational waves carries energy away from the orbiting system, causing the orbit to decay gradually. As a result, the two objects spiral inward toward each other over time, eventually merging into a single, more massive object. This prediction was made by Einstein in 1916 as a consequence of his theory of GR. However, it wasn't until 2015 that the first direct detection of gravitational waves was made by the Laser Interferometer Gravitational-Wave Observatory (LIGO) [49–52], confirming one of the most elusive predictions of Einstein's theory and opening a new era in astrophysics.

A cornerstone prediction of GR concerns the existence of black holes and their defining features, notably event horizons. According to GR, when a massive object collapses under its gravity, it can reach a point where the gravitational pull becomes so intense that even light cannot escape. This boundary, known as the event horizon, marks the limit beyond which no information or signal can reach an external observer. Inside the event horizon lies a central region of spacetime known as the singularity, where gravitational forces become infinitely strong. The existence of black holes and their event horizons is a profound consequence of GR, illustrating the extreme curvature of spacetime in regions of intense gravity. Observations across the cosmos provide compelling evidence for their ubiquity, including gravitational effects on nearby stars and gas and the detection of gravitational waves emitted during black hole mergers. Notably, the direct imaging of the central black hole in the neighboring galaxy M87 by the Event Horizon Telescope represents a groundbreaking achievement [53–58], shedding light on one of the most enigmatic and awe-inspiring phenomena in the universe. This discovery holds profound implications for our understanding of gravity, spacetime, and the nature of the cosmos.

1.2 Modified Theories of Gravity

1.2.1 Motivations of Modified Theories of Gravity

While GR is a highly successful theory in accurately describing gravity on large scales, it is acknowledged that GR is not a complete theory of gravity. There are both phenomenological and theoretical reasons for considering modifications to GR.

One of the major challenges facing GR is its compatibility with quantum mechanics. As we probe smaller length scales, quantum effects become increasingly significant. Attempts to quantize gravity within the framework of quantum field theory encounter infinities that are difficult to resolve, rendering GR a non-renormalizable theory. The term "renormalizable" refers to a crucial property that ensures consistent calculations without encountering infinite results [59]; however, GR fails to meet this criterion [60].

Various approaches modifying GR, such as string theory [61], emergent gravity [62], asymptotic safety [63] and loop quantum gravity [64], have been developed in attempts to address this fundamental problem.

One of the challenges confronting GR is the existence of spacetime singularities, such as those found at the centers of black holes and the inception of the universe, the Big Bang. For instance, a black hole forms when a massive star exhausts its nuclear fuel and undergoes gravitational collapse. As the star's density increases, reaching a critical point, a trapped surface emerges, separating the dense matter from the surrounding spacetime. The collapse continues inward until it culminates in a singularity [65]. At this point, the density and spacetime curvature become infinitely large. Singularities, or infinities, are regarded as pathologies in a theory, signifying regions where the theory breaks down and loses its predictive power.

Moreover, the problem of late-time acceleration in the universe presents a significant challenge to GR. Observations of distant supernovae in the late 1990s provided compelling evidence that the expansion of the universe is accelerating, contrary to previous expectations [66–68]. This phenomenon was unexpected within the framework of GR, which only accounted for ordinary matter and radiation. To address this discrepancy, physicists have proposed the existence of "dark energy," a mysterious form of energy that pervades space and exerts negative pressure, leading to the acceleration of cosmic expansion. Dark energy represents a departure from conventional physics as GR does not directly predict it. It may manifest as a cosmological constant, originally introduced by Einstein. Still, later discarded [69], or conceived as dynamic fields such as quintessence [70], or modifications of gravity on cosmological scales [71]. The pursuit of understanding late-time acceleration has motivated cosmologists to explore alternative models beyond GR.

1.2.2 A Guide to Modified Theories of Gravity

The limitations of classical GR become apparent when confronted with certain physical situations, such as the arguments mentioned above, necessitating its modification. The breakdown of classical GR in these scenarios suggests that additional terms or modifications beyond the standard Einstein-Hilbert action may be necessary to accurately describe nature at both low and high-energy regimes. British physicist David Lovelock highlighted a significant result in theoretical physics offering a guiding principle for the structure of gravitational theories [72], [73]. In 1971, he proved that *the Einstein field equations are the only second-order local equations of motion for a metric derivable from the Einstein-Hilbert action in four dimensions*. Lovelock's theorem holds under specific assumptions, including both the Weak and Strong Equivalence Principles, Lorentz symmetry, massless gravitons, the absence of extra fields, and second-order equations of motion. Consequently, deviating from these assumptions, which render GR unique, could give rise to various classes of modified theories of gravity (MToG), as illustrated in the mind map in Fig. (1.2).

Numerous modified theories of gravity (MToG) have been proposed in the literature. Theories with extra spatial dimensions suggest that the universe may possess additional compactified dimensions beyond the observable four. Examples of such theories include the Kaluza-Klein theory [74], the Lovelock theory [73], and string theory [75].

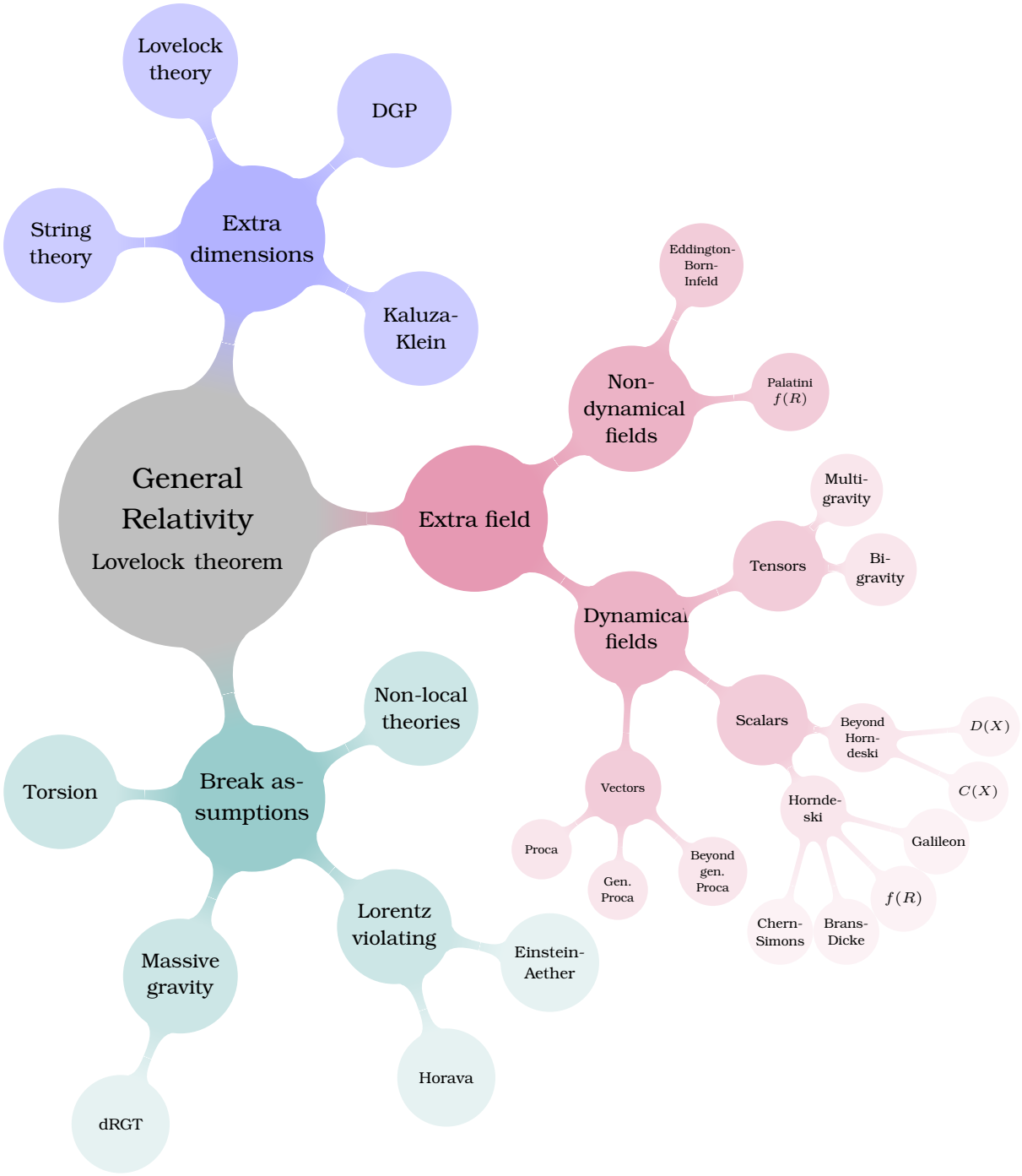

Figure 1.2: Classification of modified gravitational theories. This diagram is inspired from [76], [77]

Additionally, braneworld scenarios propose that our observable universe is a four-dimensional hypersurface (brane) embedded in a higher-dimensional spacetime (bulk). In these scenarios, gravity is confined to the brane, while other forces may propagate in the bulk. One typical example of braneworld models is the DGP model [78], [79]. GR can be modified by breaking Lorentz invariance, leading to theories such as Horava gravity [80] and Einstein-Aether [81]. A preferred time direction emerges in these theories, spontaneously breaking Lorentz symmetry. Additionally, modifications can be introduced by including inverse powers of the Laplacian operator, as $Rf(\Box^{-1}R)$ in [82], [83], or $R\frac{m^2}{\Box^2}R$ in [84], resulting in non-local theories. Giving mass to the

graviton GR is extended to Massive Gravitational Theories [85], [86]. In recent years, we have also seen a lot of interest in Torsion theories [87], where gravity is described by torsion instead of curvature.

Another way to extend GR is by introducing additional fields beyond the metric tensor, namely tensors, vectors, or scalars. Tensor theories emerge by an interaction of two or more metric tensors, resulting in Bigravity [88] and Multi-Gravity [89], respectively. The simplest vector theory is the Proca theory [90] with a kinetic term of an electromagnetic field and a mass term. At the same time, there are the Generalized Proca theory [91] and the Beyond Generalized Proca [92] with second and higher-order equations of motion, respectively.

Among MToG theories, scalar theories have received more attention than others. Although scalar fields are theoretical constructs, they find a natural place in various fundamental theories in physics. In the Standard Model of particle physics, scalar fields are present as the Higgs field. Also, scalar fields are essential in unified field theories, such as Kaluza-Klein and string theories. In Kaluza-Klein's theory, the extra dimensions are often associated with scalar fields, and in string theory, scalar fields arise as the vibrational modes of fundamental strings [93]. Therefore, while scalar fields may be hypothetical in the context of gravity theories, their existence is motivated by their presence in well-established frameworks of particle physics and unified theories. The major subclass of scalar theories is Horndeski [94] theory. It was first introduced by Gregory Horndeski in 1974 as a systematic framework for constructing viable theories of gravity with additional scalar fields. Allowing a scalar field to couple nonminimally to the curvature of spacetime introduces modifications to the gravitational interaction. Horndeski's theory is expressed by the action:

$$\mathcal{S} = \int d^4x \sqrt{-g} \left(\sum_{i=2}^{5} \mathcal{L}_i(g_{\mu\nu}, \phi) + \mathcal{L}_M(g_{\mu\nu}, \psi_i) \right), \tag{1.87}$$

where the Lagrangian densities in the sum are described as follows:

$$\mathcal{L}_2 = G_2(\phi, X), \tag{1.88}$$

$$\mathcal{L}_3 = G_3(\phi, X)\nabla^2\phi, \tag{1.89}$$

$$\mathcal{L}_4 = G_4(\phi, X)R + G_{4,X}\left[(\nabla^2\phi)^2 - (\nabla_\mu\nabla_\nu\phi)^2\right], \tag{1.90}$$

$$\begin{aligned}\mathcal{L}_5 =& G_5(\phi, X)G_{\mu\nu}\nabla^\mu\nabla^\nu\phi - \frac{1}{6}G_{5,X}\left[(\nabla^2\phi)^3 - 3(\nabla^2\phi)(\nabla_\mu\nabla_\nu\phi)^2\right. \\ &\left. +2(\nabla_\nu\nabla^\mu\phi)(\nabla_\alpha\nabla^\nu\phi)(\nabla_\mu\nabla^\alpha\phi)\right],\end{aligned} \tag{1.91}$$

where G_i are functions of ϕ and X, $X = \frac{1}{2}\nabla^\mu\phi\nabla_\mu\phi$ and $G_{i,X} = \partial G_i/\partial X$. Horndeski's theory includes various terms in the Lagrangian that can be chosen to produce specific gravitational effects, such as modifying the behavior of gravity. Hence, it encompasses several specific cases, including GR (with $G_4 = 1, G_2 = G_3 = G_5 = 0$), as well as the Brans-Dicke and $f(R)$ theories (with $G_2 = -\omega X/\phi - V(\phi), G_4 = \phi, G_3 = G_5 = 0$) [95], among numerous other scalar-tensor theories. Theories beyond Horndeski have higher order equations of motion without including additional degrees of freedom [96]. These MToG offer different perspectives on the nature of gravitational interactions and can lead to predictions that differ from GR's. They are actively studied in theoretical physics as potential extensions to GR, and they are subject to experimental and observational tests to assess their validity [97].

1.2.3 Black Holes Beyond General Relativity

No-Scalar-Hair Theorems

Black holes are a fascinating subject in the realm of MToG. They provide a unique testing ground for these alternative theories because they enable the exploration of the strong field regime, where deviations from Einstein's GR might become apparent. The No-Scalar-Hair Theorem in the context of scalar theories of gravity, proposed by physicist Jacob Bekenstein in 1972 [29], is an extension of the uniqueness theorems in black hole physics, mentioned earlier. It suggests that a stationary black hole solution with non-trivial scalar field configurations following gravitational collapse cannot exist in a classical scalar field theory coupled to gravity. According to this theorem, only three conserved quantities- mass, electric charge, and angular momentum- can fully describe a black hole solution. Any additional quantity would resemble "hair" on the black hole, with "hair" referring to any property beyond mass, charge, and angular momentum. Using natural units where $c = G = 1$ simplifies the framework.

Bekenstein considered a rotating, stationary, axisymmetric, asymptotically flat spacetime. He assumed three hypotheses, and evading one of these could lead to fundamentally different properties for black holes [98]. Firstly, he considered a canonical and minimally coupled scalar field ϕ to Einstein's gravity:

$$\mathcal{S} = \frac{1}{4\pi} \int d^4x\sqrt{-g} \left(\frac{R}{4} - \frac{1}{2}\nabla_\mu\phi\nabla^\mu\phi - V(\phi) \right). \tag{1.92}$$

The Klein-Gordon (K-G) equation, governed by the scalar fields, reads as:

$$\nabla_\mu\nabla^\mu\phi - V'(\phi) = 0. \tag{1.93}$$

Secondly, Bekenstein assumed that the scalar field inherits the spacetime symmetries. In a spherical coordinate system, $\{t, r, \theta, \varphi\}$, stationary and axisymmetric spacetime admits two independent Killing vectors. A timelike $k^\mu = \partial_t$, associated with time translations, and a spacelike $\eta^\mu = \partial_\varphi$, associated with rotations with respect to the axis of symmetry. Therefore, the scalar field obeys the following:

$$\partial_t\phi = \partial_\varphi\phi = 0. \tag{1.94}$$

Multiplying the K-G equation by ϕ and integrating over the black hole exterior spacetime results in:

$$\int d^4x\sqrt{-g}\left(\phi\nabla_\mu\nabla^\mu\phi - \phi V'(\phi)\right) = 0 \tag{1.95}$$

Integrating the first term by parts:

$$\int d^4x\sqrt{-g}\left(-\nabla_\mu\phi\nabla^\mu\phi - \phi V'(\phi)\right) + \int_{\mathcal{H}} d^3x\sigma n^\mu\phi\nabla_\mu\phi = 0, \tag{1.96}$$

where $\mathcal{H}$ denotes the boundary at horizon. Note that the boundary term at infinity vanishes since the scalar field has to guarantee the asymptotic flatness of spacetime. Note that the normal vector n^μ at the horizon is a linear combination of the Killing vectors; hence, taking into account the Eq. (1.94), it yields the vanishing of the boundary term at the horizon. Thus,

$$\int d^4x\sqrt{-g}\left(\nabla_\mu\phi\nabla^\mu\phi + \phi V'(\phi)\right) = 0. \tag{1.97}$$

Because of the spacetime symmetries, the gradient of the scalar field is orthogonal to both Killing vectors, implying that it is spacelike or zero, meaning that the first term of the above integral is non-negative $\nabla_\mu\phi\nabla^\mu\phi \geq 0$. Then, the third assumption concerns the behavior of the potential $V(\phi)$, which has to obey the inequality:

$$\phi V'(\phi) \geq 0. \tag{1.98}$$

The last assumption establishes the No-Scalar-Hair theorem. Both terms in (1.97) are non-negative; consequently, the equality holds if $\phi = 0$, leading to trivial black hole solutions.

Additional No-Scalar-Hair theorems have been developed to study black holes within the framework of MToG. Violating one of the assumptions of Bekenstein's No-Scalar-Hair conjecture, one could expect that hairy black hole solutions would be generated. A brief review of No-Scalar-Hair theorems, in subclasses of Horndeski's theory of gravity, follows.

In 1961, Robert H. Dicke and Carl H. Brans violated the first hypothesis, assuming a scalar field nonminimally coupled to the geometry [95]. The Brans-Dicke theory can be described by the action:

$$\mathcal{S} = \frac{1}{16\pi}\int d^4x\sqrt{-g}\left(\phi R - \frac{\omega}{\phi}\nabla_\mu\phi\nabla^\mu\phi - V(\phi)\right), \tag{1.99}$$

where ω is the Brans-Dicke coupling constant, which determines the coupling strength between the scalar field and matter. The nonminimal coupling can be absorbed, performing a conformal transformation of the metric $\tilde{g}_{\mu\nu} = \phi g_{\mu\nu}$ and redefining the scalar field as $d\Phi = \frac{d\phi}{\phi}\sqrt{\frac{2\omega+3}{4}}$ [99]. This yields the Brans-Dicke action in a frame where the scalar field is minimally coupled to the conformally transformed metric:

$$\mathcal{S} = \frac{1}{16\pi}\int d^4x\sqrt{-\tilde{g}}\left(\tilde{R} - \frac{1}{2}\tilde{\nabla}_\mu\Phi\tilde{\nabla}^\mu\Phi - U(\Phi)\right). \tag{1.100}$$

It is straightforward to notice that the field equations from this frame action reduce to those of GR for a trivial scalar field, thus this frame is called the Einstein frame. Hawking established the No-Scalar-Theorem for Scalar-Tensor gravity [100], showing that regular black hole solutions in Brans-Dicke theory are indistinguishable from those of GR, for a vanishing scalar field.

Then Sotiriou and Faraoni generalized the No-Scalar-Hair theorem to $f(R)$ theories of gravity [101], which under an appropriate conformal transformation can be reduced to an equivalent Brans-Dicke theory. More No-Scalar-Hair theorems developed covering scalar-tensor theories with nonminimal coupling [102–104].

Horndeski showed that Galileon theories [105], [106] can be described by the action (1.87). Considering shift symmetry, i.e., invariance under $\Phi \to \Phi + c$, implies the existence of a Noether current J^μ. Due to the conserved currents, the scalar field equation yields $\nabla_\mu J^\mu = 0$. A static and spherically symmetric spacetime is described by the line element:

$$ds^2 = -f(r)dt^2 + \frac{1}{f(r)}dr^2 + r(R)d\Omega^2. \tag{1.101}$$

The scalar field inherits all the spacetime symmetries; hence, it can be written only with radial dependence $\Phi = \Phi(r)$, hence current results in:

$$J^\mu J_\mu = \frac{(J^1)^2}{f(r)}. \tag{1.102}$$

A black hole solution supports an event horizon, where $f(r) = 0$. Therefore, the quantity described in (1.102) is well behaved at horizon only for a vanishing J^1. Integrating the scalar field equation results:

$$\nabla_\mu J^\mu = 0 \Rightarrow r(R)^2 J^1 = c, \tag{1.103}$$

where the areal radius $r(R)$ is finite and the current $J^1 = 0$ at horizon. Consequently, $J^1 = 0$ everywhere, implying that the scalar field is non-dynamical $\Phi = c$ [107].

Bekenstein, considering all these theories and the fact that some physical potentials, such as the Higgs potential, could potentially violate the third hypothesis regarding the behavior of the scalar potential $V(\phi)$ [108], proposed a novel No-Scalar-Hair theorem by analyzing the energy-momentum tensor T^μ_ν instead of the potential [109]. Assuming the validity of the first two hypotheses, he also considered the Weak Energy Condition, where the energy density is non-negative everywhere:

$$\rho \equiv T_{\mu\nu} U^\mu U^\nu \geq 0, \tag{1.104}$$

where at rest frame the timelike component of the velocity U^μ satisfies the normalization condition $g_{\mu\nu} U^\mu U^\nu = -1$. The energy momentum tensor $T_{\mu\nu}$ is given by:

$$T_{\mu\nu} = \nabla_\mu \phi \nabla_\nu \phi - \frac{1}{2} g_{\mu\nu} \partial_\kappa \phi \partial^\kappa \phi - g_{\mu\nu} V(\phi). \tag{1.105}$$

A static and spherically symmetric spacetime bequeaths its symmetries to the scalar field, which depends only on radial coordinate $\phi = \phi(r)$. Therefore, Bekenstein noticed that only the time component of the energy-momentum tensor contributes to the hypothesis (1.104), examining the sign of both T^1_1 and its first derivative $(T^1_1)'$. He computed the energy-momentum tensor using two equivalent methods: first, employing the conservation equation, and second, utilizing the field equations. This led to a contradiction, which can be resolved with a trivial scalar field.

The novel No-Scalar-Hair theorem extended to higher dimensions [110] and was modified concerning different energy conditions [111–113]. Over the years, more No-Scalar-Hair theorems have developed, reevaluating the hypothesis regarding the inherent symmetries of the scalar field [114], [115], which is a natural hypothesis, but not mandatory at all.

Hairy Black Hole Solutions

The most straightforward approach to acquiring black hole solutions, as a dynamical endpoint of gravitational collapse, with scalar hair is evading the No-Scalar-Hair theorem by violating Bekenstein's first and third hypotheses. In the literature, many of MToG admit a solution described by a stationary, spherically symmetric, asymptotically flat black hole with mass M, electric charge Q, angular momentum L, and a scalar charge D, which is not associated with the Gauss Law. These solutions exhibit two types of "hair": primary and secondary. Primary hair refers to the existence of an independent scalar charge $D \neq D(M, Q, L)$, while secondary hair corresponds to a non-independent scalar charge $D = D(M, Q, L)$ from the standard global charges, which are associated with the Gauss Law. Focusing on four dimensions, hairy black hole solutions are generated.

Scalar-tensor theories described by the action (1.92) admit hairy black hole solutions with a negative potential $V(\phi)$. This kind of potential provides an additional

repulsive force, allowing the scalar field to create a hairy configuration at the would-be-horizon. For example, in [116], a hairy black hole solution emerges with a scalar potential:

$$V(\phi) = -\frac{15}{2}\lambda e^{\phi^2/2}W(\phi) + \frac{1}{2D}\left((1+2e^{\phi^2})(\phi^2-3) + \frac{W(\phi)^2-27}{\phi^2-3}\right), \tag{1.106}$$

where

$$W(\phi) \equiv 3\phi + \sqrt{\frac{\pi}{2}}e^{\phi^2/2}(\phi^2-3)\,\mathrm{erf}\,(\frac{\phi}{\sqrt{2}}). \tag{1.107}$$

Assuming the metric ansatz for a stationary and spherically symmetric spacetime in spherical coordinates as:

$$ds^2 = -N(r)\sigma^2(r)dt^2 + \frac{dr^2}{N(r)} + r^2 d\Omega^2, \quad N(r) \equiv 1 - \frac{2m(r)}{r}, \tag{1.108}$$

the solution reads as follows:

$$\begin{aligned} m(r) =& \frac{r^3}{D^2}\left(1 + \frac{D^2}{r^2} + e^{D^2/r^2}\left(\frac{225}{8}\lambda^2 D^4 - 1\right)\right. \\ & \left. -\frac{1}{2}e^{D^2/r^2}\left(\frac{15}{2}\lambda D^2 - \frac{D}{r}e^{-D^2/(2r^2)} + \sqrt{\frac{\pi}{2}}\,\mathrm{erf}\,(\frac{D}{\sqrt{2}r})\right)^2\right), \end{aligned} \tag{1.109}$$

$$\sigma(r) = e^{D^2/(2r^2)}, \tag{1.110}$$

$$\phi(r) = -\frac{D}{r}. \tag{1.111}$$

Note that the constant λ serves as a parameter of the theory, describing the interaction strength between the scalar field and gravity. The black hole solution is characterized by two parameters: the mass M and the scalar charge D of the secondary type. Particularly, the non-independent scalar charge is determined first from the theory by the coupling constant λ and then by the black hole mass that can support "hair."

This example emphasizes the possibility of generating hairy black holes by constructing exotic negative potentials, such as the one described in (1.106). There are several other similar examples, like the one mentioned above, where hairy black holes are constructed with both analytical methods [117–122], and numerical ones [123–126].

Under certain conditions that violate the first assumption of the no-hair conjecture, one can expect the emergence of hairy black hole solutions. One of the earliest examples of a hairy black hole solution in an asymptotically flat spacetime was obtained in [127], where the scalar field ϕ is nonminimally coupled to the Ricci scalar R, through the term $R\phi^2$ in the action principle. In this context, it is also possible to circumvent the no-hair theorem by nonminimally coupling the scalar field to quadratic curvature terms. This has been done recently in a subsector of Horndeski's theory by considering a nonminimal coupling to the Gauss-Bonnet invariant [128]. The action reads as follows:

$$\mathcal{S} = \frac{1}{4\pi}\int d^4x\sqrt{-g}\left(\frac{R}{4} - \frac{1}{2}\nabla_\mu\phi\nabla^\mu\phi + \alpha\phi\mathcal{R}^2_{GB}\right), \tag{1.112}$$

where $\mathcal{R}^2_{GB} = R^2 - 4R_{\mu\nu}R^{\mu\nu} + R_{\mu\nu\rho\sigma}R^{\mu\nu\rho\sigma}$ denotes the Gauss-Bonnet invariant. Hairy black holes can be formed with a minimum size determined by the coupling constant α, resulting in slight deviations from GR.

Hence, various hairy black holes can emerge through different nonminimal couplings between the scalar field and gravity. By substituting the term $\alpha\phi\mathcal{R}^2_{GB}$ by $\alpha e^{\beta\phi}\mathcal{R}^2_{GB}$ in (1.112), the Einstein-Gauss-Bonnet-dilaton (EGBd) model arises, leading to the formation of hairy black holes [129–131]. Stationary, axisymmetric hairy black holes were found in EGBd in both slow-rotation [132] and high-rotation approximations [133]. A Plethora of hairy black hole solutions can be found in [77]. The production of hairy black holes thus continues without end.

Conceptually, in such theories, the scalar field can become trapped in bound states, determined by a negative effective potential, at the would-be event horizon, thereby forming a hairy black hole.

1.3 Scalarization Phenomenon

1.3.1 The Scalarization Mechanism

In scalar-tensor theories of gravity, a different mechanism for the formation of hairy solutions was first proposed by Damour and Esposito-Farèse in 1993, in systems involving neutron stars [134], and later extended to systems involving black holes [135], [136]. This mechanism, known as spontaneous scalarization, describes a natural process by which compact objects are endowed with scalar hair. Under certain conditions that violate the No-hair theorems, these objects can undergo a phase transition where the scalar field becomes dynamically significant, resulting in the object being "dressed" with scalar hair. This mechanism distinguishes scalarization from other models that generate hairy black holes, which is why the term "scalarized black hole" is used for a black hole that has emerged through the scalarization mechanism.

Specifically, consider the first model of a scalar-tensor theory, inspired by [137], with a canonical and nonminimally coupled scalar field to the curvature of gravity as:

$$\mathcal{S} = \frac{1}{4\pi}\int d^4x\sqrt{-g}\left(\frac{R}{4} - \frac{1}{2}\nabla_\mu\phi\nabla^\mu\phi - f(\phi)\mathcal{I}_M(g_{\mu\nu})\right), \tag{1.113}$$

where $\mathcal{I}_M(g_{\mu\nu})$ is the Lagrangian that includes curvature terms, such as Ricci scalar or Gauss-Bonnet scalar. Then, the equation of motion of the scalar can be written as:

$$\Box\phi - f'(\phi)\mathcal{I}_M(g_{\mu\nu}) = 0, \tag{1.114}$$

where the prime denotes differentiation with respect to the scalar field ϕ. Obviously, for a vanishing scalar field and if $f'(\phi)|_{\phi=0} = 0$, the theory admits the Schwarzschild metric (1.58), which is referred to as the vacuum solution of the theory. Hence, the $|_{\phi=0}$ will denote the vacuum geometry. Stability analysis of the vacuum solution can be done by performing small perturbations around the vacuum solution. The metric perturbations $\delta g_{\mu\nu}$ are decoupled from the scalar perturbations $\delta\phi$, leading to the same metric perturbations as those in the pure GR. Hence, one can only focus on scalar perturbations. Small scalar perturbations $\delta\phi$, around the vacuum solution $\phi = 0$, are governed by the following equation:

$$\left(\Box - \mu^2_{\text{eff}}\right)|_{\phi=0}\delta\phi = 0, \tag{1.115}$$

where the effective mass squared is described as $\mu^2_{\text{eff}} = f''(\phi)\mathcal{I}_M(g_{\mu\nu})$. In curved spacetimes, if the effective mass squared becomes negative enough for long enough, the

mass term may become imaginary when squared. This implies that the perturbation oscillates with an exponentially growing or decaying amplitude. A perturbation that grows over time indicates instability, referred to as tachyonic instability. This instability arises when the curvature becomes strong enough to require an additional degree of freedom for description. Tachyonic instability is quenched by a dynamical phase transition, giving rise to scalarized black hole configurations.

The unstable quasinormal modes correspond to the bound states associated with the negative minimum of the effective potential governing the linear perturbations of the scalar field [138]. In the first panel of Fig. (1.3), we see that when the effective mass squared μ_{eff}^2 is positive, the effective potential well admits a stable ground state (the minimum of the potential well) where the trivial scalar field resides. In the second panel of Fig. (1.3), we see that as μ_{eff}^2 decreases below zero, the effective potential changes shape, taking the form of a Mexican hat, which results in the generation of additional ground states. Tachyonic instability then drives the scalar field away from the unstable local maximum of the potential toward a stable minimum [137].

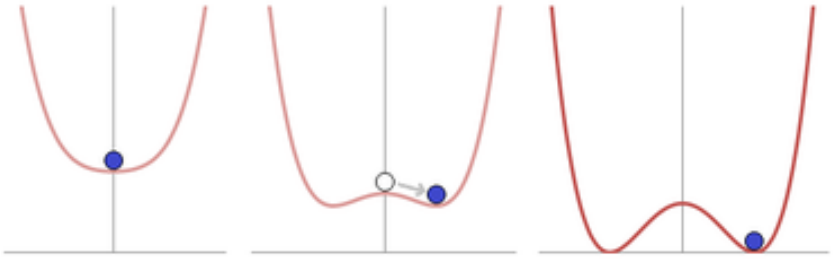

Figure 1.3: Effective potential well.

The tachyonic instability indicates the existence of new scalarized black hole solutions with nontrivial scalar hair, which bifurcate from the trivial solution at critical parameters [138]. A broad spectrum of new non-unique solutions can be found, considering that the number of nontrivial black hole solutions corresponds one-to-one with the number of bound states of the scalar effective potential.

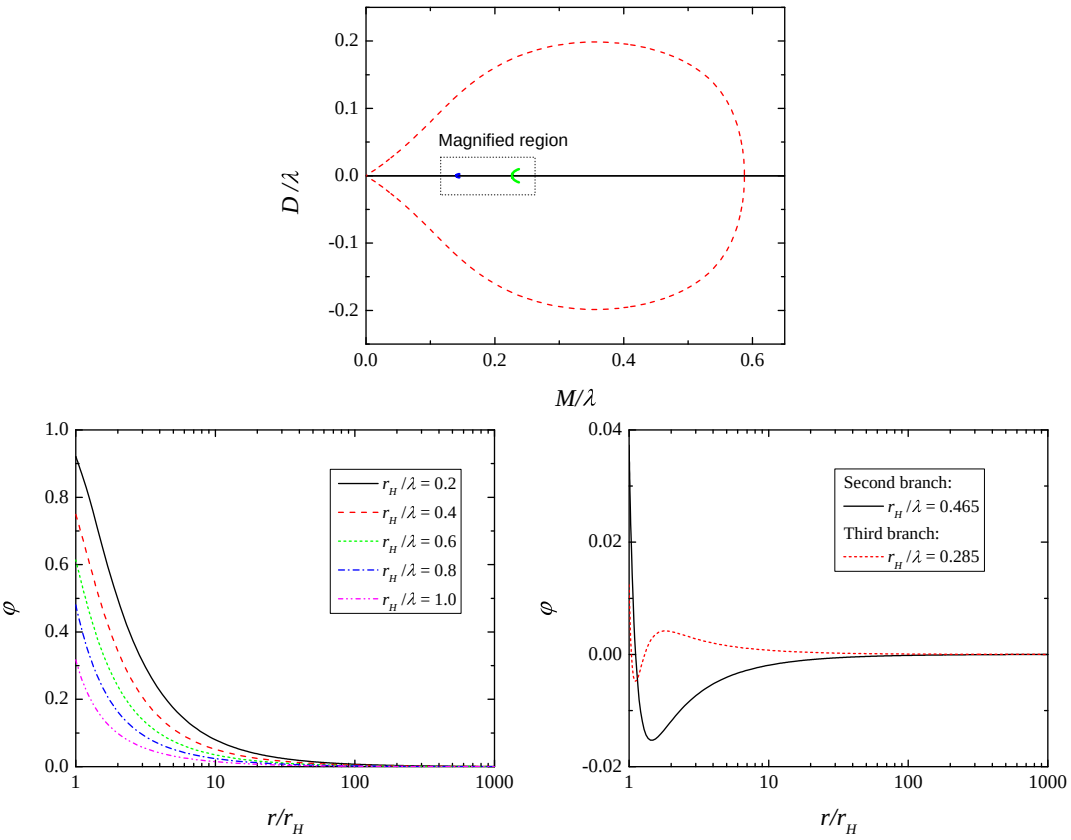

Figure 1.4: Curvature induced scalarization of the Schwarzschild black hole, [135].

In Fig. (1.4), we present the curvature-induced scalarization of the Schwarzschild black hole, [135]. In the first panel of Fig. (1.4), the scalar charge D is shown as a function of the black hole mass M. The Schwarzschild black hole solutions lie along the horizontal axis, where the scalar charge is trivial $(D = 0)$. At a critical mass M, the effective potential becomes sufficiently negative to support one bound state, and a bifurcation point appears. As the interaction between the scalar field and the curvature of gravity becomes stronger, the effective potential deepens, the number of bound states increases, and with each additional bound state in the spectrum, a new bifurcation point appears. In the first panel of Fig. (1.4), we see three bifurcation points corresponding to the first three bound states, which describe the first three unstable modes.

Each bifurcation point defines a branch of scalarized solutions with nontrivial scalar hair ($D \neq 0$). Therefore, the onset of the instability and the generation of scalarized black hole branches are controlled by curvature coupling constants. Each branch of solutions is characterized by a scalar field profile related to the unstable quasinormal modes of the vacuum solution. Since the scalar perturbations are perturbative solutions of the field equations describing static and spherically symmetric trivial black holes near the bifurcation points, we expect that the scalar field of the scalarized black hole solutions originating at the bifurcation point should have the same behavior as the corresponding unstable mode [138].

In the second and third panels of Fig. (1.4), we present three different profiles of the scalar field. The number of zeros in each profile is associated with a specific unstable mode. The monotonic profiles, which asymptotically vanish, correspond to the first scalarized branch of solutions. The asymptotically vanishing profile with one zero

corresponds to the second scalarized branch of solutions, and this pattern continues for subsequent branches.

Stability analysis of the scalarized black hole solutions indicates that only the first branch is stable, corresponding to the fundamental unstable quasinormal mode, [139]. Consequently, the first branch of scalarized solutions is called the fundamental branch.

Scalarized black holes are described as hairy black holes with an additional parameter, the scalar charge D, generated through the scalarization mechanism. These solutions bifurcate from their GR counterparts when tachyonic instabilities emerge beyond a threshold, resulting in significant deviations in the strong-field regime while remaining indistinguishable from GR in the weak-field regime.

1.3.2 Types of Scalarization

The black hole scalarization mechanism has been extensively explored by the scientific community in recent decades, including within the scope of this PhD thesis.

By modifying the action described above (1.113), one can introduce nonminimally coupled scalar fields to matter, such as linear and nonlinear electrodynamics. These additional terms contribute to the effective mass squared, acting as sources for tachyonic instabilities beyond a certain threshold. This threshold is no longer controlled by the nonminimal coupling to gravity but by the nonminimal coupling to electromagnetic gauge fields. Moreover, it has been found that spin can itself induce a scalarization mechanism when a scalar field is suitably coupled with gravity. Another way to extend this mechanism is to consider different fields, such as vectors or tensors, which can undergo a dynamical phase transition from a trivial to a non-trivial configuration, thereby broadening the scope of scalarization phenomena. Consequently, various types of this phenomenon can occur depending on the onset of scalarization, as illustrated in the mind map in Fig. (1.5).

Curvature Induced Scalarization

The prototypical MToG that exhibits black hole scalarization is the EsGB theory, which allows solutions of GR [135], [136]. In this theory, the term $f(\phi)\mathcal{R}^2_{GB}$ in the action contributes to small linear scalar perturbations, leading to the condition of the effective mass squared μ^2_{eff}, such as $f''(\phi)\mathcal{R}^2_{GB}|_{\phi=0} > 0$ for the presence of tachyonic unstable modes. Consequently, the curvature in spacetime can induce scalarization effects, a phenomenon referred to as curvature-induced scalarization. New scalarized black hole solutions emerge as branches bifurcating from the Schwarzschild black hole branch once the black hole mass surpasses a certain threshold. These solutions exhibit notable deviations from GR in the strong-field regime and minor deviations in the weak-field regime.

In the EsGB theory, two choices of the coupling function $f(\phi)$ were under consideration, described respectively by a Gaussian model and a quadratic model as follows:

$$f(\phi) = \frac{\lambda^2}{12}\left(1 - e^{-6\phi^2}\right), \tag{1.116}$$

$$f(\phi) = \frac{\eta}{8}\phi^2, \tag{1.117}$$

where λ, η denote the coupling constants. Both choices converge in the limit of a small scalar field ϕ, thus yielding the same prediction for the scalarization threshold.

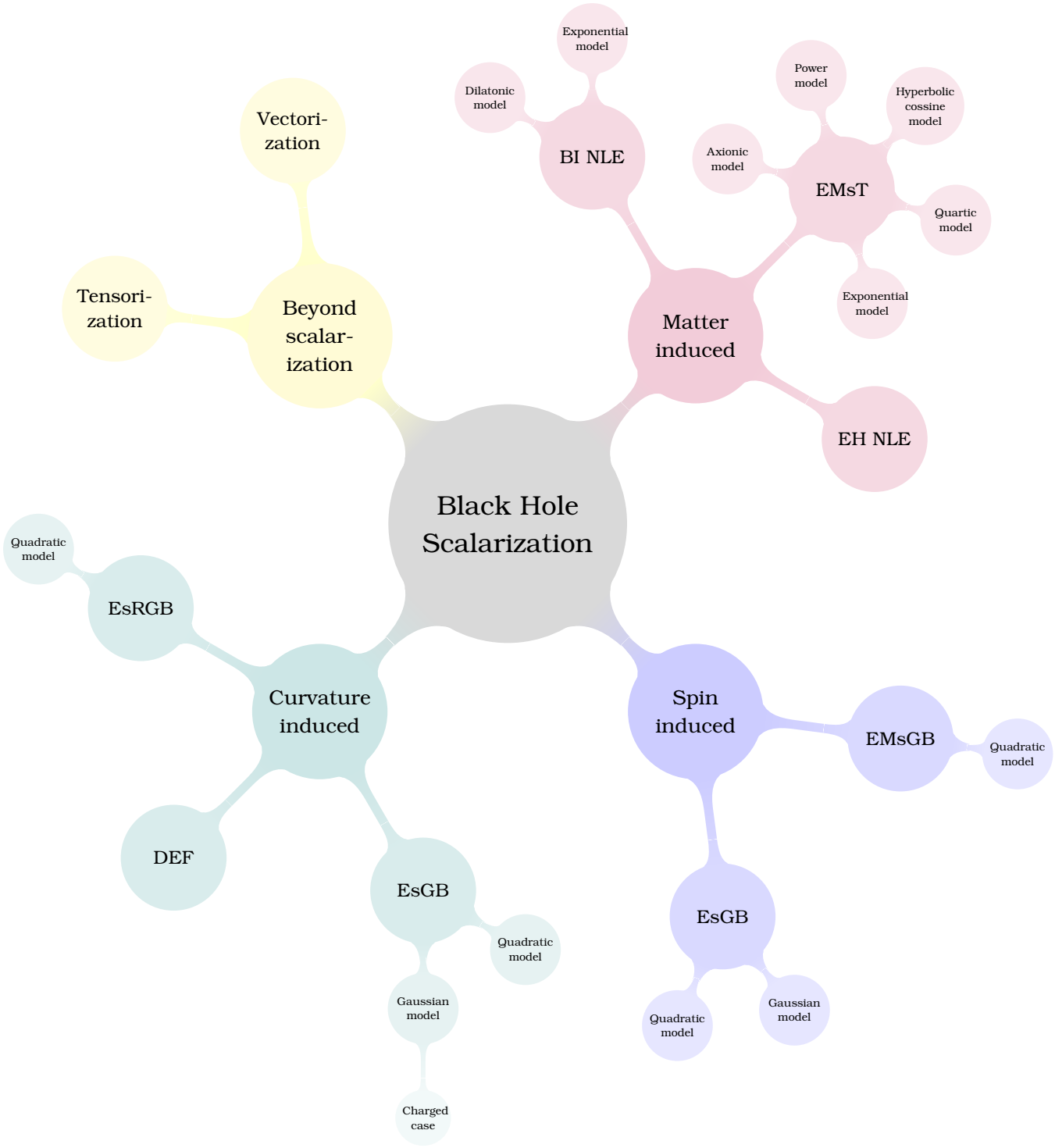

Figure 1.5: Classification of scalarization phenomenon. This diagram is inspired from [137].

However, differences arise in the properties of scalarized black hole solutions. The expansion of the Gaussian model (1.116) involves nonlinear interactions that become significant as the scalar field grows. These higher-order interactions determine the endpoint of each scalarized black hole branch. Consequently, as anticipated theoretically, the domain of existence of scalarized solutions in the Gaussian model (1.116) is larger compared to that of the quadratic model (1.117).

A natural extension of the EsGB theory involves considering the presence of an electromagnetic field and examining the scalarization phenomenon in Reissner-Nordström

black holes. This case is described analytically in Chapter 2, utilizing a Gaussian model [1].

In the context of quantum field theory in curved spacetime, an often used non-minimal coupling between a scalar field and curvature takes the form $\xi\phi^2 R$, [140]. This type of interaction arises from a suitable scalar field redefinition of the initially proposed interaction by Damour and Esposito-Farése in their study of neutron star scalarization, which is commonly referred to as the Damour-Esposito-Far'ese (DEF) model. Herdeiro and Radu explored the scalarization phenomenon of Schwarzschild black holes within the framework of the DEF model, where (quantum-corrected) black holes branch off into an effective field theory triggered by the interaction $\xi\phi^2 R$ [141].

Andreou et al. in [142] extended the study of scalarization by identifying all the terms in the Horndeski action (1.87) that contribute to the linearized equations of motion and exhibit tachyonic instabilities thereby triggering the mechanism. The minimal action reads as follows:

$$\mathcal{S} = \frac{1}{16\pi}\int d^4x\sqrt{-g}\Bigg(R - 2\Lambda + (\gamma_1 + \gamma_2 R)X + \gamma_2 R_{\mu\nu}\nabla^\mu\phi\nabla^\nu\phi \\ - \frac{m_\phi^2\phi^2 - \alpha\phi^2 R - \beta\phi^2\mathcal{R}^2_{GB}}{2} + \mathcal{L}_M\Bigg), \tag{1.118}$$

where $\alpha, \beta, \gamma_1, \gamma_2$ and m_ϕ^2 can be expressed in terms of G_i functions and their derivatives evaluated at the specific vacuum under consideration. This result has attracted the interest within the scientific community in the scalarization phenomenon involving Gauss-Bonnet and Ricci scalar couplings [143], [144], [145].

Matter Induced Scalarization

The effective mass squared μ^2_{eff} doesn't solely arise from terms representing non-minimal couplings between the scalar field and gravity. Still, it may also include couplings between the scalar field and other matter fields. This interpretation is based on the concept that black holes interact with surrounding matter, such as accretion disks or galaxies, potentially leading to scalarization. This phenomenon, known as matter-induced scalarization, describes the dynamical process by which black holes are scalarized due to their interaction with surrounding matter. This scalarization mechanism involves a scalar field coupled to non-linear electrodynamics, which is described by the general action:

$$\mathcal{S} = \frac{1}{16\pi}\int d^4x\sqrt{-g}\left(R - 2\nabla_\mu\phi\nabla^\mu\phi + 4f^4(\phi)\mathcal{I}_M(X,Y)\right), \tag{1.119}$$

where $\mathcal{I}_M(X,Y)$ represents the matter Lagrangian of the electromagnetic field, which interacts with the scalar field ϕ through the coupling function $f(\phi)$ and the quantities X, Y reads as:

$$X = \frac{f^{-4}(\phi)}{4}F_{\mu\nu}F^{\mu\nu}, \;\; Y = \frac{f^{-4}(\phi)}{4}F_{\mu\nu}(\star F)^{\mu\nu}, \tag{1.120}$$

where " $\star$ " stands for the Hodge dual. For a trivial scalar field, this theory admits the Schwarzschild black hole as a solution when $f'(\phi)\_\phi = 0$. Small scalar perturbations in the background exhibit tachyonic instability when the following condition is met:

$$-4f^3(\phi)\left(\mathcal{I}_M(X,Y) - X\partial_X\mathcal{I}_M(X,Y) - Y\partial_Y\mathcal{I}_M(X,Y)\right)\Big|_{\phi=0} < 0. \tag{1.121}$$

In the literature, various choices of the matter Lagrangian within models featuring different coupling functions have pointed to a threshold beyond which new scalarized charged black holes emerge.

The first scalarized charged black hole solutions have been studied with a couple to Born-Infeld nonlinear electrodynamics [146], [147], described by the following Lagrangian:

$$\mathcal{I}_{BI} = 2b\left(1 - \sqrt{1 + \frac{X}{b} - \frac{Y^2}{64b^2}}\right). \tag{1.122}$$

Nonlinear electrodynamics was initially introduced by Born and Infeld with the assumption of an upper limit on the field strength b [148]. The electric-magnetic duality in this theory enables the study of magnetically charged black holes ($Y = 0$), thereby simplifying the analysis. New scalarized branches of solutions bifurcate from a Schwarzschild-like black hole beyond a certain mass threshold. These branches extend in different ways with variations in a coupling parameter β (which is included in the coupling function $f(\phi)$). When $\beta > \beta_{\text{crit}}$, two branches coexist in the domain of existence of the new solutions: the background branch and the scalarized branch, with the latter appearing to be thermodynamically favored. Conversely, when $\beta < \beta_{\text{crit}}$, three branches coexist. The first branch is always trivial, followed by the emergence of the second branch, known as the middle branch, through scalarization. At a particular turning point, the third branch, known as the outer branch, emerges and changes direction. Thermodynamic analysis indicates the stability of the outer branch, which terminates as a configuration with a zero event horizon radius and a finite mass value, leading to a naked singularity.

A variety of scalarization models have been studied in the simplest Einstein-scalar-Maxwell theories, where the matter Lagrangian is described by:

$$\mathcal{I}_{EM} = -\frac{X}{4}. \tag{1.123}$$

Assuming the scalarization conditions such as $f'(\phi)|_{\phi=0} = 0$ and $f''(\phi)F_{\mu\nu}F^{\mu\nu}|_{\phi=0}$, the Reissner -Nordströ black hole beyond a threshold of its charge Q to its mass M ratio $q = Q/M$ is tachyonically unstable. All scalarized black hole solutions bifurcate from the background and can be considered overcharged in the sense that they may carry more electric charge compared to their mass [149–153]. Numerical studies have examined electrically charged black holes, magnetically charged ones, or dyons possessing both types of charges. These studies have revealed that extremal scalarized black holes only form in the presence of a magnetic charge, while in its absence, the scalarized branches terminate as naked singularities [149]. The investigation of various forms of coupling functions results in similar behaviors in the properties of scalarized solutions, with quantitative differences emerging that are primarily controlled by the strength of the coupling constant, which governs the interaction [151].

By adding higher-order derivative gauge field corrections into the Einstein-scalar-Maxwell theory, we anticipate a more accurate classical approximation of quantum electrodynamics theory [154], [155]. This case is analytically described in Chapter 3, where new electrically charged scalarized black hole solutions emerge and exhibit thermodynamic preferability compared to existing literature [3].

Spin Induced Scalarization

A different mechanism of the scalarization phenomenon arises for non-static black holes, where spin itself can induce a tachyonic instability, resulting in spin-induced scalarization. While our research has not extensively delved into spin-induced scalarization, we will briefly overview the topic as part of this thesis.

This type of scalarization involves a scalar field coupled to the Gauss-Bonnet invariant $\mathcal{R}^2_{GB}$, which exhibits non-monotonic behavior in a stationary and axisymmetric background (Kerr solution). Consequently, the effective mass squared μ^2_{eff} of small scalar perturbations indicates two possible instabilities stemming from $\mathcal{R}^2_{GB}$ rather than the nature of the coupling. The first instability is the tachyonic one, while the second arises from superradiance, resulting from the extraction of rotational energy from the black hole by the field due to wave-particle interactions [156]. Extensive studies on small linear perturbations have demonstrated that the dominant instability is the tachyonic one, leading to spin-induced scalarization [157–159]. Analytical and numerical results from both Gaussian and quadratic models indicate that spin-induced scalarized black hole solutions emerge with a minimal necessary spin value and may violate the Kerr bound on black hole spins [160–162].

Moreover, charged spin-induced scalarized black holes, as studied in [163], exhibit resistance to the dynamical phase transition in the presence of a magnetic field, necessitating a larger minimal required spin.

Regarding spin-induced scalarization, extensions have also focused on investigating the effects of a Ricci coupling in EsGB theories within a stationary and axisymmetric spacetime [164].

Beyond Scalarization

In black hole physics, the scalarization phenomenon has been extended beyond scalar fields, as the mechanism is independent of the nature of the field. This concept briefly suggests that other fields, such as vectors or tensors coupled to gravity or matter, may develop nontrivial configurations around a black hole solution of GR through mechanisms termed vectorization and tensorization, respectively. The key difference lies in the types of instabilities: instead of tachyonic instabilities, these theories are susceptible to ghost and gradient instabilities, potentially triggering dynamical phase transitions. For instance, Oliveira et al. [165] investigated spontaneous vectorized charged black hole solutions, wherein a vector field B_μ couples with the electromagnetic field A_μ through an exponential coupling function. The vectorized branches of solutions bifurcate from the Reissner-Nordström black hole branch, triggered by ghost instabilities, reaching a critical undercharged black hole solution rather than an extremal black hole or a naked singularity. This paragraph serves as a quick reference on this topic as we explore black hole scalarization in this thesis.

1.4 Thesis Outline

The main goal of this thesis is to analyze black hole scalarization in scalar-tensor theories of gravity, focusing on the role of the electromagnetic field and the exploration of holographic aspects. The structure of this thesis is organized as follows. Chapter 2 extends the pioneering work on the scalarization of Schwarzschild black

holes by incorporating an electromagnetic field, thereby studying the scalarization of Reissner-Nordström black holes induced by the interaction of a scalar field with the Gauss-Bonnet curvature invariant. Chapter 3 examines the scalarization of Reissner-Nordström black holes driven by the interaction of a scalar field with matter, particularly through the nonminimal coupling of the scalar field with the Maxwell invariant and higher derivative gauge field corrections. Chapter 4 investigates curvature-induced scalarization using a holographic approach. According to the AdS/CFT correspondence, a black hole in gravity is holographically dual to a specific state in the dual theory. Thus, we assume that trivial and scalarized black holes correspond to different states in the conformal field theory, and we explore the resulting phase transition at the boundary. The final Chapter 5 presents the conclusions derived from this research.

Chapter 2

Charged Gauss-Bonnet black holes with curvature induced scalarization in the extended scalar-tensor theories

2.1 Introduction

Black hole scalarization was first studied in Einstein-scalar-Gauss-Bonnet (EsGB) gravitational theories [135]. EsGB gravity is an extension of GR that includes additional scalar fields and higher-order curvature terms. The Gauss-Bonnet (GB) term is a particular combination of curvature invariants, whose curvature tensor is quadratic in its ordinary contractions and arises naturally in higher-dimensional Horndeski theory [94] and string theory [166]. In particular, the Gauss-Bonnet invariant represents the $\mathcal{O}(\alpha')$ R^2 correction to the Einstein action in ten-dimensional heterotic string theory, disregarding matter gauge fields [167]. In four dimensions, it is given by:

$$\mathcal{R}^2_{GB} = R^2 - 4R_{\mu\nu}R^{\mu\nu} + R_{\mu\nu\rho\sigma}R^{\mu\nu\rho\sigma}. \tag{2.1}$$

The GB term is topological in four dimensions, meaning it does not directly contribute to the field equations unless coupled to a scalar field. The action for EsGB gravity includes the standard Einstein-Hilbert term, a canonical kinetic term for the scalar field, and a coupling between the scalar field and the GB term:

$$\mathcal{S} = \frac{1}{16\pi}\int d^4x\sqrt{-g}\left(R - 2\nabla_\mu\phi\nabla^\mu\phi + f(\phi)\mathcal{R}^2_{GB}\right), \tag{2.2}$$

where $f(\phi)$ is a function of the scalar field ϕ that dictates the coupling strength between the scalar field and the GB term.

EsGB gravity allows for new black hole solutions that evade the No-hair theorems, exhibiting distinct properties compared to those in GR. Numerous hairy, spherically symmetric, and asymptotically flat black hole solutions have been found [168–175]. This theory is considered a good approximation in strong gravity regimes where the curvature is large, and the GB term significantly contributes to the system dynamics, making EsGB theory eagerly anticipated to be tested through astrophysical observations.

Within this framework, it was shown that beyond a certain mass threshold, the Schwarzschild black hole solution of GR becomes unstable due to tachyonic instabilities, triggering the scalarization mechanism. New hairy black hole branches bifurcate

from the Schwarzschild solution, characterized by a secondary hair, and the scalar charge D. Each branch comprises a discrete family of solutions labeled by the number of zeros (nodes) of the scalar field. Investigation of the linear stability of radial perturbations revealed that the fundamental branch (with a scalar field with no nodes) is stable for certain choices of the coupling function, while the higher-order branches (with scalar fields having one, two, or more nodes) are always unstable [139].

A natural extension of this theory is to add an electromagnetic field and investigate the scalarization mechanism of the Reissner-Nordström black hole. New scalarized black hole branches are anticipated to bifurcate from their GR counterparts, but only the fundamental one is expected to be stable. Therefore, this chapter focuses solely on presenting the fundamental branch of solutions.

The chapter is organized as follows: Firstly, we describe the specific theoretical framework under investigation and study the linear stability of the Reissner-Nordström black hole solution. Then, we present the newly obtained hairy black hole solutions through the scalarization mechanism and analyze their thermodynamic properties. Finally, the chapter concludes with a summary of our results.

2.2 The Theoretical Framework

We study the scalarization phenomenon in EsGB gravity theories with an electromagnetic field being present [1]. The action reads as:

$$\mathcal{S} = \frac{1}{16\pi}\int d^4x\sqrt{-g}\left[R - 2\nabla_\mu\phi\nabla^\mu\phi + \lambda^2 f(\phi)\mathcal{R}^2_{GB} + F_{\mu\nu}F^{\mu\nu}\right], \tag{2.3}$$

where ϕ denotes a neutral scalar field, $F_{\mu\nu}$ denotes the Faraday tensor, and $\mathcal{R}^2_{GB}$ is the Gauss-Bonnet invariant. The coupling function $f(\phi)$ depends only on the scalar field ϕ, determining how the scalar field is coupled with the spacetime curvature. The coupling constant λ has a dimension of length and shows how strong the coupling of the scalar field to the spacetime curvature is.

Varying the action by all the dynamical fields of our theory, the metric tensor $g^{\mu\nu}$, the scalar field ϕ and the electromagnetic potential A^μ, which is defined through the Faraday tensor as $F^{\mu\nu} = \nabla^\mu A^\nu - \nabla^\nu A^\mu$, leads to the following field equations:

$$\begin{aligned}
&R_{\mu\nu} - \frac{1}{2}Rg_{\mu\nu} + \Gamma_{\mu\nu} = 2\nabla_\mu\phi\nabla_\nu\phi - g_{\mu\nu}\nabla_\alpha\phi\nabla^\alpha\phi + 2\left(F_{\mu\alpha}F_\nu{}^\alpha - \frac{1}{4}g_{\mu\nu}F_{\alpha\beta}F^{\alpha\beta}\right),\\
&\nabla_\alpha\nabla^\alpha\phi = -\frac{\lambda^2}{4}\frac{df(\phi)}{d\phi}\mathcal{R}^2_{GB},\\
&\nabla_\mu F^{\mu\nu} = 0,\\
&\nabla_{[\mu}F_{\alpha\beta]} = 0,
\end{aligned} \tag{2.4}$$

where the $\Gamma_{\mu\nu}$ is defined by:

$$\begin{aligned}
\Gamma_{\mu\nu} =& -R\left(\nabla_\mu\Psi_\nu + \nabla_\nu\Psi_\mu\right) - 4\nabla^\alpha\Psi_\alpha\left(R_{\mu\nu} - \frac{1}{2}Rg_{\mu\nu}\right) + 4R_{\mu\alpha}\nabla^\alpha\Psi_\nu + 4R_{\nu\alpha}\nabla^\alpha\Psi_\mu\\
&- 4g_{\mu\nu}R^{\alpha\beta}\nabla_\alpha\Psi_\beta + 4R^\beta{}_{\mu\alpha\nu}\nabla^\alpha\Psi_\beta,
\end{aligned} \tag{2.5}$$

with

$$\Psi_\mu = \lambda^2\frac{df(\phi)}{d\phi}\nabla_\mu\phi. \tag{2.6}$$

As we are interested in black hole solutions, we assume a static and spherically symmetric spacetime with metric ansatz as follows:

$$ds^2 = -e^{2\Phi(r)}dt^2 + e^{2\Lambda(r)}dr^2 + r^2(d\theta^2 + \sin^2\theta d\varphi^2). \tag{2.7}$$

The scalar field and the electromagnetic potential inherit the spacetime symmetries; thus, they depend only on the radial coordinate. Moreover, we consider a Coulomb-like electric potential without considering any magnetic charges. Hence, the aforementioned fields read as:

$$\phi = \phi(r), \quad A^\mu = \left(\frac{Q}{r}, 0, 0, 0\right), \tag{2.8}$$

where Q is the electric charge. Then, the independent nontrivial field equations reduce to the form:

$$\frac{2}{r}\left(1 + \frac{2}{r}(1 - 3e^{-2\Lambda})\Psi_r\right)\frac{d\Lambda}{dr} + \frac{e^{2\Lambda} - 1}{r^2} - \frac{4}{r^2}(1 - e^{-2\Lambda})\frac{d\Psi_r}{dr} - \left(\frac{d\phi}{dr}\right)^2 - e^{-2\Phi}\frac{Q^2}{r^4} = 0, \tag{2.9}$$

$$\frac{2}{r}\left(1 + \frac{2}{r}(1 - 3e^{-2\Lambda})\Psi_r\right)\frac{d\Phi}{dr} - \frac{e^{2\Lambda} - 1}{r^2} - \left(\frac{d\phi}{dr}\right)^2 + e^{-2\Phi}\frac{Q^2}{r^4} = 0, \tag{2.10}$$

$$\begin{aligned}\frac{d^2\Phi}{dr^2} &+ \left(\frac{d\Phi}{dr} - \frac{d\Lambda}{dr}\right) + \frac{4e^{-2\Lambda}}{r}\left(3\frac{d\Phi}{dr}\frac{d\Lambda}{dr} - \frac{d^2\Phi}{dr^2} - \left(\frac{d\Phi}{dr}\right)^2\right)\Psi_r \\ &- \frac{4e^{-2\Lambda}}{r}\frac{d\Phi}{dr}\frac{d\Phi_r}{dr} + \left(\frac{d\phi}{dr}\right)^2 - e^{-2\Phi}\frac{Q^2}{r^4} = 0,\end{aligned} \tag{2.11}$$

$$\begin{aligned}\frac{d^2\phi}{dr^2} &+ \left(\frac{d\Phi}{dr} - \frac{d\Lambda}{dr} + \frac{2}{r}\right)\frac{d\phi}{dr} \\ &- \frac{2\lambda^2}{r^2}\frac{df(\phi)}{d\phi}\left((1 - e^{-2\Lambda})\left(\frac{d^2\Phi}{dr^2} + \frac{d\Phi}{dr}\left(\frac{d\Phi}{dr} - \frac{d\Lambda}{dr}\right)\right) + 2e^{-2\Lambda}\frac{d\Phi}{dr}\frac{d\Lambda}{dr}\right) = 0,\end{aligned} \tag{2.12}$$

where

$$\Psi_r = \lambda^2\frac{df(\phi)}{d\phi}\frac{d\phi}{dr}. \tag{2.13}$$

2.3 Tachyonic Instabilities

The scalarization phenomenon describes the black hole solution of GR, undergoing a dynamical phase transition triggered by tachyonic instabilities. For a vanishing scalar field $\phi = 0$, the field equations (2.4) reduce to the Einstein field equations in the vacuum with a present electric field if the coupling function satisfies the condition $f'(\phi)|_{\phi=0} = 0$. Then, the theory admits the Reissner-Nordstr$\acute{}$om solution as a background solution:

$$\begin{aligned}ds^2 =& -f(r)dt^2 + \frac{dr^2}{f(r)} + r^2(d\theta^2 + \sin^2\theta d\varphi^2), \\ f(r) =& 1 - \frac{2M}{r} + \frac{Q^2}{r^2}.\end{aligned} \tag{2.14}$$

Instabilities arise under small perturbations of all the dynamical fields. The equation of the scalar perturbation $\delta\phi$ decouples from the equations of metric $\delta g_{\mu\nu}$ and electromagnetic δA_μ perturbations, which coincide with those of Einstein-Maxwell theory. As a result, instabilities are determined through the scalar perturbation equation, which reads as:

$$\left(\Box + \frac{1}{4}\lambda^2 f''(\phi)\mathcal{R}^2_{GB}\right)|_{\phi=0}\delta\phi = 0, \tag{2.15}$$

where $|_{\phi=0}$ denotes the Reissner-Nordstŕom geometry. The presence of a negative effective mass squared indicates tachyonic instabilities. Here, $\mu^2_{eff} = -\frac{1}{4}\lambda^2 f''(\phi)\mathcal{R}^2_{GB}|_{\phi=0}$ resulting to the scalarization condition $f''(\phi)|_{\phi=0} > 0$. The second derivative of the coupling function $f(\phi)$ with respect to the scalar field is a constant quantity, which can always be normalized to unity, rescaling the coupling constant λ. Then, the scalar perturbation equation takes the form:

$$\left(\Box + \frac{1}{4}\lambda^2\mathcal{R}^2_{GB}\right)|_{\phi=0}\delta\phi = 0. \tag{2.16}$$

Since this form indicates tachyonic instability, we examine this equation more, searching for a sufficient condition that provides the threshold of scalarization.

In a static and spherically symmetric spacetime, the scalar perturbation can be decomposed in the standard way $\delta\phi = \frac{u(r)}{r}e^{-i\omega t}Y_{lm}(\theta,\varphi)$, where $Y_{lm}(\theta,\varphi)$ are the spherical harmonic functions. Substituting into (2.16), a Schrödinger-like equation arises as:

$$\frac{d^2u}{dr_*^2} + \left(\omega^2 - U(r)\right)u = 0, \tag{2.17}$$

where $U(r)$ denotes an effective potential as:

$$U(r) = f(r)\left(\frac{2M}{r^3} - \frac{2Q^2}{r^4} + \frac{l(l+1)}{r^2} - 2\lambda^2\left(\frac{5Q^4}{r^8} - \frac{12MQ^2}{r^7} + \frac{6M^2}{r^6}\right)\right). \tag{2.18}$$

Note that, r_* denotes the tortoise coordinate defined as $dr_* = \frac{dr}{f(r)}$, mapping the region outside the outer event horizon $r \in (M + \sqrt{M^2 - Q^2}, +\infty)$ to the hole space $r_* \in (-\infty, +\infty)$. The one-dimensional potential (2.18) supports at least one bound state when it develops a negative well outside the Reissner-Nordström black hole horizon [176]. Mathematically, this condition reads as:

$$\int_{-\infty}^{+\infty} U(r_*)dr_* = \int_{r_H}^{+\infty}\frac{U(r)}{f(r)}dr < 0. \tag{2.19}$$

Assuming only the zero mode for $l = 0$, because of spherical symmetry and normalizing, for convenience, the charge Q and the coupling constant λ to the black hole mass M as:

$$\tilde{Q} = \frac{Q}{M}, \quad \tilde{\lambda} = \frac{\lambda}{M}, \tag{2.20}$$

the condition (2.19) leads to the following inequality:

$$\left(1 + 2\sqrt{1-\tilde{Q}^2}\right)\left(1 + \sqrt{1-\tilde{Q}^2}\right)^3 - \frac{6}{35}\tilde{\lambda}^2\left(\left(2 + 5\sqrt{1-\tilde{Q}^2}\right)^2 - 7\right) < 0. \tag{2.21}$$

Note that the first term is positively defined. Therefore, for the inequality to be satisfied, a new necessary condition arises as follows:

$$\left(2+5\sqrt{1-\tilde{Q}^2}\right)^2-7>0 \Rightarrow \frac{|Q|}{M}<\frac{1}{5}\sqrt{14+4\sqrt{7}}\approx 0.9916, \tag{2.22}$$

which ensures that the electric charge does not dominate the gravitational effects of the black hole, guaranteeing that the background solution is described by the Reissner-Nordström black hole. Consequently, the latter becomes unstable under scalar perturbations if the normalized coupling parameter $\tilde{\lambda}$ exceeds a certain threshold, as described by the following relation:

$$\tilde{\lambda}^2>\frac{35}{6}\frac{\left(1+2\sqrt{1-\tilde{Q}^2}\right)\left(1+\sqrt{1-\tilde{Q}^2}\right)^3}{\left(2+5\sqrt{1-\tilde{Q}^2}\right)^2-7}. \tag{2.23}$$

The qualitative behavior of this relation is presented in Fig. (2.1), showing the lower threshold value of the dimensionless coupling parameter $\tilde{\lambda}$, which is sufficient to ensure tachyonic instability for a particular charge to mass ratio Q/M. We observe that as the ratio Q/M increases, the threshold value of $\tilde{\lambda}$ decreases. This means that the Reissner-Nordström black hole becomes more susceptible to tachyonic instability when it carries a sufficiently large electric charge Q compared to its mass M. The repulsive electromagnetic force becomes comparable to the attractive gravitational force, resulting in scalar perturbations becoming trapped in a potential well outside the event horizon, destabilizing the spacetime. As the Reissner-Nordström black hole approaches its near-extremal limit, the behavior of the coupling parameter $\tilde{\lambda}$ is reversed. The background solution experiences a balance between the two aforementioned forces, making it difficult for tachyonic instabilities to appear.

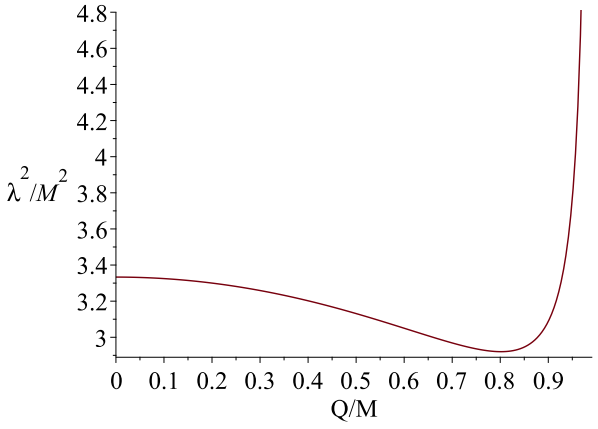

Figure 2.1: Lower threshold of the existence of scalarized solutions in EsGB theory with an electromagnetic field.

2.4 Scalarized Charged Black Hole Solutions

As the onset of the instability is controlled by the coupling parameter λ, defining the interaction between the scalar field and the curvature invariant, we expect

curvature-induced scalarization to occur. The scalarization mechanism implies that the Reissner-Nordström solution may undergo a phase transition to a stable hairy black hole configuration.

To investigate new scalarized charged black hole solutions, we solve the system of the field equations numerically (2.9)-(2.11) with a shooting procedure in the Wolfram Mathematica software. We are interested in asymptotically flat and regular on the black hole horizon r_H solutions. Asymptotic flatness implies that the geometry approaches flat Minkowski spacetime as you move infinitely far away from the gravitational source. Consequently, the boundary conditions at spacetime infinity, $r \to +\infty$, are imposed as follows:

$$\Phi|_{r\to\infty} \to 0, \;\; \Lambda|_{r\to\infty} \to 0, \;\; \phi|_{r\to\infty} \to 0. \tag{2.24}$$

On the other hand, the behavior of the metric functions Φ, Λ in the near-horizon region can be imposed in such a way as to ensure the presence of a horizon while adhering to the following relations:

$$e^{2\Phi}|_{r\to r_H} \to 0, \;\; e^{-2\Lambda}|_{r\to r_H} \to 0. \tag{2.25}$$

The regularity of the scalar field at the black hole horizon also suggests the regularity of its first and second derivatives, leading to the boundary conditions as:

$$\begin{aligned} \phi|_{r\to r_H} &= \phi_H, \\ \left(\frac{d\phi}{dr}\right)_{r\to r_H} &= -\frac{1}{4\Phi_1 r_H^2 f_1(\phi)\left(r_H^6 - 4Q^2 f_1^2(\phi)\right)}\Big[(Q^2+\Phi_1 r_H^3)(r_H^6 - 8Q^2 f_1^2(\phi)) \\ &\quad \pm r_H^2\sqrt{r_H^8(Q^2+\Phi_1 r_H^3)^2 - 8\Phi_1 r_H f_1^2(\phi)(2Q^2+3\Phi_1 r_H^3)(r_H^6 - 4Q^2 f_1^2(\phi))}\Big], \end{aligned} \tag{2.26}$$

where ϕ_H is a non-zero constant value and we use the notations $\Phi_1 = \left(de^{2\Phi}/dr\right)_{r\to r_H}$ and $f_1 = \left(df(\phi)/dr\right)_{r\to r_H}$. We notice that only the plus sign recovers the Reissner-Nordström black hole for a trivial scalar field, hence we reject the condition with the minus sign.

Furthermore, the expression under the square root in equation (2.26) must be positive, considering a regular scalar field. This imposes a constraint that all values of the fields at the horizon must adhere to. This constraint can be expressed as follows:

$$f_1^2(\phi)\left(r_H^6 - 4Q^2 f_1^2(\phi)\right) < \frac{r_H^7\left(Q^2+\Phi_1 r_H^3\right)^2}{8\Phi_1\left(2Q^2+3\Phi_1 r_H^3\right)}. \tag{2.27}$$

We investigate the scalarization phenomenon in three different cases, each governed by a different coupling function $f(\phi)$. These functions adhere to conditions conducive to scalarization, namely $f'(\phi)|_{\phi\to 0} = 0$ and $f''(\phi)_{\phi\to 0} > 0$. The first coupling function corresponds to Case I, and it is given by:

$$f(\phi) = \frac{1}{2\beta}\left(1 - e^{-\beta\phi^2}\right), \tag{2.28}$$

where β is a constant. This coupling function is described as a Gaussian model, inspired by studies on the scalarization phenomenon in Schwarzschild black holes within EsGB gravity theories, [135], and the subsequent demonstration of the stability

of scalarized black holes, as shown in [139]. Two additional study cases are considered to explore the sensitivity of the dynamic process to each particular model. The Case II is described by the following coupling function:

$$f(\phi) = \frac{1}{\beta^2}\left(1 - \frac{1}{\cosh\beta\phi}\right), \tag{2.29}$$

while the Case III is described by:

$$f(\phi) = \frac{\phi^2}{2\left(1+\beta^2\phi^2\right)}. \tag{2.30}$$

To summarize, the system of field equations (2.9)-(2.12) can be simplified to two independent second-order equations for both the functions $\Phi(r)$ and $\phi(r)$, as in [177]. The scale of our theory is the horizon r_H, which is set to $r_H = 1$. We solve by integrating numerically the system for the function $\Phi(r)$ and $\phi(r)$. In contrast, a dependent equation involving the aforementioned two functions defines the function $\Lambda(r)$. Then, we employ a shooting procedure, imposing the boundary conditions at infinity as described in (2.24), while searching for solutions that meet the boundary conditions at the horizon, as outlined in (2.25) and (2.26), and ensuring satisfaction of the constraint (2.27).

The obtained scalarized black hole solutions are characterized by three parameters associated with the conserved mass M, electric charge Q, and the scalar charge D of the black hole. The electric charge Q is defined by the electric potential (2.8). The mass M and the scalar charge D are defined by the asymptotic expansions of the metric and scalar functions at infinity, as follows:

$$\Phi|_{r\to+\infty} \approx -\frac{M}{r} + \mathcal{O}\left(\frac{1}{r^2}\right), \quad \phi|_{r\to+\infty} \approx \frac{D}{r} + \mathcal{O}\left(\frac{1}{r^2}\right) \tag{2.31}$$

As mentioned earlier, scalarized uncharged solutions in the EsGB theory were extensively studied in [135]. Each family of solutions forms a branch characterized by the number of nodes in the scalar field. Specifically, solutions without zeros in the scalar field constitute the fundamental branch, while those with one zero form the second branch, and so on. The fundamental branch bifurcates at a particular mass, with additional scalarized branches bifurcating at progressively smaller masses. Stability analysis under linear perturbations [139] demonstrated that only the fundamental branch is stable, while the others are unstable. Therefore, although we expect similar behavior for scalarized charged solutions, only the fundamental branches of solutions are viable, as the additional ones violate the constraint (2.27).

We present the scalarized charged black hole solutions in Fig. (2.2), showing how the scalar charge D varies with the black hole mass M across different electric charge values Q. Normalizing all the quantities to the parameter λ, the parameter β represents the coupling constant of the theory. For each study case, we investigate two regimes: the strong-field regime, represented by the value $\beta = 6$, and the weak-field regime, represented by the value $\beta = 12$. Note that the choice of the value $\beta = 6$ was motivated by the numerical results, as this value yielded "nice" branches of solutions that extended to the mass limit $M = 0$, which we will analyze later.

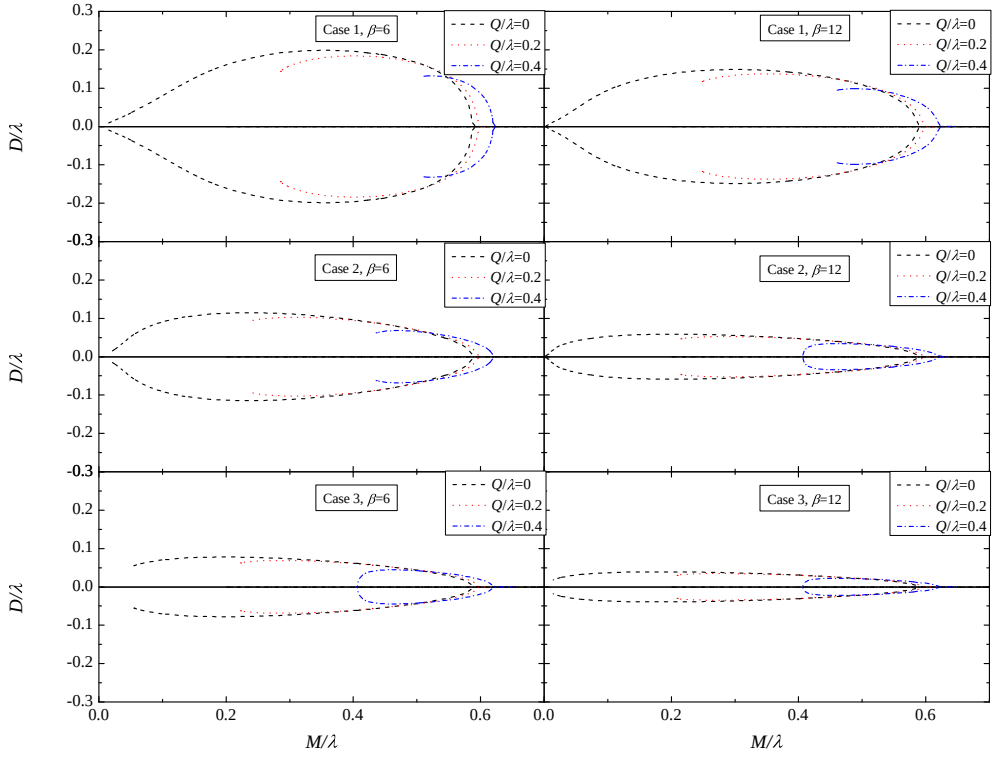

Figure 2.2: The scalar charge D of the black hole as a function of its mass M. Figures for all three cases are shown (Case I, II, and III) for $\beta = 6$ and $\beta = 12$. In each figure three black hole charge $Q/\lambda = 0, Q/\lambda = 0.2$ and $Q/\lambda = 0.4$ are shown.

The horizontal axis represents the GR black hole solution as the background solution for a trivial scalar field, where $D = 0$. It is evident that in all three cases and both regimes, the fundamental branch of solutions bifurcates from the trivial solution at the same specific mass for both uncharged and charged black hole solutions, represented by the black dotted line and the red and blue dotted lines, respectively. This occurs because the bifurcation point depends solely on the constant λ and is independent of the particular coupling function β, as demonstrated in the effective potential (2.18).

As the electric charge increases, the bifurcation point shifts to higher masses. Moreover, the branches of the scalarized black hole solutions become shorter and narrower in both strong and weak gravity regimes, regardless of the choice of the coupling function.

Near the bifurcation points, the new scalarized solutions exhibit slight deviations from their GR counterparts. As the branches extend to lower masses, these deviations become more pronounced. Specifically, the deviations in the strong-field regime ($\beta = 6$) are greater than those observed in the weak-field regime ($\beta = 12$). These deviations are reflected in the scalar charge D. As the parameter β decreases, indicating stronger gravitational interaction, the scalar charge D of the black hole increases. This behavior holds in all three cases, and what differs is only the magnitude of the scalar charge, which is controlled by the value of the coupling constant β. Note that these deviations are consistent with the expected minor departure from GR in the weak-field regime

through the scalarization mechanism.

As observed, the scalarized charged branches of solutions may either terminate at a scalarized charged black hole configuration, where $D \neq 0$, or they converge back to the Reissner-Nordström black hole where $D = 0$. This outcome is determined solely by the constraint (2.27) for the charged branches. In contrast, for the uncharged branches, it is determined either by the constraint (2.27) or by a limiting configuration with $M = 0$.

Before reaching its endpoint, the scalar charge D peaks at an intermediate-mass along the scalarized branch. This peak signifies the greatest deviation from the GR solution, as the scalar charge D decreases with decreasing masses thereafter. This behavior is consistent across all three cases, while the maximal absolute value of the scalar charge increases as gravity becomes stronger.

Furthermore, for a fixed charge Q, the branches of solutions shorten as gravity strengthens, with a decreasing coupling constant β. Consequently, as gravitational interaction strengthens, we anticipate the branches of solutions to progressively shorten. Stability analysis in [139] under the limit of $\beta = 0$ and $Q = 0$ demonstrated that the fundamental branch is exceedingly short and unstable, motivating the choice $\beta = 6$.

2.5 Thermodynamic Properties

We further discuss the thermodynamic properties of the obtained scalarized black hole solutions, including the horizon area, entropy, and temperature. Examining these properties not only offers indications about the stability of the new solutions but also provides a deeper understanding of gravitational theories beyond GR while simultaneously serving as indicators of deviation from GR.

The area of the black hole horizon, $A_H = 4\pi r_H^2$, is illustrated in Fig. (2.3). In the three different cases, solid lines denote the GR solutions, while dotted lines represent the scalarized ones, with parameter choices matching those in Fig.(2.2). We observe that in all cases, both at strong and weak field regimes, the new scalarized charged black hole solutions are smaller than their GR counterparts. The largest deviation from the Reissner-Nordström black holes occurs at a specific intermediate mass, consistent with the findings depicted in Fig. (2.2). This relationship is evident from the observation that as the horizon area increases, the quantity of 'hair' or the deviation from the GR solution decreases. Non-negligible deviations emerge for sufficiently small values of the parameter β.

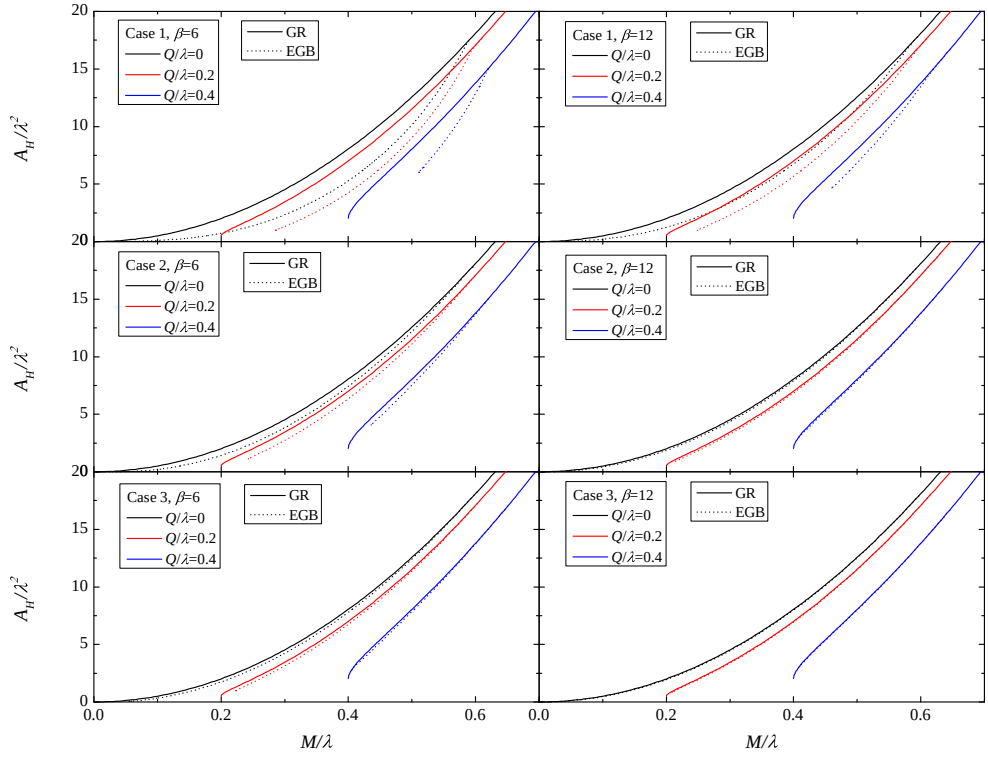

Figure 2.3: The horizon area of the scalarized charged black hole solutions.

The study of entropy can illuminate the thermodynamic behavior of scalarized black holes. In EsGB gravitational theories, entropy is not solely determined by the horizon area; instead, it incorporates contributions from the interaction term of the scalar field with the Gauss-Bonnet invariant. Following the method outlined by Wald and Iyer in [178], [179], the quantity playing the role of black hole entropy is 2π times the integral over the horizon surface H of the Noether charge associated with the horizon Killing field (i.e., the Killing field which vanishes on H), normalized to have unit surface gravity, which leads to the expression:

$$S_H = 2\pi \int_H \frac{\partial \mathcal{L}}{\partial R_{\mu\nu\alpha\beta}} \varepsilon_{\mu\nu}\varepsilon_{\alpha\beta}. \tag{2.32}$$

The Wald entropy results in the analytic formula:

$$S_H = \frac{1}{4}A_H + 4\pi\lambda^2 f(\phi_H), \tag{2.33}$$

and it is illustrated as a function of the black hole mass M in Fig. (2.4). The notations are kept the same. Remarkably, all scalarized charged black hole solutions exhibit greater entropy than their GR counterparts. This suggests thermodynamic stability against thermal fluctuations, making the new solutions thermodynamically favored over the GR solutions. Near the bifurcation point, deviations from GR are slight, but as the solutions extend to lower masses, these deviations become more pronounced

without reaching a maximum or minimum. Only the fundamental branches of the scalarized solutions appear here, as other branches are forbidden due to the constraint (2.27) violation. However, we examined the uncharged case for consistency, where this constraint is invalid, leading to the emergence of additional branches. Similarly to the entropy behavior of scalarized Schwarzschild black hole branches, the fundamental branch exhibits the highest entropy, suggesting potential instability in the other branches.

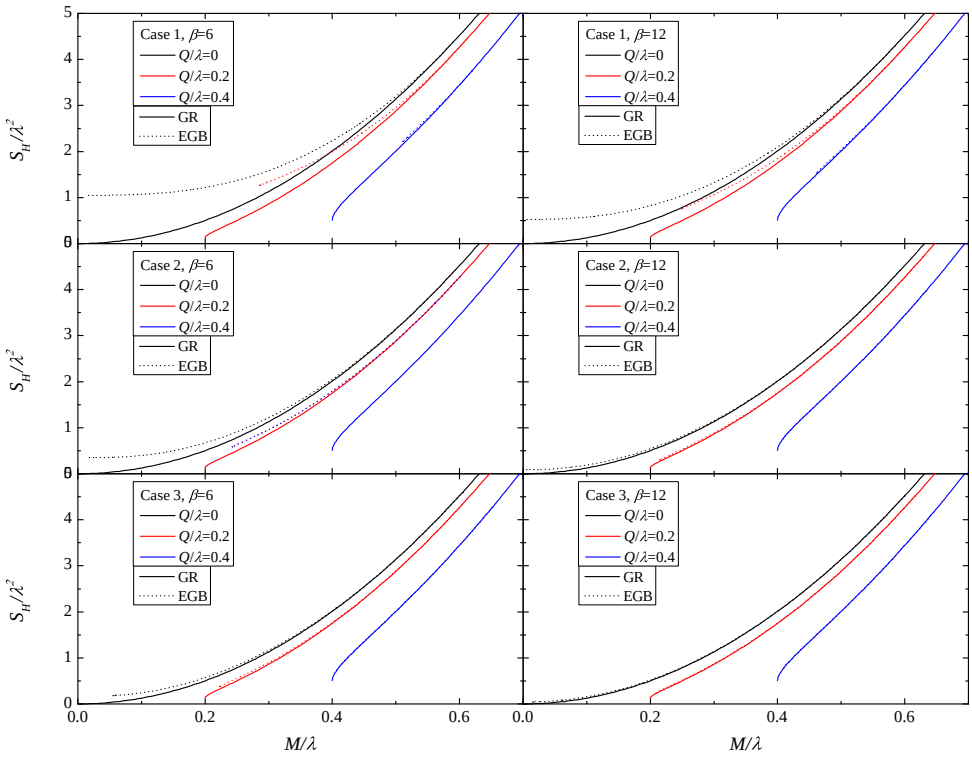

Figure 2.4: The Wald entropy of the scalarized charged black hole solutions.

The temperature of the spherical symmetric scalarized charged black holes is derived from the surface gravity k_H at the event horizon as in [180], [181]:

$$T = \frac{k_H}{2\pi} = \frac{1}{4\pi}\left(\frac{1}{\sqrt{|g_{tt}g_{rr}|}}\left|\frac{dg_{tt}}{dr}\right|\right)_{r_H} . \tag{2.34}$$

The behavior of the temperature of scalarized solutions compared to their GR counterparts is depicted in Fig. (2.5). While Reissner-Nordström black hole branches may reach an extremal configuration with $T = 0$, ceasing to radiate, scalarized black hole branches typically fail to reach this limit. This failure can be attributed to the violation of constraint (2.27) or to the scalar field becoming trivial, causing the hairy configuration to merge with the Reissner-Nordström black hole. Despite conducting a numerical study involving a large number of cases with varying electric charges and coupling parameters, we did not find extremal scalarized solutions.

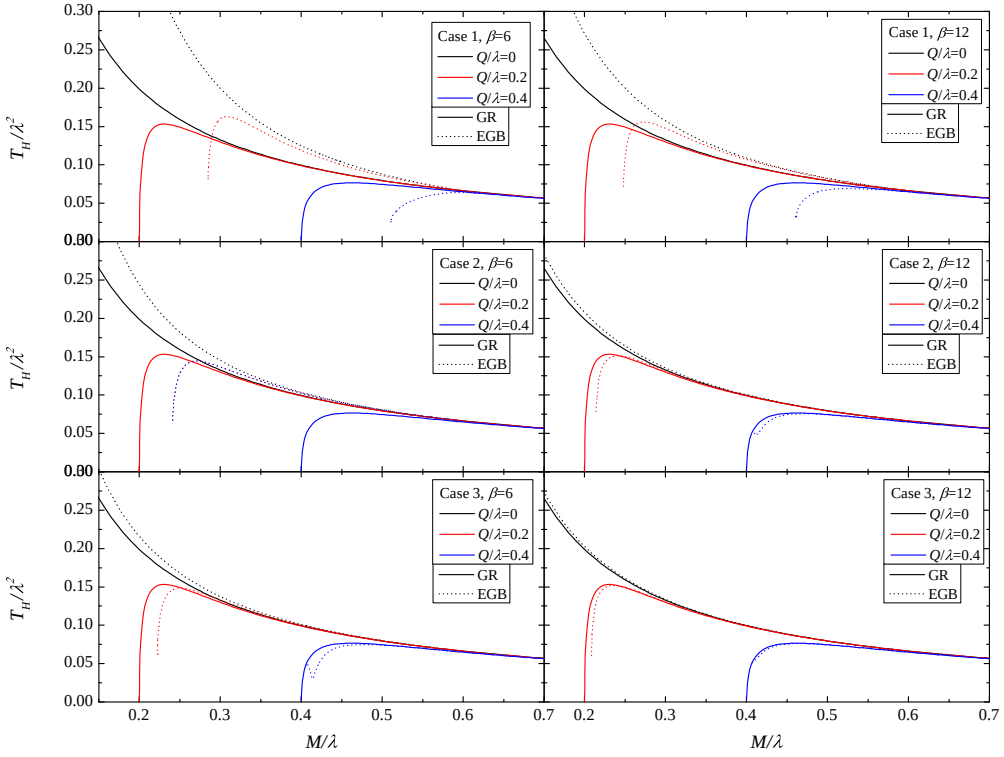

Figure 2.5: The temperature of the scalarized charged black hole solutions.

2.6 Discussion

In this chapter, we extended previous studies within the scientific community on the phenomenon of scalarization in EsGB gravitational theories by adding an electromagnetic field.

The Reissner-Nordström black hole of GR, as a background solution of our theory, experienced tachyonic instabilities under small linear perturbations. These instabilities led to a dynamical phase transition, resulting in the formation of a hairy charged black hole. Numerically, we obtained spherically symmetric and asymptotically flat scalarized black holes characterized by mass M, electric charge Q, and scalar charge D in three different cases, each characterized by a different coupling function. These solutions are also examined in both the strong and weak field regimes, where the coupling parameter β assumes small and large values, respectively.

New scalarized black hole branches bifurcate from the Reissner-Nordström black hole and may or may not merge with it again at smaller masses, reaching a peak at intermediate mass values. The amplitude of the scalar charge D shows deviations from GR. Thus, in all cases, we investigated that, these deviations become significant in strong field regimes, while they become almost imperceptible in weak field regimes.

The study of certain thermodynamic properties has unveiled intriguing features of the new scalarized black hole solutions. Firstly, the horizon area of these scalarized solutions is smaller compared to their GR counterparts. This implies that for the

same mass M, scalarized black holes possess a smaller horizon surface, consistent with the behavior of the scalar charge D. Secondly, the higher black hole entropy exhibited by the new solutions suggests their thermodynamic stability. Finally, the temperature of the scalarized solutions is higher compared to Reissner-Nordström black holes, indicating that they emit more radiation. This behavior suggests that the scalarized branches terminate in non-extremal scalarized black hole solutions, a conclusion supported by a large number of study cases.

The key point to note is that new hairy charged black hole solutions are generated through the scalarization mechanism, triggered by tachyonic instabilities. The presence of a non-trivial scalar field solution introduces a second type of "hair" to the black hole solution, meaning its dependence on both the black hole mass and electric charge.

Chapter 3

Scalarization of the Reissner-Nordström black hole with higher derivative gauge field corrections

3.1 Introduction

So far, we have explored the scalarization mechanism due to tachyonic instability involving a nonminimally coupled scalar field with gravity. The scalar field experiences an effective potential that changes shape beyond the instability threshold, causing it to acquire dynamic behavior. The nonminimal coupling to gravity describes a situation where the gravitational effects are enhanced in the strong gravity regime, necessitating an extra degree of freedom to accurately describe the black hole solution, resulting in curvature-induced scalarization.

An interesting extension of the scalarization mechanism involves introducing a nonminimally coupled scalar field with matter fields. As Chapter 1 mentions, this interaction term describes a situation where the surrounding matter could scalarize a black hole, leading to matter-induced scalarization. The simplest case of this kind of interaction is described by a nonminimally coupled scalar field with the electromagnetic field, in the well-known Einstein-Maxwell-scalar (EMs) theory described by the action:

$$\mathcal{S} = \frac{1}{16\pi}\int d^4x\,\sqrt{-g}\left(\frac{R}{2} - \frac{1}{2}\nabla_\mu\phi\nabla^\mu\phi - f(\phi)F_{\mu\nu}F^{\mu\nu} - V(\phi)\right), \tag{3.1}$$

where $f(\phi)$ is the coupling function, $F_{\mu\nu} = \nabla_\mu A_\mu - \nabla_\nu A_\mu$ is the Maxwell invariant and $V(\phi)$ is a scalar potential. The scalarization of the Reissner-Nordström black hole results in charged, nontrivial black hole solutions that reveal new physics beyond GR.

In models with different forms of the coupling function, the scalarization phenomenon has been studied, resulting in scalarized electrically charged black holes beyond a threshold of a sufficiently large charge-to-mass ratio, $q = Q/M$. EMs theories have provided deeper insights into the spontaneous scalarization of black holes [150]. The results indicate that scalarized black hole branches are thermodynamically favored compared to Reissner-Nordström black holes, with each branch terminating at a critical, singular configuration. Scalarized charged black holes may also be overcharged, meaning they may carry more electric charge relative to their mass. Both electric

and magnetic charges were considered in [149], leading to new scalarized black holes. A notable result was that scalarized dyonic black hole solutions can have a smooth extremal limit, unlike purely electric or magnetic ones.

In this Chapter, we extend the EMs theory with higher-order derivative gauge field corrections, described by the following action:

$$\mathcal{S}=\frac{1}{16\pi}\int d^4x\sqrt{-g}\left(\frac{R}{2}-\frac{1}{2}\nabla_\mu\phi\nabla^\mu\phi-\frac{1}{2}F_{\mu\nu}F^{\mu\nu}-f(\phi)F_{\mu\nu}F^{\mu\nu}+\alpha f(\phi)(F_{\mu\nu}F^{\mu\nu})^2\right), \tag{3.2}$$

where the $(F_{\mu\nu}F^{\mu\nu})^2$ term arises as $\mathcal{O}(\alpha')$ order correction, just like the Gauss-Bonnet invariant in the ten-dimensional heterotic string theory [167]. Note here that the scalar $F_\alpha{}^\sigma F_\beta{}^\alpha F_\gamma{}^\beta F_\sigma{}^\gamma$ arises also as $\mathcal{O}(\alpha')$ order correction. Still, we neglect it since it provides a contribution similar to the $(F_{\mu\nu}F^{\mu\nu})^2$ scalar for pure electric fields [182], [183].

The chapter is organized as follows: Firstly, we describe the specific theoretical framework under investigation and study the linear stability against scalar perturbations of the Reissner-Nordström black hole solution. Then, we present the hairy black hole solutions obtained through the scalarization mechanism and analyze their characteristics and thermodynamic properties. Finally, we discuss their energy conditions, and the chapter concludes with a summary of our results.

3.2 The Theoretical Framework

We study the scalarization phenomenon in nonlinear EMs gravity theories, where a scalar field is nonminimally coupled to higher order derivative gauge field corrections [3]. The action reads as:

$$S=\frac{1}{8\pi}\int d^4x\,\sqrt{-g}\left[\frac{R}{2}-\frac{1}{2}\nabla^\mu\phi\nabla_\mu\phi-\frac{1}{2}\mathcal{P}-f(\phi)\left(\mathcal{P}-\alpha\mathcal{P}^2\right)\right], \tag{3.3}$$

where we use the following notation:

$$\mathcal{P}=F_{\mu\nu}F^{\mu\nu}=-2(\mathbf{E}^2-\mathbf{B}^2), \tag{3.4}$$

and $F_{\mu\nu}=\partial_\mu A_\nu-\partial_\nu A_\mu$ is the Faraday tensor, A_μ is the electromagnetic gauge potential while the quantities **E** and **B** are the electric and magnetic fields, respectively.

Varying the action with respect to the dynamical fields ϕ, A^μ and $g^{\mu\nu}$ we can obtain the following field equations:

$$\nabla_\mu\nabla^\mu\phi-\dot{f}(\phi)\left(\mathcal{P}-\alpha\mathcal{P}^2\right)=0, \tag{3.5}$$

$$\nabla_\mu\left(2F^{\mu\nu}+f(\phi)F^{\mu\nu}-2\alpha f(\phi)\mathcal{P}F^{\mu\nu}\right)=0, \tag{3.6}$$

$$G_{\mu\nu}=\mathcal{T}^{SC}_{\mu\nu}+\mathcal{T}^{EM}_{\mu\nu}+\mathcal{T}^{INT}_{\mu\nu}, \tag{3.7}$$

where $\mathcal{T}^{SC}_{\mu\nu}$, $\mathcal{T}^{EM}_{\mu\nu}$, $\mathcal{T}^{INT}_{\mu\nu}$ are the energy-momentum tensors of the scalar field, the Maxwell invariant and the interaction term, and are given by

$$\begin{aligned}
\mathcal{T}^{SC}_{\mu\nu}&=\nabla_\mu\phi\nabla_\nu\phi-\frac{1}{2}g_{\mu\nu}\nabla_\kappa\phi\nabla^\kappa\phi,\\
\mathcal{T}^{EM}_{\mu\nu}&=2F_\mu{}^\kappa F_{\nu\kappa}-\frac{1}{2}g_{\mu\nu}\mathcal{P},\\
\mathcal{T}^{INT}_{\mu\nu}&=f(\phi)\left(4F_\mu{}^\kappa F_{\nu\kappa}-g_{\mu\nu}\mathcal{P}-8\alpha F_\mu{}^\kappa F_{\nu\kappa}\mathcal{P}+\alpha g_{\mu\nu}\mathcal{P}^2\right).
\end{aligned}$$

3.3 Tachyonic Instabilities

For a trivial scalar field $\phi = 0$, coupled with a function such that its first derivative vanishes, $f(0) = \dot{f}(0) = 0$, the field equations of motion admit the Reissner-Nordström solution as the vacuum solutions of our theory:

$$ds^2 = -N(r)dt^2 + \frac{1}{N(r)}dr^2 + r^2 d\theta^2 + r^2 \sin^2\theta d\varphi^2,\ N(r) \equiv 1 - \frac{2M}{r} + \frac{Q^2}{r^2}\ . \tag{3.8}$$

Performing small perturbations around the vacuum solution $\phi \to 0 + \delta\phi$, the equation of the scalar motion (3.5) becomes:

$$\left(\Box - \mu_{\text{eff}}^2\right)\big|_{\phi=0}\delta\phi = 0\ , \tag{3.9}$$

where the effective mass squared μ_{eff}^2 of the perturbation reads as:

$$\mu_{\text{eff}}^2 = \ddot{f}(\phi)\left(\mathcal{P} - \alpha\mathcal{P}^2\right)\Big|_{\phi=0}\ . \tag{3.10}$$

Tachyonic instabilities arise when the effective mass squared is negative, indicating that the mass term becomes imaginary when squared. As we have discussed, this implies that the perturbation may oscillate and grow over time, indicating the presence of tachyons. Therefore, observing the terms, we find that $\mathcal{P}$ is always negative for pure electric fields (and therefore $\mathcal{P}^2 > 0$), and α is related to the fine structure constant and is positive. Consequently, the necessary but not sufficient condition for tachyonic instabilities, $\ddot{f}(\phi)\big|_{\phi=0} > 0$, is required to scalarize the Reissner-Nordström black hole.

We consider a quadratic model for the coupling function, which is given by:

$$f(\phi) = \beta^2\phi^2, \tag{3.11}$$

where β is a dimensionless coupling constant, which shows the strength of the interaction.

To determine the threshold of instability, there are two possible ways: one is a dynamical (time-dependent) spherically symmetric perturbation, and the other is a static (local) spherically symmetric perturbation, as in [184]. Because of the level of complexity, we choose the second one. Performing a static (real) decomposition of the scalar field with the same symmetries of the RN background, namely $\delta\phi(r,\theta,\varphi) = u(r)Y_{lm}(\theta,\varphi)$, where $Y_{lm}(\theta,\varphi)$ are the spherical harmonic functions of degree l and order m, the Eq. (3.9) is reduced to the equation

$$\left(r^2 N(r)u'(r)\right)' - \left(l(l+1) - \frac{2Q^2\left(2\alpha Q^2 + r^4\right)f''(0)}{r^6}\right)u(r) = 0\ . \tag{3.12}$$

We are interested in the spherically symmetric $l = 0$ solutions, which are regular on and outside the horizon r_H and vanish at infinity. When these unstable modes appear, the RN solution becomes unstable, and new scalarized solutions with nontrivial scalar fields bifurcate from it.

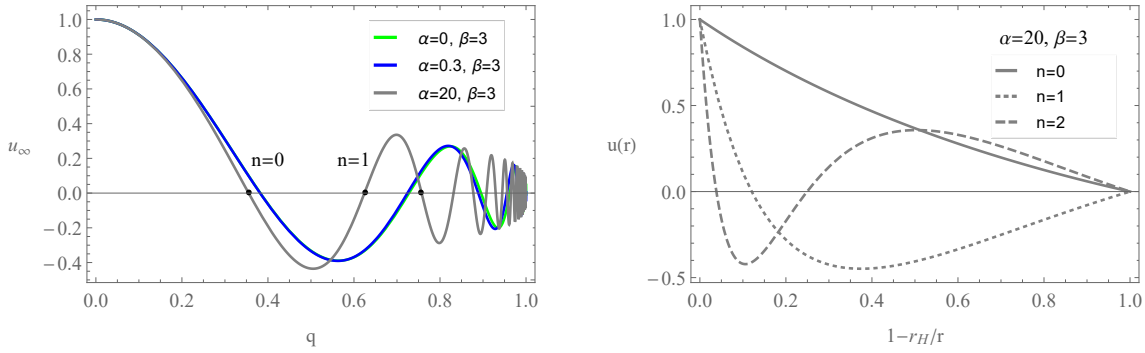

Figure 3.1: (Left) The value u_∞ as a function of the charge to mass ratio q of RN black hole. (Right) The radial profiles of perturbation $u(r)$ with a different number of nodes.

So, to determine the regions of the parameter space where the RN solution is unstable, we solve numerically Eq. (3.12), and we study the value of the perturbation at infinity u_∞, as in [149]. In Fig. (3.1) (left) we plot the u_∞ as a function of the charge to mass ratio $q = \dfrac{Q}{M}$ of the RN black hole for different values of the coupling constants α, β. The zeros of this function give us the unstable modes, which are characterized by a parameter $n = 0, 1, 2, 3, \ldots$, which is associated with the number of nodes of $u(r)$, Fig. (3.1) (right). We explore the fundamental mode (zero mode, $n = 0$), the first and the second mode ($n = 1, n = 2$ respectively) of the perturbations, [184], [138]. We call the existence value q, q_{exist} as the smallest value of q that onsets the instability of the RN solution.

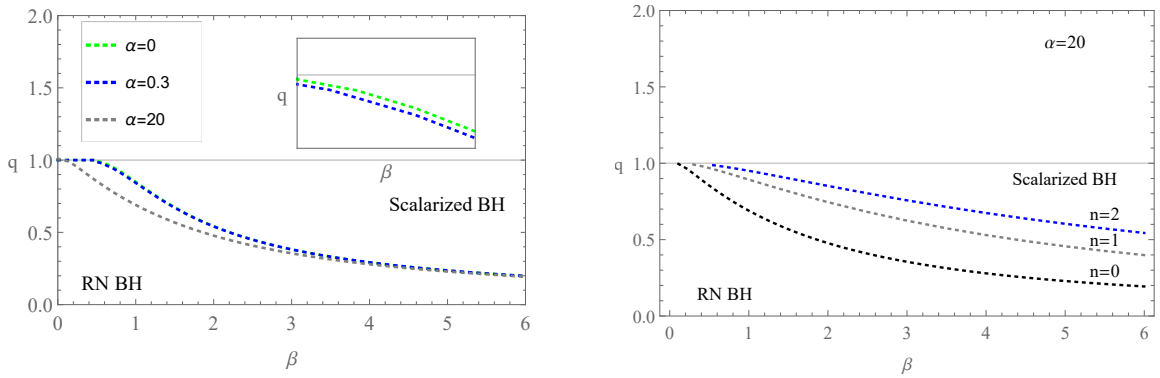

Figure 3.2: Lower threshold of the domain of existence of scalarized BHs, (left) for different values of the parameter α of the fundamental modes and (right) for three different modes with the same parameter $\alpha = 20$

.

In Fig. (3.2), we demonstrate scalarized black hole (SBH) branches of solutions, and we can see the lower threshold value q_{exist} of the domain of existence of scalarized black hole solutions for different values of the constant α. So, the dotted lines separate the region where the RN black hole is stable (under the dotted line), and the RN is unstable, and the scalarized solutions appear and bifurcate from the RN (above the dotted line). As we can notice from Fig. (3.2) (left), sufficiently large values of constant α can increase the domain of existence of scalarized solutions. As it was expected from Fig. (3.2), [138], the fundamental mode ($n = 0$) is described by smaller values of q_{exist}

and therefore the rest of the modes are less interesting.

3.4 Scalarized charged black hole solutions

In this section, we numerically solve the system of field equations. We highlight the primary findings, specifically focusing on the impact of the coupling of the scalar field to higher-order derivative gauge field corrections on the domains of existence and the profiles of radial functions of scalarized black hole solutions.

To investigate scalarized charged black hole solutions, we consider the following static and spherically symmetric ansatz for the metric

$$ds^2 = -e^{-2\delta(r)}N(r)dt^2 + \frac{dr^2}{N(r)} + r^2 d\theta^2 + r^2\sin^2\theta d\varphi^2,\ N(r) \equiv 1 - \frac{2m(r)}{r}\ , \tag{3.13}$$

where $m(r)$ is the Misner-Sharp mass function and the gauge potential A_μ

$$A_\mu = (A(r), 0, 0, 0)\ , \tag{3.14}$$

while the scalar field only depends on the radial coordinate, $\phi = \phi(r)$.
A linear combination of the Eq. (3.5),(3.7), using the integral of the Eq. (3.6) reads

$$A' = -\frac{e^{\delta} r^2\left(1 + 2f(\phi)\right)}{2\cdot 6^{1/3}\mathcal{C}} + \frac{e^{-3\delta}\mathcal{C}}{2\cdot 6^{2/3}\alpha r^2 f(\phi)}\ , \tag{3.15}$$

$$2\delta' + r\phi'^2 = 0\ , \tag{3.16}$$

$$\begin{aligned} &4rA'^2 e^{2\delta} f(\phi)\left(2\alpha A'^2 e^{2\delta} + 1\right) - r\left(N'' + N\left(-2\delta'' + 2\delta'^2 + \phi'^2\right)\right) \\ &\qquad + N'(r)\left(3r\delta' - 2\right) + 2\left(N\delta' + rA'^2 e^{2\delta}\right) = 0\ , \end{aligned} \tag{3.17}$$

$$N\phi'' + \left(N' + \frac{N(2 - r\delta')}{r}\right)\phi' + 2e^{2\delta}\dot{f}(\phi)A'^2(1 + 2\alpha e^{2\delta}A'^2) = 0\ , \tag{3.18}$$

where $\mathcal{C} = \mathcal{C}(r)$ reads as

$$\begin{aligned} \mathcal{C} = \Big(&\sqrt{6}\alpha^{3/2} r^4 e^{6\delta} f(\phi)^{3/2}\sqrt{6\left(9\alpha Q^2 + r^4\right) f(\phi) + 4r^4 f(\phi)^2(2f(\phi) + 3) + r^4} \\ &+ 18\alpha^2 Q r^4 e^{6\delta} f(\phi)^2\Big)^{1/3}\ , \end{aligned} \tag{3.19}$$

where Q is the integration constant, which is interpreted as the electric charge. Note that the primes denote derivatives with respect to the radial coordinate.
To evaluate possible singular behaviors, it's noteworthy that the expressions for the Ricci and Kretschmann scalars, considering the line-element (3.13), are as follows:

$$R = \frac{N'}{r}(3r\delta' - 4) + \frac{2}{r^2}\left(1 + N\left(r^2\delta'' - (1 - r\delta')^2\right)\right) - N''\ , \tag{3.20}$$

$$K = \frac{4}{r^4}(1 - N)^2 + \frac{2}{r^2}\left(N'^2 + (N' - 2N\delta')^2\right) + \left(N'' - 3\delta' N' + 2N(\delta'^2 - \delta'')\right)^2 \tag{3.21}$$

We construct scalarized charged black hole solutions by integrating numerically the ordinary differential equations $(3.15 - 3.18)$ using a shooting method. At the black hole

horizon $r = r_H$, the solutions are asymptotically flat and regular

$$\begin{aligned} m(r) &= \frac{r_H}{2} + m'(r_H)(r - r_H) + \dots \\ \delta(r) &= \delta(r_H) + \delta'(r_H)(r - r_H) + \dots \\ \phi(r) &= \phi(r_H) + \phi'(r_H)(r - r_H) + \dots \\ A(r) &= A(r_H) + A'(r_H)(r - r_H) + \dots \end{aligned} \tag{3.22}$$

where

$$m'(r_H) = \frac{1}{2} e^{2\delta(r_H)} r_H^2 A'(r_H)^2 \left(1 + 2f(\phi(r_H)) \left(1 + 6\alpha e^{2\delta(r_H)} A'(r_H)^2\right)\right) , \tag{3.23}$$

$$\delta'(r_H) = -\frac{2e^{2\delta(r_H)} r_H^3 A'(r_H)^4 \dot{f}(\phi(r_H)) \left(1 + 2\alpha e^{2\delta(r_H)} A'(r_H)^2\right)}{\left(-1 + e^{2\delta(r_H)} r_H^2 A'(r_H)^2 \left(1 + 2f(\phi(r_H))\right) \left(1 + 6\alpha e^{2\delta(r_H)} A'(r_H)^2\right)\right)^2} , \tag{3.24}$$

$$\phi'(r_H) = \frac{2e^{2\delta(r_H)} r_H \dot{f}(\phi(r_H)) A'(r_H)^2 \left(1 + 2\alpha e^{2\delta(r_H)} A'(r_H)^2\right)}{-1 + 2e^{2\delta(r_H)} r_H^2 A'(r_H)^2 \left(1 + f(\phi(r_H))\right) \left(1 + 6\alpha e^{2\delta(r_H)} A'(r_H)^2\right)} , \tag{3.25}$$

$$A'(r_H) = -\frac{e^{\delta(r_H)} r_H^2 \left(1 + 2f(\phi(r_H))\right)}{2 \cdot 6^{1/3} \mathcal{C}(r_H)} + \frac{e^{-3\delta(r_H)} \mathcal{C}(r_H)}{2 \cdot 6^{2/3} \alpha r_H^2 f(\phi(r_H))} . \tag{3.26}$$

The undetermined parameters $\delta(r_H)$, $\phi(r_H)$, and $A(r_H)$ are determined from the approximate behavior of the solutions at large distances via the shooting method.
At spatial infinity, the asymptotic solutions are

$$m(r) = M - \frac{2Q^2 + D^2}{4r} - \frac{MD^2}{4r^2} + \dots \tag{3.27}$$

$$\delta(r) = \frac{D^2}{4r^2} + \frac{2MD^2}{3r^3} + \dots \tag{3.28}$$

$$\phi(r) = \frac{D}{r} + \frac{MD}{r^2} + \dots \tag{3.29}$$

$$A(r) = -\frac{Q}{r} + \dots \tag{3.30}$$

where the parameters M, Q, D denote, respectively, the ADM (Arnowitt, Deser, Misner) mass, the BH electric charge, and the scalar charge at infinity. The Ricci scalar R (3.20) approaches zero as r approaches r_H, whereas the Kretschmann scalar K (3.21) is expressed as follows:

$$\begin{aligned} K = \quad & \frac{12 - 24e^{\delta(r_H)} \left(1 + 2f(\phi(r_H))\right) A'(r_H)^2}{r_H^4} \\ & + \frac{4e^{4\delta(r_H)} \left(5r_H^2 + 4f(\phi(r_H)) \left(-14\alpha + 5r_H^2 + 5r_H^2 f(\phi(r_H))\right)\right) A'(r_H)^4}{r_H^2} \\ & + 352\alpha e^{6\delta(r_H)} f(\phi(r_H)) \left(1 + 2f(\phi(r_H))\right) A'(r_H)^6 \\ & + 1600\alpha^2 e^{8\delta(r_H)} f(\phi(r_H))^2 A'(r_H)^8 + \mathcal{O}(r - r_H) . \end{aligned} \tag{3.31}$$

where the $A'(r_H)$ is given by the Eq. (3.26).

The analysis of the linear stability has shown that the RN black hole has a tachyonic instability in a certain region of the parameter space, where we obtain numerically scalarized solutions bifurcating from it, as we can see in Fig. (3.3). Notice that each dot in the plot denotes a black hole solution. Each solution is found numerically by

solving the system of equations (3.15)-(3.18) with a shooting procedure in the Wolfram Mathematica software. The parameter that determines each solution is $r_H = 1$ and there are three shooting parameters, namely, the value of the scalar field $\phi(r_H)$, the metric function $\delta(r_H)$ and the electric potential $A(r_H)$ at the horizon. The shooting method determines the aforementioned horizon quantities by the asymptotic solutions of ϕ, δ, A at infinity, (3.28)-(3.30). In Fig. (3.3), the thick black line denotes the trivial

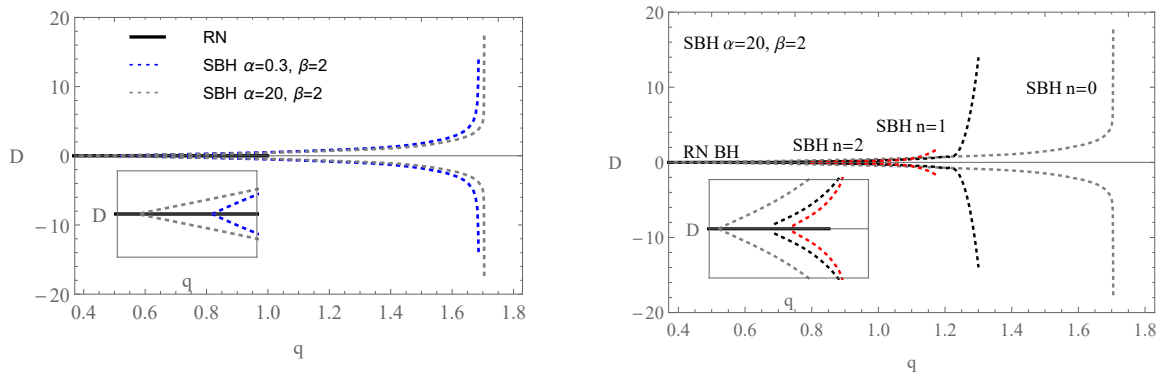

Figure 3.3: The scalar charge D as a function of the charge to mass ratio q, (left) for different values of the parameters α, β of the fundamental modes and (right) for three different modes for the same parameters α, β

.

branch of the Reissner-Nordström solution. Specifically, in Fig. (3.3) (left), the blue and gray dotted lines denote the nontrivial branches of scalarized black hole solutions for fundamental modes, and in Fig. (3.3) (right) we demonstrate the first three nontrivial branches of the fundamental, the first and the second mode, respectively. As we can notice from the domain of existence of scalarized black holes (Fig. (3.2)), the nontrivial branches bifurcate from the trivial branch, and they can reach a charge-to-mass ratio q greater than the unity. So scalarized black hole solutions can be overcharged, as they may have more electric charge than mass, while the black hole scalar charge increases to a critical value when the branch ends. The same happens for all the first three branches of nontrivial scalarized black hole solutions. Note also that the branch of the fundamental mode is bigger and tends to have a greater charge-to-mass ratio than the other branches of the first and second modes. The scalar charge D is, obviously, not independent from the black hole mass M, as the black hole charge Q, even if an explicit function that relates these quantities can not be found analytically. Hence, the hair is of a secondary kind. The endpoint of each branch exhibits a singularity, and numerical calculations indicate a divergence of the Kretschmann scalar at the horizon, as we can notice in Fig. (3.4) (left). So we call the critical value of charge to mass ratio q, q_{crit} as the value from which the Kretschmann scalar diverges. In Fig. (3.4) (right), we show the critical lines that serve as upper bounds for the domain of existence of scalarized BHs. The last one together with the Fig. (3.2) confirms that as the parameters α, β are increasing the domain of existence of scalarized black holes also is increasing. In Table. (3.1), we show the existence and critical values of charge to mass ratio, $q_{\text{exist}}, q_{\text{crit}}$ respectively, for some branches of scalarized solutions.

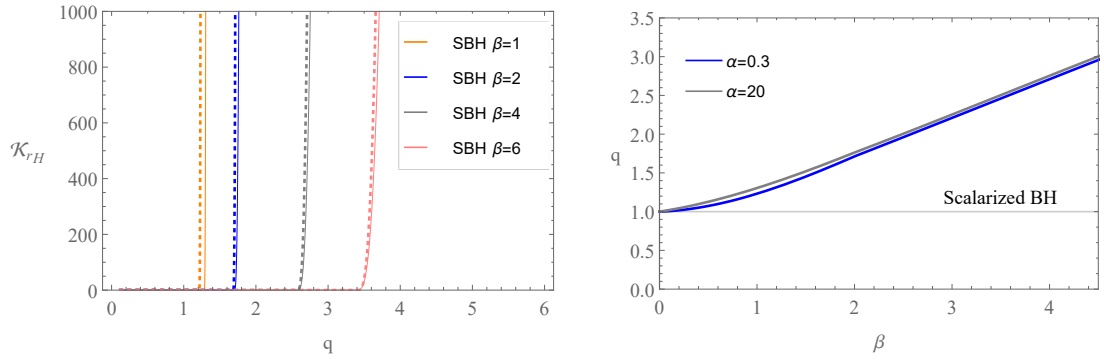

Figure 3.4: (Left) The Kretschmann scalar at the horizon $\mathcal{K}_{r_H}$. The dotted lines describe solutions for $\alpha = 0.3$, and the thin lines describe solutions for $\alpha = 20$. Moving closer to the critical point, $\mathcal{K}_{r_H}$ diverges. (Right) The upper threshold of the domain of existence of scalarized BHs.

α	β	q_{exist}	q_{crit}
0.3	2	0.54079	1.68719
20	2	0.47737	1.70369
0.3	4	0.29235	2.58449
20	4	0.27943	2.58737

Table 3.1: Threshold values of charge to mass ratio, $q_{\text{exist}}, q_{\text{crit}}$, for different branches.

We can notice from the threshold values, $q_{\text{exist}}, q_{\text{crit}}$, that the effect of the coupling constant β is more significant than the effect of the constant α, in the sense that small value changes of β will result in configurations with bigger deviations when compared to RN. In Fig. (3.5) we show such configurations for $\alpha = 0.3$, $q = 0.99$ and $\beta = 1, 2, 4$. As we can see, the scalar field configurations are characterized by the absence of zeros. All the configurations deviate from each one as the coupling constant β increases both qualitatively and quantitatively. The value of the scalar field at the horizon is decreasing while the value at infinity approaches its asymptotic value at a slower rate, as β is increasing. The components of the metric g_{tt}, g_{rr} of scalarized solutions, as well as the electric potential $A(r)$, demonstrate significant deviation from the Reissner-Nordström one, Fig. (3.5) (right), (down). In Fig. (3.6), we depict three scalar field configurations $\phi(r)$ for the first three modes, where we can notice the zeros of each mode. The fundamental mode does not develop any root, while the first and the second modes do develop one and two roots, respectively.

3.5 Thermodynamic Properties and Smarr Relation

Let us now discuss the thermodynamics of the solution obtained. We are dealing with a stationary, asymptotically flat spacetime, which therefore admits an asymptotically timelike vector field $K^\mu = (1, 0, 0, 0)$, which satisfies the Killing equation $\nabla_\mu K_\nu + \nabla_\nu K_\mu = 0$. As a result, we can define the conserved mass of the black hole as [185]

$$\mathcal{M} = -\frac{1}{8\pi} \lim_{r\to\infty} \int_\infty dS_{\alpha\beta} \nabla^\alpha K^\beta \,, \tag{3.32}$$

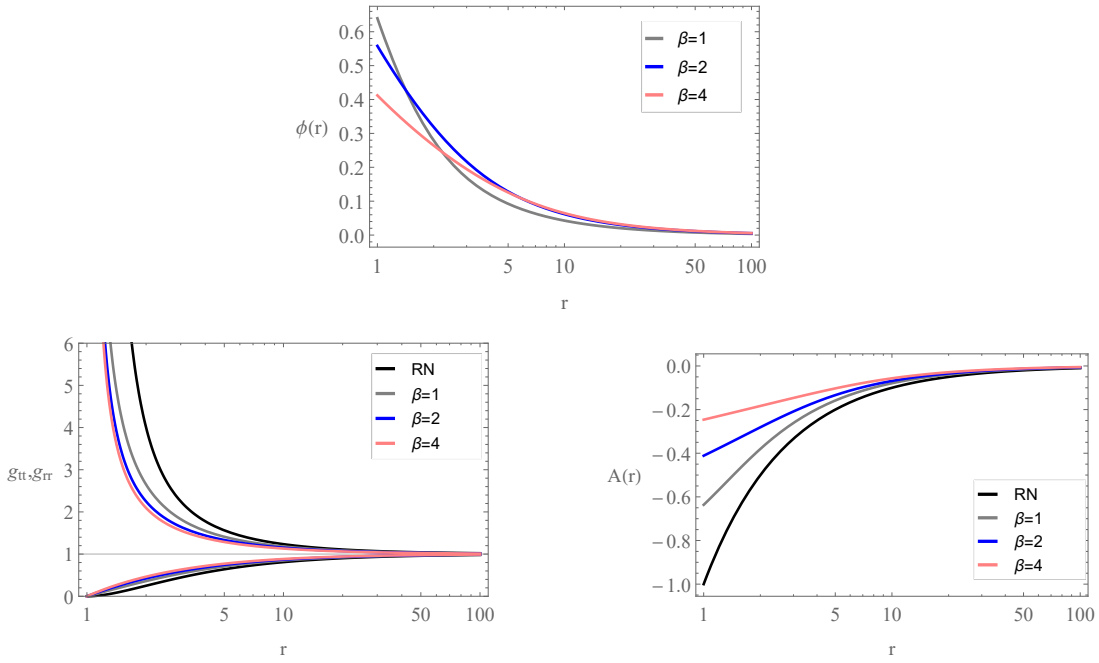

Figure 3.5: The scalar field $\phi(r)$, the metric g_{tt}, g_{rr} and the electric potential $A(r)$ as a function of the radial coordinate r. We set $\alpha = 0.3, q = 0.99$.

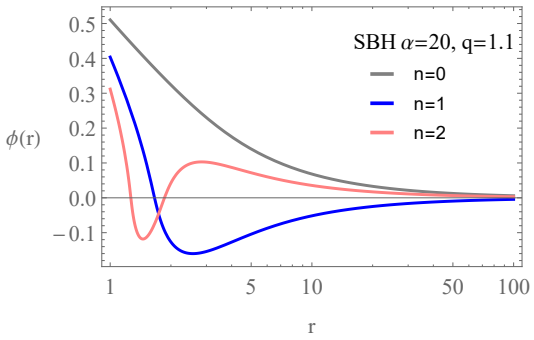

Figure 3.6: The scalar field $\phi(r)$ as a function of the radial coordinate r for the first three modes. We set $\alpha = 20, q = 1.1$.

where $dS_{\alpha\beta} = -2t_{[\alpha}r_{\beta]}\sqrt{\sigma}d\theta d\varphi$ is the surface element with $\sqrt{\sigma}$ being the induced metric on the $t = r =$ const surface: $\sqrt{\sigma} = r^2 \sin\theta$. Here t_μ is a time-like covariant vector field, normalized to unity $t_\mu = (-\sqrt{e^{-2\delta}N}, 0, 0, 0)$ and r_μ is a space-like covariant vector field normalized to satisfy $r_\mu = (0, N(r)^{-1/2}, 0, 0)$. Expanding the term $dS_{\alpha\beta}\nabla^\alpha K^\beta$ we have

$$\begin{aligned} dS_{\alpha\beta}\nabla^\alpha K^\beta = -2t_{[\alpha}r_{\beta]}\nabla^\alpha K^\beta\sqrt{\sigma}d\theta d\varphi =& (-t_\alpha r_\beta \nabla^\alpha K^\beta + t_\beta r_\alpha \nabla^\alpha K^\beta)\sqrt{\sigma}d\theta d\varphi \\ =& -2t_\alpha r_\beta \nabla^\alpha K^\beta \sqrt{\sigma}d\theta d\varphi \ . \end{aligned} \tag{3.33}$$

Evaluating the above relation for our line element, we have that

$$2t_\alpha r_\beta \nabla^\alpha K^\beta = -2t_t r_r \Gamma^r_{tt} K^t \sim -2Mr^2 \ , \tag{3.34}$$

where we have used the asymptotic form of the solution given in equations (3.28)- (3.30) and kept only the highest order term since the integral is evaluated at a $2-$sphere at

infinity. Finally evaluating the integral (3.32) we obtain

$$\mathcal{M} = -\frac{1}{8\pi}(-8\pi M) = M \ , \tag{3.35}$$

which ensures that indeed M is the ADM mass as measured by a far-away observer.

Now, since the Killing equation is antisymmetric, it satisfies the following identity:

$$\oint_{\partial\Sigma} \nabla^\alpha K^\beta dS_{\alpha\beta} = 2\int_\Sigma \nabla_\beta \nabla^\alpha K^\beta d\Sigma_\alpha \ , \tag{3.36}$$

which might be re-written as

$$\oint_{\partial\Sigma} \nabla^\alpha K^\beta dS_{\alpha\beta} = 2\int_\Sigma R^\alpha{}_\beta K^\beta d\Sigma_\alpha \ , \tag{3.37}$$

if one uses the antisymmetric nature of the Killing equation and the equation $\Box K^a = -R^a{}_b K^b$. The left-hand side of (3.36) contains two contributions from the cross-section defined by $t = r = \text{const}$, one at the event horizon of the black hole and another one at infinity. As a result, we can break this term into two pieces

$$\oint_{\partial\Sigma} \nabla^\alpha K^\beta dS_{\alpha\beta} = \oint_H \nabla^\alpha K^\beta dS_{\alpha\beta} + \oint_\infty \nabla^\alpha K^\beta dS_{\alpha\beta} \ , \tag{3.38}$$

and we have already calculated the term at infinity, which will give $-8\pi M$. Evaluating the integral at the horizon, we have

$$\oint_H \nabla^\alpha K^\beta dS_{\alpha\beta} = 4\pi r^2 e^{-\delta} N'\Big|_{r_H} \ . \tag{3.39}$$

As a result, one may now write

$$-8\pi M + 4\pi r^2 e^{-\delta} N'\Big|_{r_H} = 2\int_\Sigma R^\alpha{}_\beta K^\beta d\Sigma_\alpha \rightarrow M = \frac{1}{2} r^2 e^{-\delta} N'\Big|_{r_H} - \frac{1}{4\pi}\int_\Sigma R^\alpha{}_\beta K^\beta d\Sigma_\alpha \ . \tag{3.40}$$

The area of the event horizon of the black hole is given by [185]

$$\mathcal{A}(r_H) = \int_0^{2\pi} d\varphi \int_0^\pi r_H^2 \sin\theta = 4\pi r_H^2 \ . \tag{3.41}$$

The temperature of the black hole at the event horizon is $T_H = N' e^{-\delta}/4\pi\Big|_{r_H}$ [185]. Now we can rewrite (3.40) as

$$M = \frac{1}{2}\mathcal{A}T - \frac{1}{4\pi}\int_\Sigma R^\alpha{}_\beta K^\beta d\Sigma_\alpha \ . \tag{3.42}$$

Moreover, the $t = \text{const}$ hypersurface element reads

$$d\Sigma_\alpha = -t_\alpha \sqrt{h} \ , \tag{3.43}$$

where $h = r^2 \sin\theta \sqrt{1/N}$ is the induced metric on the spacelike hypersurface. Now, by using Einstein's equation, we may rewrite the above equation as

$$M = \frac{1}{2}\mathcal{A}T + \frac{1}{4\pi}\int_{r_H}^\infty dr \int_0^\pi \sin\theta d\theta \int_0^{2\pi} d\varphi \left\{ -\sqrt{e^{-2\delta} N} r^2 \sqrt{\frac{1}{N}} \right.$$
$$\left. \left(-e^{2\delta} \left(A'\right)^2 \left(f(\phi) \left(4\alpha e^{2\delta} \left(A'\right)^2 + 2 \right) + 1 \right) \right) \right\} \ , \tag{3.44}$$

where we have used the trace of the energy-momentum tensor

$$\mathcal{T} = -16\alpha e^{4\delta} \left(A'\right)^4 f(\phi) - r \left(\phi'\right)^2 \ . \tag{3.45}$$

Notice here the absence of any $A'(r)^2$ term because Maxwell's theory is traceless in four dimensions. Now (3.44) reads

$$M = \frac{1}{2}\mathcal{A}T + \int_{r_H}^{\infty} dr \left(e^{\delta} r^2 \left(A'\right)^2 \left(2f(\phi) + 1\right) + 4\alpha e^{3\delta} r^2 \left(A'\right)^4 f(\phi) \right) \ , \tag{3.46}$$

and this is the Smarr relation that our solution satisfies. For the free scalar field theory where $\phi = f(\phi) = \delta = 0$ one can see that

$$M = \frac{1}{2}\mathcal{A}T + \Phi_{RN} Q \ , \tag{3.47}$$

where $\Phi_{RN} = Q/r_H$ is the electrostatic potential of the RN black hole, and hence one obtains the usual Smarr formula.

The charge of the scalar field might also be computed by using the relation of the dilaton charge, mostly used in string theory [131, 186]

$$D = -\frac{1}{4\pi} \int d^2\Sigma^{\mu} \nabla_{\mu} \phi \ , \tag{3.48}$$

where the integral is evaluated over a two-sphere with infinite radius and $-1/4\pi$ is a normalization constant. It might not be clear from this expression; however, the scalar field dresses the black hole with a secondary scalar hair since the scalar charge is not independent of the mass of the black hole or the electric charge, as we mentioned above, and as can be seen in Fig. (3.3).

Moreover, as is well known, the entropy will be related to the area of the black hole solution [30]. It has also been proven that the entropy will be associated with the gravitational theory under consideration through Wald's formula [178]. In this work, we considered the framework of GR to describe gravitation, and consequently, the entropy will be given by

$$\mathcal{S} = \frac{\mathcal{A}(r_H)}{4} \ , \tag{3.49}$$

since we have set Newton's constant to unity. As a result, examining the area of the black hole is the same as examining the entropy.

We introduce the dimensionless standard reduced quantities

$$a_H \equiv \frac{\mathcal{A}_H}{16\pi M^2} \ , \ t_H \equiv 8\pi T_H M \ . \tag{3.50}$$

In Fig. (3.7), we plot the reduced temperature and the area of the RN black hole solution as well as of some scalarized branches of solutions.

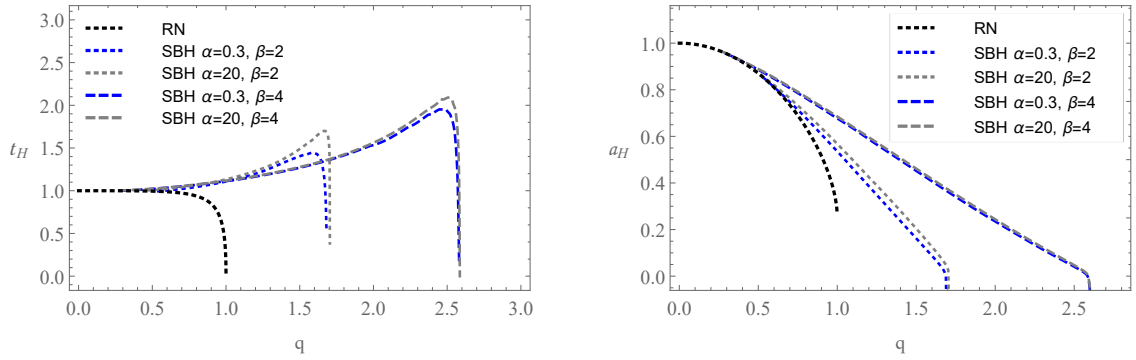

Figure 3.7: (Left) Reduced temperature t_H as a function of the charge to mass ratio q. (Right) Reduced area a_H as a function of the charge to mass ratio q.

As we discussed above, we can notice in Fig. (3.7) that for a given set of constants α and β, nontrivial scalarized black holes emerge through bifurcation from the corresponding Reissner-Nordström black hole with a specific charge to mass ratio q_{exist}. The branches of solutions have a finite range and end up at a critical configuration with a different ratio q_{crit}. The resulting solution features a singular horizon, evidenced by the evaluation of the Kretschmann scalar (Fig. (3.4) (left)). As the critical solution is approached, the horizon area tends to zero, and the temperature remains finite and decreases as long as the coupling gets stronger. It is essential to mention that there are BHs that are hot, as indicated by the peaks in the reduced temperature plot. In the parameter space region where both scalarized and RN black holes coexist for the same charge q, it is consistently observed that scalarized solutions are entropically favored over RN black holes, as evident in Fig. (3.7) (right). In Fig. (3.8), we can notice the same behavior of the reduced temperature and area of all of the first three nontrivial branches. The fundamental mode exhibits higher entropy than the other modes, so the non-fundamental modes are not thermodynamically preferred.

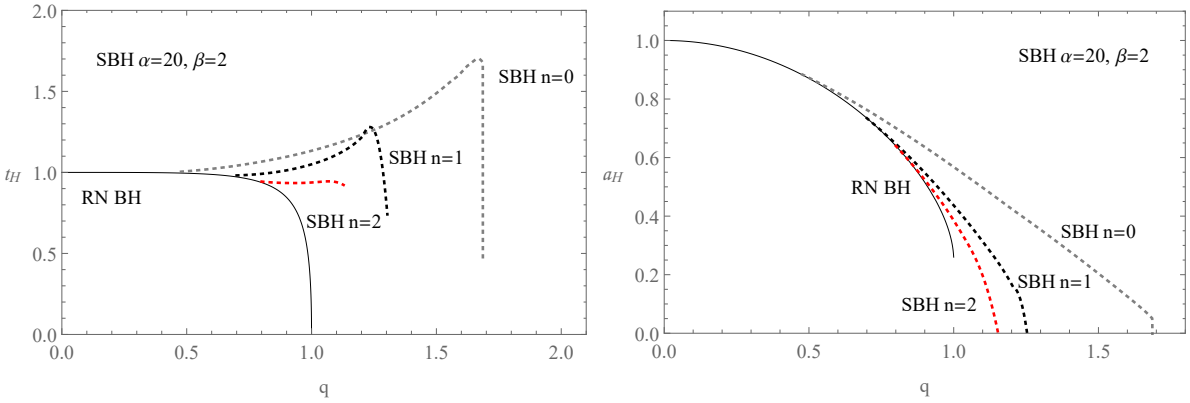

Figure 3.8: (Left) Reduced temperature t_H as a function of the charge to mass ratio q for the first three nontrivial branches. (Right) Reduced area a_H as a function of the charge to mass ratio q. for the first three nontrivial branches.

3.6 Energy Conditions

This section will discuss the nature of the energy-momentum tensor threading the black hole spacetime by analyzing the energy conditions [187]. By considering the

proper reference frame where an observer will remain at rest for constant r, θ, φ [188], we may identify the energy density and the principal pressures as follows

$$\rho \equiv -\mathcal{T}_t^t = e^{2\delta} \left(A'\right)^2 \left(2f(\phi) \left(6\alpha e^{2\delta} \left(A'\right)^2 + 1\right) + 1\right) + \frac{1}{2} N \left(\phi'\right)^2 \ , \tag{3.51}$$

$$p_r \equiv \mathcal{T}_r^r = \frac{1}{2} N \left(\phi'\right)^2 - e^{2\delta} \left(A'\right)^2 \left(2f(\phi) \left(6\alpha e^{2\delta} \left(A'\right)^2 + 1\right) + 1\right) \ , \tag{3.52}$$

$$p_\theta = p_\varphi \equiv \mathcal{T}_\theta^\theta = e^{2\delta} \left(A'\right)^2 \left(f(\phi) \left(4\alpha e^{2\delta} \left(A'\right)^2 + 2\right) + 1\right) - \frac{1}{2} N \left(\phi'\right)^2 \ . \tag{3.53}$$

Without referring to the exact form of the solutions, the energy density of the black hole spacetime is always positive *by construction* in the exterior region of the black hole $r > r_H$ where $N > 0$, since to have scalarized solutions we assumed that $f(\phi) > 0$ for a positive α. As a result, the Weak Energy Condition, which implies the non-negativity of the energy density, is respected. Moreover, the Null Energy Condition (NEC) states that the sum of the energy density with the radial pressure is non-negative. For our scenario, we have

$$\rho + p_r = N \phi'^2 \ , \tag{3.54}$$

which is positive in the causal region of spacetime, and the NEC again holds *by construction* since we used a regular scalar field to construct hairy black hole solutions and not a phantom one (with a negative kinetic energy term in the Lagrangian). The Strong Energy Condition (SEC) states that the sum of the energy density and the principal pressures is non-negative, which, in our case, reads

$$\rho + p_r + p_\theta + p_\varphi = 2e^{2\delta} \left(A'\right)^2 \left(f(\phi) \left(4\alpha e^{2\delta} \left(A'\right)^2 + 2\right) + 1\right) \ , \tag{3.55}$$

which is also non-negative for our system. Hence, the WEC, NEC, and SEC are all satisfied in the causal region of spacetime for our solution since the pressure of the matter threading the black hole spacetime is tangential dominated [189]. In Fig. (3.9), we plot the components of the energy-momentum tensor of our theory. All components are finite at the event horizon of the black hole, while at infinity, they tend to zero, following asymptotic flatness.

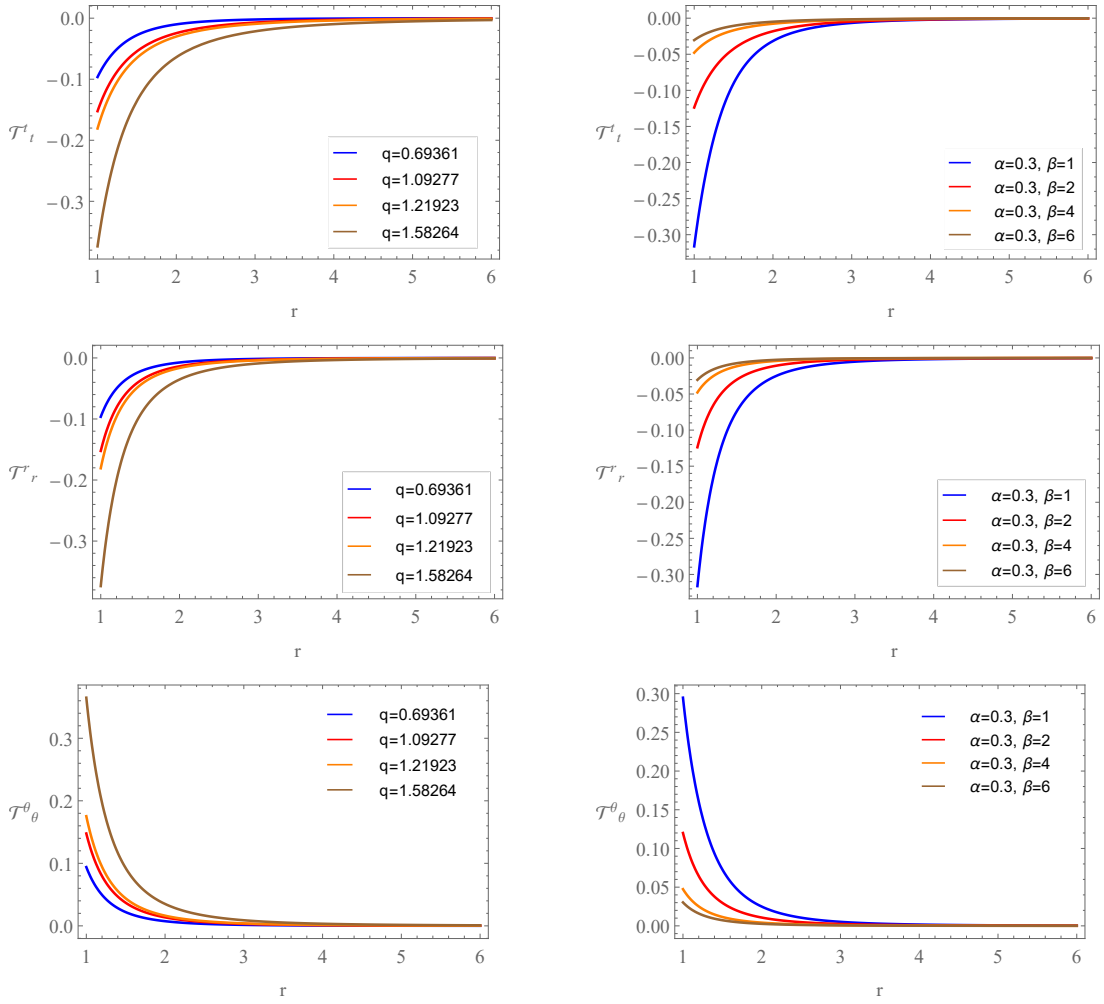

Figure 3.9: The components of the energy-momentum tensor for scalarized BHs for different scenarios. (Left) We set $\alpha = 0.3, \beta = 2$ (Right) We set $q = 0.99$.

In Fig. (3.9) (left), we set $\alpha = 0.3$ and $\beta = 2$ so we plot the components $\mathcal{T}^{\mu}_{\mu}$ for some scalarized BH solutions with different charge to mass ratio q. We can notice that as the BHs get overcharged, the magnitude of all components increases at the horizon while it reaches its asymptotic value at a slower rate. In the right column, we set $\alpha = 0.3, q = 0.99$ while we increase the strength of the interaction of the scalar field with the electromagnetism. As the coupling constant β is increasing, the magnitude of all the components is decreasing.

3.7 Conclusions

In this work, we considered the EMs model with higher derivative gauge field corrections, a scenario that arises in string theory setups, as well as dimensionally reduced Lovelock theories. We investigated the conditions under which the background solution of our theory (the RN black hole) develops a tachyonic instability, indicating in this way the spontaneous dressing of the RN black hole with the scalar field of the theory. Then, we numerically solved the system of the field equations, and we found scalarized black hole solutions that carry a non-trivial scalar field. The branches of our black hole solutions end with a curvature singularity and not with an extremal black hole, which

is in agreement with [1]. We investigated the thermodynamics of our system, derived the Smarr relation of our black hole spacetime, and defined the mass and the scalar charge of our solution through hypersurface integrals. By examining the temperature of the black hole, we found that there is a critical value of the electric charge-to-mass ratio for which the black holes are hot. The area of the scalarized black hole solutions is bigger when compared to the area of the RN black hole, as well as, to the area of the EMs scalarized black holes without the higher derivative gauge field corrections. This result indicates that our solutions are thermodynamically preferred when compared to the existing literature.

Chapter 4

Spontaneous Holographic Scalarization of Black Holes in Einstein-Scalar-Gauss-Bonnet Theories

4.1 Introduction

4.1.1 The Holographic principle and the AdS/CFT correspodence

The holographic principle is a revolutionary idea in theoretical physics suggesting that all the information contained within a volume of space can be represented as a "hologram" -a theory located on the boundary of that space [190–192]. Black holes have an entropy that scales with their surface area, which arises from a precise equivalence between seemingly very different concepts. Specifically, certain theories of quantum gravity in D dimensions (possibly more than four) are exactly equivalent to ordinary gauge field theories, conformal field theory (CFT) in $D-1$ dimensions. This means that curved spacetimes undergoing quantum mechanical fluctuations are exactly equivalent to ordinary particle theories without any gravity but in one lower number of dimensions. The first example of holographic duality was proposed by Maldacena in 1997 [193]. He formulated the conjecture that an $\mathcal{N}=4SU(N)$ Yang-Mills theory in R^{3+1} Minkowski spacetime with 4 supersymmetries is dual to a type IIB supergravity theory in a five-dimensional Anti-de Sitter AdS_5 spacetime, whose boundary coincides with theR^{3+1} Minkowski spacetime. In this correspondence, the two theories are inversely related: the strongly coupled CFT is dual to a weakly coupled quantum gravity theory. The holographic correspondence represents a highly effective approach for addressing strongly interacting systems in condensed matter physics [194–198].

States of the dual theories must be in a $1-1$ correspondence. Note that the identification between operators and gravitational fields is done at $r\to\infty$; consequently, the CFT is referred to as the boundary theory, with the asymptotically AdS spacetime considered the bulk. A field that scales as z^{Δ} near the AdS boundary maps to a gauge invariant operator of dimension Δ. Thus, the CFT operators are related to the bulk field as:

$$\mathcal{O}(x)=C_0\lim_{z\to 0} z^{-\Delta}\phi(x,z), \tag{4.1}$$

where C_0 is a normalization factor.

To verify that the operator has dimension Δ, let us study a scalar bulk field. Since the field is scalar, rescaling the coordinates by ζ implies $\phi(x,z) \to \phi(\zeta x, \zeta z)$. Thus:

$$\mathcal{O}(x) \to C_0 \lim_{z\to 0} z^{-\Delta}\phi(\zeta x, \zeta z) = \zeta^{\Delta} C_0 \lim_{z\to 0} z^{-\Delta}\phi(x,z) = \zeta^{\Delta}\mathcal{O}(x), \tag{4.2}$$

which is precisely the scale transformation of an operator of dimension Δ.

Specifically, in AdS$_{d+1}$, the mass of the field is related to its dimension as follows:

$$m^2 L^2 = \Delta(\Delta - d), \tag{4.3}$$

therefore, there are two possible dimensions for each given mass. These dimensions are related to the boundary conditions of the bulk field at $z \to 0$ as:

$$\phi(x,z) = z^{\Delta_+}\left(\phi_{\Delta_+}(x) + O(z^2)\right) + z^{\Delta_-}\left(\phi_{\Delta_-}(x) + O(z^2)\right), \tag{4.4}$$

where

$$\Delta_\pm = \frac{1}{2}\left(d \pm \sqrt{d^2 + 4m^2L^2}\right). \tag{4.5}$$

The field ϕ_{Δ_-} is a non-normalizable term and represents the coupling of external sources to the gravitational theory, whereas the field ϕ_{Δ_+} is a normalizable term and is related to the expectation value of the operator $\mathcal{O}$.

Notice that in AdS, the mass term m^2 may be negative and still correspond to real dimensions Δ for a scalar, meaning that the scalar field solutions are normalizable as long as the following inequality holds:

$$m^2 L^2 \geq -\frac{d^2}{4}, \tag{4.6}$$

which is the Breitenlohner-Freedman bound [199]. This bound is a consequence of the AdS geometry, giving the possibility for the existence of tachyonic scalar fields.

Regarding a gauge field with a time component as $A_t = \phi(z)$, the asymptotic behavior ($z \to 0$) is obtained as:

$$\phi(z) = \mu + \rho z^{d-2} + \ldots, \tag{4.7}$$

where the asymptotic coefficients μ and ρ are identified holographically with the chemical potential and the charge density, respectively.

4.1.2 Black Holes in Holography

One useful application of hairy black holes in holography is the study of problematic systems, such as high-temperature superconductors, using holographic techniques. High-temperature superconductors are materials that exhibit superconductivity at relatively high temperatures ($30K$ and higher) compared to traditional superconductors and involve strongly correlated electrons. In these systems, the interactions between electrons are so significant that they cannot be described by conventional theories of metals, such as Fermi liquid theory.

The BCS (Bardeen-Cooper-Schrieffer) theory is a microscopic theory of superconductivity based on the concept of quasi-particle fermionic interaction. It predicts the creation of electron pairs, known as Cooper pairs, which are bound together in such a way that they do not scatter by the lattice. This causes the electrical resistance to drop

abruptly to zero below a critical temperature T_c. The Cooper pairs form a "particle" with different properties from the individual electron. Finally, all Cooper pairs condense into a single macroscopic quantum state, described by a coherent wave function.

In s-wave superconductors (conventional materials) such as lead, tin, and mercury, the electron pairs have a spherically symmetric wavefunction, as they are made of one electron with spin up and one with spin down, resulting in no net angular momentum. In p-wave superconductors, the pairs have an angular momentum of one, and the electrons pair with parallel spins, leading to an asymmetrical wavefunction. In d-wave superconductors, the Cooper pairs have an angular momentum of two, and the electrons pair with antiparallel spins, resulting in a more complex, cloverleaf-shaped wavefunction. The strong electron-electron interactions in these materials lead to complex behavior that is difficult to model and predict.

Holographic superconductors use the AdS/CFT duality and can provide a natural theoretical definition of superconductivity in the strong-coupling regime [200]. The first holographic superconductor with quite similar behavior to real superconductors was obtained in GR theory minimally coupled to a Maxwell field and a charged complex scalar with a potential term in AdS spacetime [201], [202]. Below a critical temperature, T_c, the charged black hole solutions undergo a phase transition through classical instability, developing non-trivial hair. In terms of the dual field theory, a $U(1)$ symmetry breaks through thermal fluctuations, and a holographic phase transition appears below T_c at a finite charged density due to the condensation of a charged scalar. Therefore, the superconductivity is characterized by the condensation of a charged operator $\mathcal{O}$ for low temperatures $T < T_c$. This model inherently manifests s-wave superconductors.

For completeness, we refer to the investigation of p-wave superconductors explored in references [203], [204], while d-wave superconductors have been examined in [205–207].

Despite the success of holographic superconductors, there remains a need to investigate more generalized nonminimal holographic superconductors. This exploration is essential to incorporate additional features of superconductors found in real physical systems and potentially uncover the dual description of real superconductors.

4.1.3 Holographic Scalarization

Holographic phase transitions are often characterized by changes in the dual gravitational theory, exemplified by phenomena such as the formation of hairy black holes, as discussed previously. In AdS spacetime, a black hole on the gravitational side is holographically dual to a specific state in the dual CFT, implying that the Schwarzschild-AdS black hole and the hairy AdS black hole correspond to different states in the boundary CFT.

Similarly, spontaneous scalarization involves alterations in the gravitational field surrounding compact objects due to the amplification of scalar fields. While one might initially consider spontaneous scalarization as a holographic phase transition, it's important to note that traditional holographic phase transitions are typically accompanied by symmetry breaking. The mechanism of scalarization, however, leads to a phase transition unrelated to symmetry breaking. As a result, it likely describes a specific quantum phase transition occurring at absolute zero temperature.

In this chapter, we explore the phenomenon of holographic scalarization through

two distinct analyses. Firstly, we examine holographic scalarization in AdS EsGB theory with a neutral scalar field coupled to the Gauss-Bonnet invariant. Our goal is to study the resulting phase transition from both the bulk gravity and boundary CFT perspectives without invoking any symmetry breaking. Since this model lacks $U(1)$ symmetry breaking, we anticipate that the dual theory will not exhibit superconducting behavior but rather undergo condensation $\mathcal{O}_\phi$. Secondly, we investigate holographic scalarization in AdS EsGB theory in the presence of an electromagnetic field and a charged scalar field. This allows us to examine the combined effects of two different phase transition mechanisms, potentially leading to a wider and deeper effective mass and hastening the formation of hairy black holes. In this case, the presence of $U(1)$ symmetry breaking results in a holographic superconducting condensation when the temperature drops below a critical value.

4.2 Scalarization analysis and holography in Einstein-scalar-Gauss-Bonnet theory

4.2.1 The Theoretical Framework

The EsGB theory is described by the following action:

$$\mathcal{S} = \frac{1}{16\pi G_N}\int d^4x\sqrt{-g}\left(R + \frac{6}{L^2} - \nabla_\mu\phi\nabla^\mu\phi - m^2\phi^2 + f(\phi)\mathcal{R}^2_{GB}\right), \tag{4.8}$$

where G_N is the Newton's constant, L is the curvature radius of AdS spacetime, $\phi = \phi(r)$ is a neutral real scalar field with mass m, and $f(\phi)$ is the coupling function of the scalar field and the Gauss-Bonnet invariant term.

Varying the action with respect to all dynamical fields yields the following field equations:

$$\begin{aligned} &R_{\mu\nu} - \frac{1}{2}Rg_{\mu\nu} - \frac{3}{L^2}g_{\mu\nu} + \Gamma_{\mu\nu} = \nabla_\mu\phi\nabla_\nu\phi - \frac{1}{2}g_{\mu\nu}\nabla_\alpha\phi\nabla^\alpha\phi - \frac{1}{2}m^2g_{\mu\nu} \\ &\nabla_\mu\nabla^\mu\phi - \left(m^2 - \frac{1}{2}f'(\phi)\mathcal{R}^2_{GB}\right) = 0, \end{aligned} \tag{4.9}$$

where

$$\begin{aligned} \Gamma_{\mu\nu} =& -R\left(\nabla_\mu\Psi_\nu + \nabla_\nu\Psi_\mu\right) - 4\nabla^\alpha\Psi_\alpha\left(R_{\mu\nu} - \frac{1}{2}Rg_{\mu\nu}\right) + 4R_{\mu\alpha}\nabla^\alpha\Psi_\nu + 4R_{\nu\alpha}\nabla^\alpha\Psi_\mu \\ &- 4g_{\mu\nu}R^{\alpha\beta}\nabla_\alpha\Psi_\beta + 4R^\beta_{\ \mu\alpha\nu}\nabla^\alpha\Psi_\beta, \end{aligned} \tag{4.10}$$

with

$$\Psi_\mu = \frac{df(\phi)}{d\phi}\nabla_\mu\phi. \tag{4.11}$$

As highlighted by Witten [208], in the limit of a large Schwarzschild-AdS black hole, the topology transitions from $\mathbf{S}^1 \times \mathbf{S}^{d-1}$ to $\mathbf{S}^1 \times \mathbf{R}^{d-1}$, where a Schwarzschild black hole is approximated by a planar black hole with a translationally invariant horizon. Hence, we can conclude that the planar Schwarzschild-AdS black hole emerges as an

admissible solution of our theory if $f'(0) = 0$, where the field equations reduce to the Einstein field equations for a trivial scalar field, which we set to zero ($\phi = 0$):

$$\begin{aligned} ds^2 =& -g(r)dt^2 + \frac{1}{g(r)}dr^2 + r^2(dx^2 + dy^2) \\ g(r) =& \frac{r^2}{L^2} - \frac{M}{r}, \end{aligned} \tag{4.12}$$

where M is the black hole mass. We expect tachyonic instabilities to arise if the coupling function also satisfies the condition $f''(0) > 0$, as discussed in [135]. Therefore, we choose:

$$f(\phi) = \frac{\lambda^2}{2\beta}\left(1 - e^{-\beta\phi^2}\right), \tag{4.13}$$

Here, λ represents the coupling constant of our theory, while β serves as a parameter that has a minor impact on our analysis; thus, we set $\beta = 1$ for the subsequent study.

4.2.2 (In)stability analysis for a neutral scalar field

We are interested in studying the possible instabilities of the background solutions in our theory. As in the previous chapter, these instabilities manifest through the scalar perturbation equation:

$$\left(\Box - \left(m^2 - \frac{1}{2}f''(\phi)\mathcal{R}^2_{GB}\right)\right)\Big|_{\phi=0}\delta\phi = 0, \tag{4.14}$$

where $\Box$ is the d'Alambert operator and the Gauss-Bonnet invariant is calculated with the planar Schwarzschild-AdS metric as:

$$\mathcal{R}^2_{GB} = \frac{4}{r^2}\left(g'(r)^2 + g(r)g''(r)\right) = \frac{24}{L^2} + \frac{12M^2}{r^6}. \tag{4.15}$$

As we expected, the effective mass term may become sufficiently negative, resulting in tachyonic instabilities, due to the presence of a negative term, as follows:

$$m^2_{eff} = m^2 - \frac{\lambda^2}{2}\mathcal{R}^2_{GB}. \tag{4.16}$$

A more analytical approach involves a dynamical analysis of the Schwarzschild AdS black hole, we consider the time-dependent radial perturbation given by $\phi = \epsilon\frac{\phi(r,t)}{r}$. Consequently, the Klein-Gordon equation, expressed under the tortoise coordinate $r_* = \int g^{-1}dr$, is as follows:

$$-\frac{\partial^2\phi(r,t)}{\partial t^2} + \frac{\partial^2\phi(r,t)}{\partial r_*^2} - V(r)\phi(r,t) = 0, \tag{4.17}$$

where the effective potential reads as:

$$V(r) = g\left(\frac{g'}{r} + m^2 - \frac{2\lambda^2}{r^2}(g'^2 + gg'')\right). \tag{4.18}$$

We present the profile of the effective potential in the left panel of Fig. (4.1). As expected, the potential may form well outside the horizon radius r_h, which, when deep

enough, results in tachyonic instabilities. As the coupling constant λ increases, the interaction between the scalar field and gravity strengthens, destabilizing the background spacetime. The critical coupling is approximately $\lambda \approx 0.6$. Note that in the right panel of Fig. (4.1), we present the effective potential for the flat Schwarzschild AdS case, i.e., $L \to \infty$. This clearly shows smaller and shallower potential wells, implying that instabilities arise more easily for planar Schwarzschild black holes in AdS spacetime compared to flat spacetime.

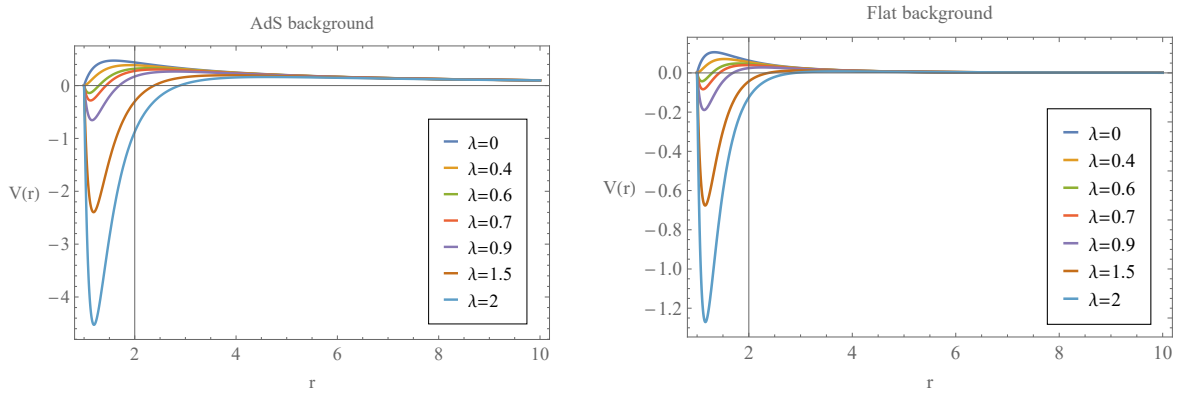

Figure 4.1: (Left) The behavior of the effective potential for the AdS black hole as the function of the radial coordinate. Right: The effective potential for the flat case with $L \to \infty$ with the same value of parameters. Here we have set $r_h = 1$ and $m^2L^2 - 12\frac{\lambda^2}{L^2} = -2$ without loss of generalization, while the mass M is the root of the metric function $g(r)$.

In Fig. (4.2), we present the time domain profile of the scalar field. Below a critical value of the coupling, the scalar field decays over time, indicating stability. However, when the coupling constant λ exceeds the critical value of approximately $\lambda \approx 0.678$, the scalar field grows over time. This behavior aligns with the analysis of the effective potential.

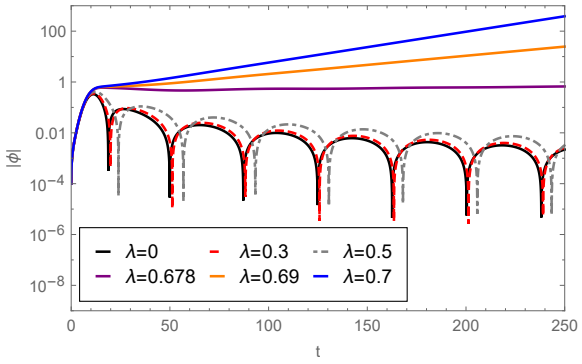

Figure 4.2: The time domain profile of the scalar field at fixed radial coordinate $r = 1000$.

4.2.3 Signal of scalarization in the probe limit

The analysis in the preceding section was conducted from the gravity side, involving a dynamical analysis of scalar perturbations within the background geometry. This analysis revealed the onset of tachyonic instability beyond a critical coupling threshold, approximately $\lambda \approx 0.678$. Consequently, it is anticipated that the scalar field will condense on the boundary on the gauge side.

The Klein-Gordon equation governing a radial scalar field $\phi = \phi(r)$ under the planar AdS Schwarzschild background is given by:

$$\phi''(r) + \left(\frac{2}{r} + \frac{g'(r)}{g(r)}\right)\phi'(r) - \frac{m^2}{g(r)}\phi(r) + \frac{\lambda^2}{2g(r)}\mathcal{R}^2_{GB}\frac{df(\phi)}{d\phi} = 0, \tag{4.19}$$

which, near the black hole horizon, reduces to:

$$\phi' - \frac{1}{3}\left(-3 - m^2 - 18\lambda^2 e^{-\phi^2}\right)\phi = 0. \tag{4.20}$$

At the AdS boundary, $r \to \infty$, the scalar field behavior reads as:

$$\phi(r) = \frac{\phi_-}{r^{\Delta_-}} + \frac{\phi_+}{r^{\Delta_+}}, \tag{4.21}$$

where $\Delta_\pm = \frac{3\pm\sqrt{9+4m_e^2}}{2}$ and $m_e^2 = m^2L^2 - 12\frac{\lambda^2}{L^2}$. According to the gauge/gravity duality, a condensate will form in the boundary theory if m_e^2 holds the Breitenlohner-Freedman (BF) bound, i.e., if $m_e^2 < m_{BF}^2$ [199], [209]. For $(3+1)$ dimensional asymptotically flat AdS spacetime with AdS radius $L = -\frac{3}{\Lambda}$, the BF bound is $m_{BF}^2 = -\frac{d^2}{4L^2} = -\frac{9}{4L^2}$. Therefore, it sets a lower limit on the effective mass squared of a scalar field to ensure stability:

$$m_e^2 > -\frac{9}{4L^2}. \tag{4.22}$$

Hence, for simplicity, we set $m_e^2 = -2$, resulting in the values $\Delta_- = 1$ and $\Delta_+ = 2$. We then solve Eq. (4.19) numerically, imposing the following boundary conditions:

$$\phi_+ = 0, \text{ and } \phi_- = \langle \mathcal{O}_\phi \rangle \tag{4.23}$$

In the probe limit, the behavior of ϕ_- as a function of the coupling constant λ is presented in Fig. (4.3). The dual CFT suggests a strong indication of spontaneous scalarization beyond a critical coupling constant value of approximately $\lambda_c \approx 0.64$, where the condensate of the scalar field emerges rapidly.

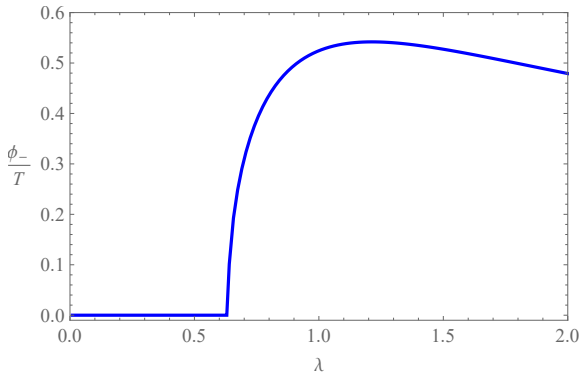

Figure 4.3: The boundary condensate parameter ϕ_- as a function of the Gauss-Bonnet coupling constant λ.

Moreover, in Fig. (4.4), we present the scalar field profiles for different coupling constants that exceed the threshold, $\lambda > \lambda_c$. This figure confirms the presence of nontrivial scalar fields triggered by tachyonic instabilities.

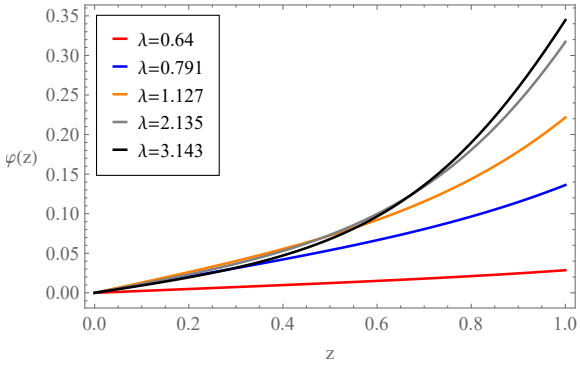

Figure 4.4: The profile of the scalar field as the function of the coordinate $z = \frac{r_h}{r}$ here we set the horizon $r_h = 1$. We see that the scalar field condensates near the horizon, contributing to the black hole hair for some intermediate λ.

4.2.4 Scalarized hairy black hole solution

Considering the backreaction of the scalar field on the background geometry, we solve the field equations (4.9) in this section using the following ansatz for the planar metric:

$$ds^2 = \frac{1}{z^2}\left(-(1-z)p(z)U(z)dt^2 + \frac{1}{(1-z)p(z)U(z)}dz^2 + V(z)dx^2 + V(z)dy^2\right), \quad (4.24)$$

where $z = r_h/r$, $p(z) = 1 + z + z^2$, so the horizon is now located at $z = 1$ and the asymptotic boundary at $z \to 0$. The functions $U(z)$ and $V(z)$ are the metric functions.

The Klein-Gordon equation takes the following form:

$$\begin{aligned}\phi''(r)+&\left(\frac{p'(z)}{p(z)}+\frac{U'(z)}{U(z)}+\frac{V'(z)}{V(z)}-\frac{z-2}{z(z-1)}\right)\phi'(z)\\ &+\frac{1}{(z-1)z^2p(z)U(z)}\left(m^2\phi(z)+\frac{\lambda^2}{2}\frac{df(\phi)}{d\phi}\mathcal{R}^2_{GB}\right)=0,\end{aligned} \quad (4.25)$$

and the nontrivial field equations read as:

$$\begin{aligned}&U'\left[2z(z-1)pV^2\left(zV'-2V\right)+\lambda^2\frac{df(\phi)}{d\phi}UM\right]+U[(z-1)z^2V\left(2pVV'-pV'^2\right)\\ &-4z(z-1)V^3p'+2pV^3(-6+4z+(z-1)z^2\phi'^2)-2zpV^2((3z-4)V'-2z(z-1)V'')]\\ &+\lambda^2\frac{df(\phi)}{d\phi}U^2[\frac{p'}{p}M+4(z-1)^2z^4p^2V'\phi'(2V''-V'^2)+8z(z-1)p^2V^3N\\ &+2(z-1)z^3p^2VV'^2(N+4(z-1)\phi')-8(z-1)z^2p^2V^2(2z(z-1)\phi'V''+NV')]\\ &+2V^3(6-m^2\phi^2)\end{aligned} \quad (4.26)$$

$$\begin{aligned}&V'^2\left[(z-1)z^2pU+\frac{z^2}{4}X\right]+VV'[2(z-1)z^2(Up'+pU')-2z(3z-4)pU-zX]\\ &+V^2\left[12-2m^2\phi^2-4z(z-1)(Up'+pU')+X-2pU(6-4z+(z-1)z^2\phi'^2)\right],\end{aligned} \quad (4.27)$$

$$V''[-2(z-1)z^2pU+2\phi'\lambda^2\frac{df(\phi)}{d\phi}(2(z-1)(z-2)z^3p^2U^2-(z-1)^2z^4(p^2U^2)')]$$
$$+\frac{V'^2}{V}[(z-1)z^2pU+\frac{z^2}{12}X]+V'[2z(z-2)pU-2(z-1)z^2pU'-2Y]+V[-12+2m^2\phi^2$$
$$+2pU(2(3-z)-(z-1)z^2\phi'^2)+4z(z-2)Up'+2(z-1)z^2(2p'U'+Up'')$$
$$+2zp(2(z-2)U'-z(z-1)U'')+\frac{4}{z}Y] \quad (4.28)$$

where

$$\begin{aligned}
M &= 6(z-1)^2p^2V\phi'(4V^2-4zVV'+z^2V^2)\ ,\\
N &= (z+2)\phi'+2(z-1)z\phi'',\\
X &= 12\phi'\lambda^2\frac{df(\phi)}{d\phi}[(z-1)^2z^2(p^2U^2)'-2z(z-1)(z-2)p^2U^2]\ ,\\
Y &= \lambda^2\frac{df(\phi)}{d\phi}\{[(z-1)^2z^4\phi'(U^2p^2)']'-2(z-1)z^4\phi'(U^2p^2)'-Q\}\ ,\\
Q &= 2z^2p^2U^2[(z^2-2)\phi'+z(z^2-3z+2)\phi'']\ . \qquad (4.29)
\end{aligned}$$

We verify that when $U(z)=V(z)=1$ and $\phi=0$, the Schwarzschild-AdS geometry becomes a solution to the above system. Therefore, we impose the following boundary conditions ($r\to\infty,\ z\to 0$):

$$U(z\to 0)=V(z\to 0)=1,\ \phi(z\to 0)=\phi_-z^{\frac{3-\sqrt{9+4m_e^2}}{2}}+\phi_+z^{\frac{3+\sqrt{9+4m_e^2}}{2}}. \qquad (4.30)$$

By setting the model parameters to those of the probe limit, we numerically solve the nontrivial field equations for values of the coupling parameter close to the critical value found in the previous analyses. The profiles of the metric functions $U(z)$ and $V(z)$, along with the nonvanishing scalar field $\phi(z)$, are illustrated in Fig. (4.5). Near the critical value, the metric functions $U(z)$ and $V(z)$ approach unity, and the scalar field begins to manifest as hair. As λ surpasses the critical value, new scalarized black hole solutions emerge, causing the metric functions to deviate from unity and the scalar field from zero.

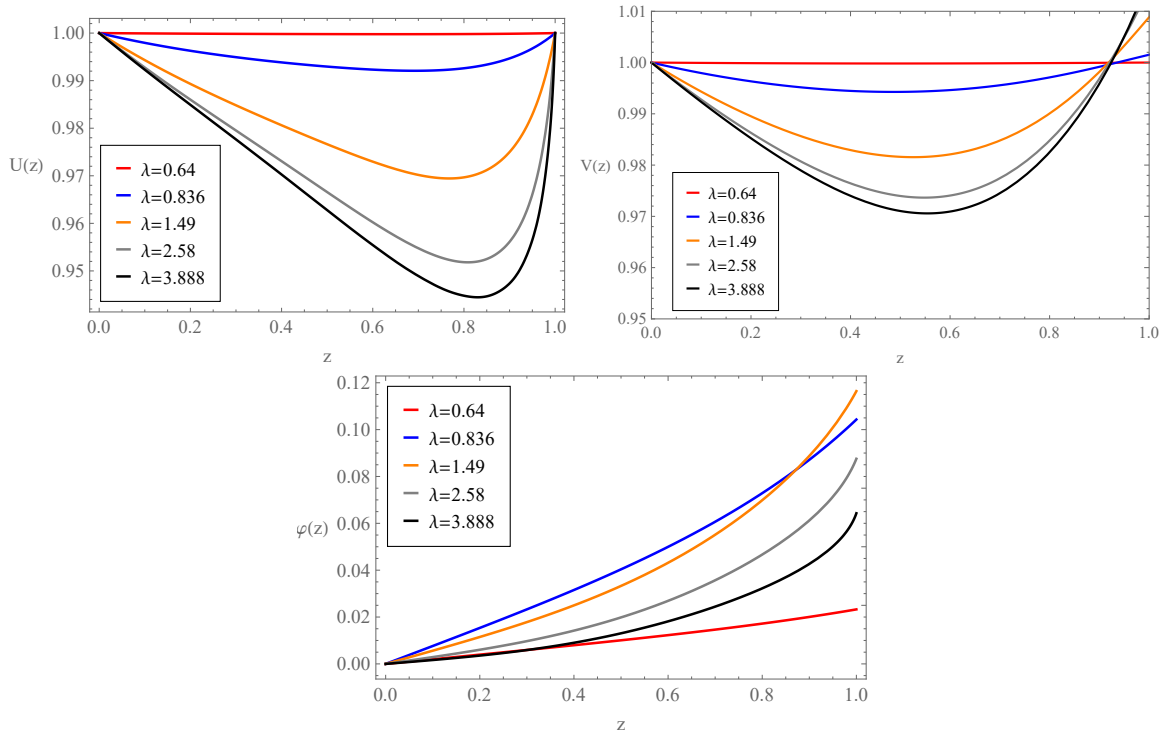

Figure 4.5: The profiles of the metric function U, V and the scalar function ϕ of the hairy black hole as the function of the coordinate $z = \frac{r_h}{r}$.

According to the AdS/CFT correspondence, the scalar field ϕ expressed in (4.30) is dual to a scalar operator $\mathcal{O}_\phi$ in the boundary theory. As before, we set the boundary conditions $\phi_+ = 0$ and ϕ_- represents the vacuum expectation value (VEV) in the dual theory. In Fig. (4.6), we present the VEV as a function of the coupling parameter. Similar to the probe limit, ϕ_- becomes nonzero around 0.64 and sharply increases, indicating the condensation of hair. It's worth noting that after reaching a maximum VEV, the behavior changes, suggesting that the scalar field may face difficulty in forming a stable configuration of a scalarized black hole[1].

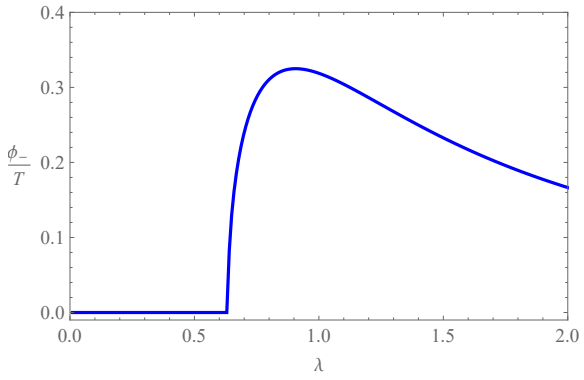

Figure 4.6: The boundary condensate parameter ϕ_- as a function of the coupling parameter λ. The condensate merges around $\lambda_c \approx 0.64$, which are the same as the results in the probe limit.

To discuss these results briefly, we aim to clarify the two dual descriptions of the phase transition occurrence. On the bulk gravity side, we observe the formation of

[1]The presence of nonlinear terms leads to numerical breakdown for large coupling

scalarized black hole solutions triggered by tachyonic instability resulting from the interaction of the scalar field with higher-order curvature terms. This occurs even if the effective mass of the scalar field does not violate the BF bound. In the boundary field theory, a black hole on the gravity side is holographically dual to a thermal state. Conversely, there is a distinct phase transition from a normal state with a vanishing VEV to a condensed matter state with a nonvanishing VEV. The absence of $U(1)$ symmetry breaking results in the phase transition in the CFT not being a holographic phase transition but rather a quantum phase transition at a finite temperature.

4.2.5 Holographic entanglement entropy as a probe

In this subsection, we will investigate the scalarization mechanism by calculating the dual theory's holographic entanglement entropy (HEE). As previously mentioned, HEE is one of the boundary theory's most important characteristic scales. We anticipate that HEE will serve as a useful probe of scalarization, enabling us to characterize the phase transition in the dual boundary theory.

In the case of Lovelock gravity, the correct holographic entanglement entropy does not be described by Wald's formula. The appropriate function for describing holographic entanglement entropy is the one introduced in [210]. We will utilize the Ryu-Takayanagi proposal [211] to compute the sector's holographic entanglement entropy (HEE). For this purpose, we focus on subsystem A, which has a straight strip geometry defined by $\frac{l}{2} \leq x \leq \frac{l}{2},\ 0 \leq y \leq L$, where l is the size of A and L serves as a regulator, which can be set to infinity. Ryu and Takayanagi proposed that the HEE S_A is determined by the radial minimal extended surface γ_A bounded by the A as:

$$S_A = \frac{Area(\gamma_A)}{4G_N}, \tag{4.31}$$

in Einstein's gravity. A general expression for HEE in higher derivative gravity is given by [212]:

$$\begin{aligned} S_A &= -2\pi \int_\Xi d^2x\sqrt{h}\frac{\partial L}{\partial R_{\mu\nu\rho\sigma}}\varepsilon_{\mu\nu}\varepsilon_{\rho\sigma} + \text{Anomaly term} \\ &= -2\pi \int_\Xi d^2x\sqrt{h}\left(\frac{\partial L}{\partial R_{\mu\rho\nu\sigma}}\varepsilon_{\mu\rho}\varepsilon_{\nu\sigma} - \sum_\alpha \left(\frac{\partial^2 L}{\partial R_{\mu_1\rho_1\nu_1\sigma_1}\partial R_{\mu_2\rho_2\nu_2\sigma_2}}\right)_\alpha \frac{2K_{\lambda_1\rho_1\sigma_1}K_{\lambda_2\rho_2\sigma_2}}{q_{\alpha+1}}\right. \\ &\left.\times[(n_{\mu_1\mu_2}n_{\nu_1\nu_2} - \varepsilon_{\mu_1\mu_2}\varepsilon_{\nu_1\nu_2})n^{\lambda_1\lambda_2} + (n_{\mu_1\mu_2}\varepsilon_{\nu_1\nu_2} + \varepsilon_{\mu_1\mu_2}n_{\nu_1\nu_2})\varepsilon^{\lambda_1\lambda_2}]\right), \end{aligned} \tag{4.32}$$

The first term represents the Wald entropy [178], [179], while the second term is the anomaly term of HEE, representing the corrections involving extrinsic curvature. q_α denotes "anomaly coefficients," L is the Lagrangian density, and h denotes the determinant of the induced metric on the extended surface Ξ, which minimizes the functional S_A. Our theory yields the HEE for the dual theory, evaluated as:

$$S_A = \frac{1}{4}\int_\Xi dx^2\sqrt{h}\left[1 - f(\phi)\left(2R - 4(R^a_a - \frac{1}{2}K_aK^a) + 2(R^{ab}R_{ab} - K_{aij}K^{aij})\right)\right], \tag{4.33}$$

where K_{aij} is the extrinsic curvature tensor and K_a is defined as $K_a \equiv K_{aij}h^{ij}$.

We explain the notations used in the two formulas as follows: The Greek letters $\mu, \nu, \ldots$ serve as indices for the four-dimensional bulk geometry, while $i, j, \ldots$ are

indices for the two-dimensional extended surface Ξ. The Latin letters $a, b, \ldots$ are indices for the two-dimensional space orthogonal to Ξ. In terms of two orthogonal unit vectors $n_\mu^{(a)}$, we define $n_{\mu\nu} = n_\mu^{(a)} n_\nu^{(b)} G_{ab}$, which projects onto the induced two-dimensional metric G_{ab} in the x^a directions. Then, the tensor $\varepsilon_{\mu\nu}$ can be constructed as $\varepsilon = n_\mu^{(a)} n_\nu^{(b)} \varepsilon_{ab}$, where ε_{ab} is the usual Levi-Civita tensor and $\varepsilon_{\mu\nu}$ is the Levi-Civita tensor in the two orthogonal directions with all other components vanishing.

We denote the HEE of the Schwarzschild-AdS black hole as S_{A0}, which is a constant since it is independent of the coupling constant λ. Thus, S_A represents the HEE entropy of the scalarized black hole. In Fig. (4.7), we present the relation between the difference $\Delta S = S_A - S_{A0}$, which encapsulates the information arising from the interaction between the scalar field and the GB invariant, and the coupling constant λ. Aligned with the previous results, when the coupling constant is less than the critical value $\lambda_c \approx 0.64$, the background solution is the physically favorable one. However, as the coupling constant exceeds the critical value, the HEE increases rapidly, and new scalarized black holes become physically favorable, possessing larger HEE.

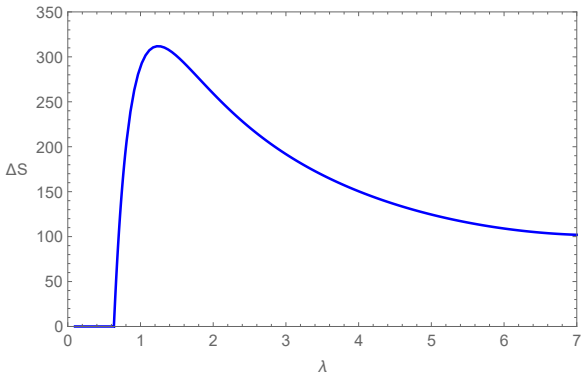

Figure 4.7: The difference of holographic entanglement entropy $\Delta S = S_A - S_{A0}$ as a function of the GB coupling.

As the HEE serves as a measure of the degree of freedom within a system, introducing the scalar field should augment the degree of freedom in the boundary theory corresponding to the hairy black hole, thereby increasing HEE after scalarization. It's noteworthy to highlight that this behavior of HEE contrasts significantly with that observed in holographic superconductors. In such systems, the hairy superconducting state typically exhibits lower HEE than the normal state. This discrepancy arises because the emergence of Cooper pairs in the superconducting state reduces the degree of freedom of the system. For further insights, refer to [**?**, **?**, **?**], and references therein.

Moreover, scalarization implies the formation of a halo of matter at small distances $r < r_h$. This is a dynamic process driven solely by gravitational force. Fig. (4.7) illustrates that the HEE initially increases from λ_c and then decreases until it stabilizes. This behavior indicates that the black hole acquires hair, with the scalar field penetrating the black hole horizon until stabilization is achieved. As this process occurs on a small scale, the corresponding dual boundary theory can only be described as a quantum physics effect. From this perspective, we can argue that the scalarization discussed may correspond to a certain quantum phase transition; however, further investigation is required to delve deeper into the underlying physics.

4.3 Holography phase transition in Einstein-scalar-Gauss-Bonnet theory in the presence of an electromagnetic field

4.3.1 The Theoretical Framework

In this section, we investigate the holographic phase transition in EsGB theory in the presence of an electromagnetic field $A_\mu = (A_t(r), 0, 0, 0)$ and a massive charged real scalar field ϕ, which is described by the following action:

$$\mathcal{S} = \frac{1}{16\pi G_N}\int dx^2\sqrt{-g}\left(R + \frac{6}{L^2} - \frac{1}{4}F_{\mu\nu}F^{\mu\nu} - D_\mu\phi(D^\mu\phi)^* - m^2|\phi|^2 + f(\phi)\mathcal{R}^2_{GB}\right), \tag{4.34}$$

where $D_\mu = \nabla_\mu - iqA_\mu$, $F_{\mu\nu} = \nabla_\mu A_\nu - \nabla_\nu A_\mu$ is the Maxwell invariant, $L = -\frac{3}{\Lambda}$ is the AdS radius and m, q denote the mass and the charge of the scalar field. The modified Einstein field equations of all the dynamical fields $g_{\mu\nu}, A_\mu$ and ϕ read as:

$$\begin{aligned}
R_{\mu\nu} - \frac{1}{2}Rg_{\mu\nu} - \frac{3}{L^2}g_{\mu\nu} + \Gamma_{\mu\nu} =& \nabla_\mu\phi\nabla_\nu\phi - \frac{1}{2}g_{\mu\nu}\nabla_\alpha\phi\nabla^\alpha\phi \\
&- \left(\frac{1}{2}m^2 g_{\mu\nu} + \frac{1}{2}q^2 A_\alpha A^\alpha g_{\mu\nu} - q^2 A_\mu A_\nu\right)\phi^2 \\
&+ \frac{1}{2}\left(F^{\mu\alpha}F^{\nu}_{\ \alpha} - \frac{1}{4}F_{\alpha\kappa}F^{\alpha\kappa}g_{\mu\nu}\right), \\
\nabla_\alpha F^{\alpha\mu} =& \, 2q^2 A^\mu\phi^2, \\
\nabla_\mu\nabla^\mu\phi - \left(m^2 + q^2 A_\mu A^\mu\right)\phi + \frac{1}{2}f'(\phi)\mathcal{R}^2_{GB} =& \, 0,
\end{aligned} \tag{4.35}$$

where $\Gamma_{\mu\nu}$ is defined as in (4.10). As in the previous section, choosing the coupling function $f(\phi) = \frac{\lambda^2}{2\beta}\left(1 - e^{-\beta\phi^2}\right)$ with $\beta = 1$ and the condition $f'(0) = 0$ results in the Reissner-Nordström-AdS solution as the vacuum solution of this theory, as follows:

$$\begin{aligned}
ds^2 =& -g(r)dt^2 + \frac{1}{g(r)}dr^2 + r^2\left(dx^2 + dy^2\right), \\
g(r) =& \frac{r^2}{L^2} - \frac{2M}{r} + \frac{Q^2}{4r^2}.
\end{aligned} \tag{4.36}$$

4.3.2 (In)stability analysis for a charged scalar field

Moreover, this coupling function form satisfies the spontaneous scalarization condition. Specifically, small linear perturbations around the background solution are governed by the Klein-Gordon equation:

$$\left(\Box - \left(m^2 + q^2 A_\mu A^\mu\right) + \frac{1}{2}f''(\phi)\mathcal{R}^2_G B\right)\delta\phi = 0, \tag{4.37}$$

where the effective mass squared takes the form as follows:

$$m^2_{eff} = m^2 - \frac{q^2 A_t(r)^2}{g(r)} - \frac{\lambda^2}{2}\mathcal{R}^2_{GB}, \tag{4.38}$$

where $A_t(r)$ denotes the electric potential. If the m^2_{eff} remains sufficiently negative for a long enough period, it may become tachyonic, breaking the $U(1)$ symmetry. Consequently, we expect the scalarization mechanism to mimic a holographic superconducting phase transition at a certain critical temperature of the black hole [200], [202]. The Hawking temperature of the Reissner-Nordström-AdS black hole is given by:

$$T = \frac{g'(r_h)}{4\pi}. \tag{4.39}$$

We avoid analyzing the stability behavior of the background metric and proceed directly to investigating scalarization in the probe limit. This approach is justified by the expectation that similar to the neutral case without the electromagnetic field, the dynamical analysis of the background solution aligns with the condensation analysis in the probe limit.

4.3.3 Holographic superconducting condensation

The equations governing the scalar and electromagnetic fields are depicted as:

$$\phi''(r) + \left(\frac{2}{r} + \frac{g'(r)}{g(r)}\right)\phi'(r) + \frac{q^2 A_t(r)^2 - m^2 g(r)}{g(r)^2}\phi(r) + \frac{df(\phi)}{d\phi}\frac{\mathcal{R}^2_{GB}}{2g(r)} = 0, \tag{4.40}$$

$$A_t''(r) + \frac{2}{r}A_t'(r) - \frac{2q^2\phi(r)^2}{g(r)}A_t(r) = 0. \tag{4.41}$$

We are interested in asymptotically AdS solutions, which are regular on the horizon. Therefore, the boundary conditions near the horizon are given by:

$$A_t(r_h) = 0,\ \phi'(r_h) = \frac{L^2}{3r_h}\left(m^2 - \frac{18\lambda^2 e^{-6\phi(r_h)^2}}{L^4}\right)\phi(r_h), \tag{4.42}$$

while the boundary conditions at infinity are given by:

$$A_t(r) = \mu - \frac{\rho}{r},\ \phi(r) = \frac{\phi_-}{r^{\Delta_-}} + \frac{\phi_+}{r^{\Delta_+}}. \tag{4.43}$$

The asymptotic coefficients μ and ρ are holographically associated with the charge density and the chemical potential, respectively, and $\Delta_\pm = \frac{3\pm\sqrt{9+4m_e^2}}{2}$ with $m_e^2 = m^2 - 12\lambda^2$. We fix $L = M = q = 1,\ m_e^2 L = -2$, and then solve the system of equations numerically using the specified boundary conditions.

The scalar field condensates at the critical temperature T_c, triggered by tachyonic instabilities due to interactions between the scalar field and both the gauge field and gravity. In the left panel of Fig. (4.8), we present the phase diagram $\lambda - T_c$. This result is consistent with findings from [213–215], and [216], which indicate that in the presence of strong curvature effects outside the horizon of a five-dimensional Gauss-Bonnet-AdS black hole, the effectiveness of the holographic superconducting mechanism diminishes as the GB coupling increases. The critical temperature T_c of the holographic superconducting phase transition is the particular temperature above which the trivial black hole is physically stable. In contrast, below it, the black hole is stabilized in a superconducting state with non-vanishing ϕ_-. This figure shows that the critical temperature first slightly increases as the GB coupling λ increases. When

the coupling goes to a critical value $\lambda_{cc} \approx 0.6339$, T_c increases dramatically and then becomes divergent, it implies that the holographic superconducting phase transition only can occur when $\lambda < \lambda_{cc}$ and when $\lambda \leq \lambda_{cc}$; a hairy black hole does not form in the gravity sector while on the boundary there is no any holographic superconducting phase.

This result indicates that as the GB coupling λ becomes larger than a critical value, the gravitational attraction from the GB high curvature term becomes stronger, and the formation of the scalarized black hole is not possible. A similar effect was observed in [213] as well as [214–216] and therein. It was found that with the strong curvature effects outside the horizon of a five-dimensional Gauss-Bonnet-AdS black hole, the holographic superconducting mechanism is less effective as the GB coupling is increased.

Note also that in the limit $\lambda = 0$, the dynamics of the scalar field and its interactions mimic the behavior of an s-wave superconductor [200].

In the right panel of Fig. (4.8), we present the phase diagram $q - T_c$, which shows that the critical temperature increases as the scalar charge increases.

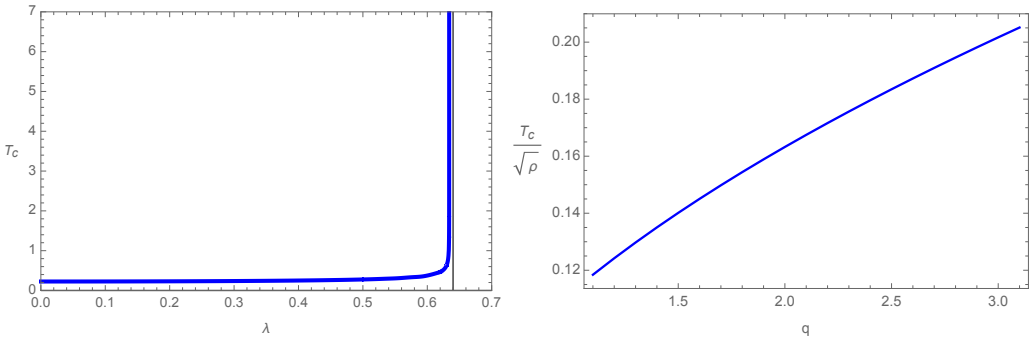

Figure 4.8: (Left) The phase diagram $\lambda - T_c$. (Right) The phase diagram $q - T_c$.

We display the scalar condensation in Fig. (4.9). For values smaller than the critical coupling constant λ_{cc}, we observe a suppression in the condensation gap, indicating a reduction in Cooper pairs within the dual boundary theory. We confirm these results by examining the conductivity in the following subsection.

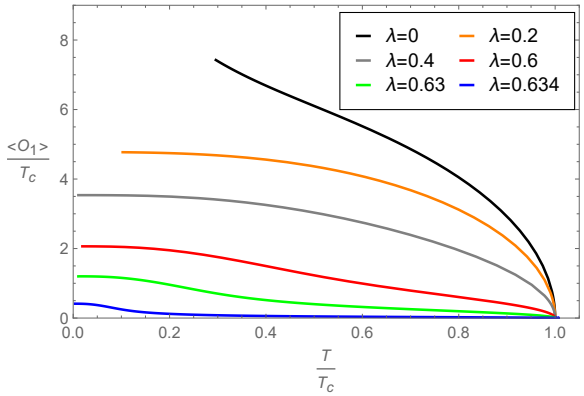

Figure 4.9: The condensation of scalar field as the function of the temperature T/T_c with different couplings.

4.3.4 Optical conductivity

The conductivity of the dual superconductor is calculated through linear perturbations of the electromagnetic potential $A_t(r) = A_x(r)e^{-i\omega t}$ in the probe limit:

$$A_x''(r) + \frac{g'(r)}{g(r)}A_x'(r) + \left(\frac{\omega^2}{g(r)^2} - \frac{2q^2\phi(r)^2}{g(r)}\right)A_x(r) = 0. \tag{4.44}$$

The boundary condition at the horizon is described by an ingoing wave, given by:

$$A_x(r) \propto g(r)^{-i\omega/3r_h}\Big|_{r\to r_h}, \tag{4.45}$$

while the asymptotic behavior at infinity is described as:

$$A_x = A_x^{(0)} + \frac{A_x^{(1)}}{r} + \dots, \tag{4.46}$$

where $A_x^{(0)} = A_x$ represents the dual source in the boundary theory that couples to a current operator and $A_x^{(1)} = \langle J_x \rangle$ the expectation value for the current due to this coupling. Then, the conductivity obeys Ohm's Law, resulting to:

$$\sigma(\omega) = -\frac{iA_x^{(1)}}{\omega A_x^{(0)}}. \tag{4.47}$$

Therefore, to determine the electric conductivity, numerical calculations are necessary to obtain the values of $A_x^{(0)}$ and $A_x^{(1)}$ on hairy black hole backgrounds with varying temperatures for different values of λ. In Fig. (4.10), we observe the expected behavior of the conductivity, specifically the real part of σ. As the coupling of the scalar field with the GB invariant strengthens, it increases to unity, indicating a weaker conductivity. Ultimately, the system mimics the behavior of a metal at a fixed temperature.

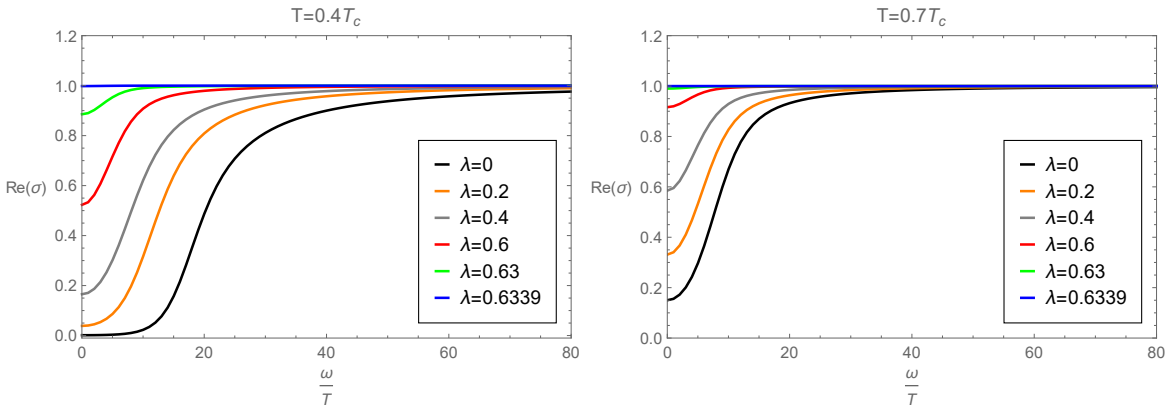

Figure 4.10: The real part of optical conductivity, $Re(\sigma)$, as the function of $\frac{\omega}{T}$ at the temperature $0.4T_c$ and $0.7T_c$, respectively.

We can also examine the conductivity's behavior at extremely low frequencies. When $T < T_c$, the real part of the conductivity exhibits a delta function at zero frequency, while the imaginary part displays a pole. These features can be attributed to the Kramers-Kronig relations:

$$\mathrm{Im}(\sigma(\omega)) = -\frac{1}{\pi}\mathcal{P}\int_{-\infty}^{\infty}\frac{\mathrm{Re}(\sigma(\omega'))}{\omega' - \omega}d\omega'. \tag{4.48}$$

In more detail, as ω approaches zero, the imaginary part behaves as $\mathrm{Im}(\sigma) \sim n_s/\omega$. According to the Kramers-Kronig relations, the real part takes the form $\mathrm{Re}(\sigma) \sim \pi n_s \delta(\omega)$. Here, the coefficient n_s of the delta function is defined as the superfluid density. By fitting data near the critical temperature, we observe that the superfluid density exhibits the following behavior with various couplings:

$$n_s \simeq C_1 T_c (1 - T/T_c), \tag{4.49}$$

meaning that the n_s vanishes linearly as T approaches T_c. The different values of the coefficient C_1 are presented in Table (4.1). C_1 decreases significantly, resulting in the suppression of the superfluid density as the coupling increases. This trend aligns with the condensation depicted in Fig. (4.9), where a stronger coupling corresponds to a reduced condensation gap.

λ	0	0.2	0.4	0.6	0.63	0.633	0.6339
C_1	16.92	10.95	4.04	0.46	0.09	0.04	0.01

Table 4.1: The coefficient C_1 of the superfluid density near the critical temperature for different coupling.

4.4 Conclusions

In this chapter, we conducted a holographic investigation of the scalarization mechanism in two EsGB theories featuring a negative cosmological constant. When the scalar field is neutral, increasing the coupling constant λ sufficiently triggers tachyonic instabilities, leading to the formation of a hairy black hole. We numerically constructed this scalarized solution in the bulk theory. According to gauge/gravity duality, the emergence of a hairy black hole in the bulk corresponds to non-zero condensation, resembling a certain holographic phase transition in the dual boundary theory, despite occurring without any symmetry breaking. Subsequently, we explored this phase transition by computing the $\lambda-$dependent vacuum expectation value of the dual scalar operator and the entanglement entropy in the boundary theory. The observed properties indicate a quantum-type phase transition.

In the other case, we investigated an EsGB theory featuring an electromagnetic field and a real charged scalar field. Holographic scalarization was observed below a critical temperature. We analyzed the scalar condensation and the optical conductivity. The results also revealed a critical value of the coupling constant beyond which the background solution remains stable under small linear perturbations, implying the absence of a holographic superconducting phase transition on the boundary. This phenomenon can be attributed to the strengthening gravitational attraction from the Gauss-Bonnet high curvature term above λ_{cc}, rendering the formation of a scalarized black hole unfeasible.

In conclusion, the stability analysis indicates that the combined effect of two different scalarization mechanisms (interaction between the scalar field and the Gauss-Bonnet curvature correction and interaction between the scalar and the $U(1)$ electromagnetic field) accommodates a broader and deeper effective mass, expediting the formation of hairy black holes. Correspondingly, in the boundary theory, we demonstrated that above a certain critical temperature, only a specific phase transition induced by a sufficiently large coupling constant could occur, resulting in the formation

of scalar hair. However, when the temperature drops below a critical value, holographic superconducting condensation comes into play, exerting combined stronger effects on the formation of hairy black holes.

Chapter 5

Conclusions

Experimental and observational data have established GR as the most successful framework for describing gravitational interaction during the last century. However, this overwhelming evidence falls in its vast majority under the weak gravitational field regime, leaving an unexplored gap in the strong field regime. Similarly, at large scales, there are still some unanswered questions, such as the cosmological constant problem, the Hubble tension, and the nature of dark matter and dark energy, which strongly suggest the existence of a more fundamental theory. Although there are already many proposed quantum gravity theories, they are incomplete. They still need to overcome major conceptual problems and be tested at scales whose realization is not promising. Such theories suggest that GR acquires additional degrees of freedom besides the metric ones at the low-energy limit.

Following these clues and given the lack of a complete theory of quantum gravity, MToG emerges as a modest response to face the current challenges of gravitational physics. In general, an MToG can be seen as an effective field theory of an underlying fundamental theory. In particular, scalar-tensor theories have attracted much attention regarding their applications to issues in cosmology. On the other hand, given the imminent gravitational wave astronomy, compact objects are suitable for exploring scalar-tensor theories in strong-field regimes.

In this context, it has been recently shown that scalar-tensor theories can predict strong gravity phase transitions, commonly called spontaneous scalarization. Scalar-tensor theories usually admit black hole or star solutions that are different from the corresponding vacuum solution. When the effective mass for the scalar mode is tachyonic, the vacuum solution becomes unstable in regions of strong curvature, while the stable black hole or star acquires scalar hair.

This research has contributed to the exploration of black hole scalarization in scalar-tensor theories of gravity, particularly focusing on the role of the electromagnetic field and the exploration of holographic aspects.

In Chapter 2 of this research, we extended existing investigations on black hole scalarization induced by curvature by incorporating an electromagnetic field. A non-minimally coupled scalar field with the Gauss-Bonnet invariant led to the discovery of tachyonic instabilities under small linear perturbations, causing a phase transition from Reissner-Nordström black holes to scalarized charged black holes. These scalarized black holes, characterized by mass M, electric charge Q, and scalar charge D, displayed significant deviations from GR in strong field regimes while remaining almost indistinguishable in weak field regimes.

The presence of the electromagnetic field shifted the bifurcation point of the scalarized branches of black hole solutions to larger masses while the branches themselves became shorter and narrower. In some cases, there are two bifurcation points. The second bifurcation point of the scalarized charged branches may be located at the trivial branch of solutions, meaning that a scalarized charged black hole may merge with the Reissner-Nordström black hole again, indicating a phase transition through a mechanism of de-scalarization.

The thermodynamic analysis revealed that scalarized black holes have a smaller horizon area, higher entropy, and higher temperature than their GR counterparts, indicating their thermodynamic preferability and enhanced radiation emission.

In Chapter 3, we analyzed matter-induced scalarization in the EMs model with higher derivative gauge field corrections. The interaction between the scalar field and the electromagnetic field describes a scenario in which black holes interact with surrounding matter, leading to tachyonic instabilities that trigger the formation of scalarized black hole solutions. As this interaction becomes stronger, the domain of existence for scalarized solutions expands, introducing new physics beyond GR.

The new scalarized branches of charged black hole solutions bifurcate from the trivial one at a specific electric charge to mass ratio $q_{\text{exist}} < 1$ and extend to overcharged configurations. This implies that scalarized charged black holes may carry more electric charge than their mass, violating the extremality condition. The divergence of the Kretschmann scalar at the horizon indicates that the endpoint of each scalarized branch exhibits a naked singularity at a particular electric charge to mass ratio $q_{\text{crit}} > 1$.

We investigated the thermodynamic properties of the obtained scalarized charged black holes. By examining their temperature, we found a critical value of the electric charge-to-mass ratio at which the scalarized black holes reach a maximum temperature. The area of the nontrivial solutions is larger compared to the area of the RN black hole, as well as the area of the scalarized charged black holes without the higher derivative gauge field corrections. This indicates thermodynamic preferability over the solutions in the existing literature.

In Chapter 4, we conducted a holographic investigation of scalarization in EsGB theories with a negative cosmological constant, where a scalar field is nonminimally coupled with the Gauss-Bonnet invariant. According to gauge/gravity duality, a black hole in AdS spacetime on the gravity side is holographically dual to a particular state in the dual CFT. Thus, a trivial black hole without a scalar charge and a scalarized black hole can be assumed to correspond to different states in the boundary CFT. We performed this analysis in two separate cases: in the first case, we considered the absence of an electromagnetic field and the presence of a neutral scalar field; in the second case, we considered the presence of an electromagnetic field and an electrically charged scalar field.

In the first case, the planar Schwarzschild-AdS black hole was the vacuum solution of the theory under consideration. By increasing the coupling constant λ sufficiently beyond a critical value, the effective potential of the nonminimally coupled neutral scalar field became deep enough for the scalar field to grow over time, resulting in tachyonic instabilities, which indicated the formation of scalarized black holes in the bulk theory. This corresponded to a quantum-type phase transition in the dual boundary theory, as indicated by the sharp increase in the vacuum expectation value of the dual scalar operator, showing the condensation of hair.

Moreover, we explored the entanglement entropy, which increased rapidly when the coupling constant exceeded a critical value λ_c. Entanglement entropy serves as a measure of the degrees of freedom within a system. The introduction of the scalar field increased the degrees of freedom, thereby increasing the entropy after scalarization. This behavior contrasted significantly with that observed in holographic superconductors, where the hairy superconducting state typically exhibited lower entropy than the normal state because the emergence of Cooper pairs in the superconducting state reduced the degrees of freedom of the system. Therefore, the scalarization mechanism could not be interpreted as a superconducting phase transition holographically.

In the second case, when considering an EsGB theory with an electromagnetic field and a charged scalar field, scalarization was observed below a critical temperature, revealing a phase transition akin to holographic superconductivity. Our findings demonstrate that the interaction between the scalar field and both the Gauss-Bonnet curvature correction and the $U(1)$ electromagnetic field accommodates a wider and deeper effective potential, triggering the formation of hairy black holes. Correspondingly, in the boundary theory, we showed that when the temperature drops below a critical value, the holographic superconducting condensation participates, and the combined effects of the couplings are stronger on the formation of hairy black holes. When the coupling constant exceeds a critical value, the divergence of the critical temperature implies that a hairy black hole can not form. At the same time, in the CFT, there is no holographic superconducting phase. The optical conductivity and the superfluid density were calculated, showing that as the coupling constant exceeds the corresponding critical value at the gravity theory, then the system is dual to a metal at a fixed temperature.

This research reveals new physics beyond GR by highlighting the role of the intricate interaction between scalar fields, electromagnetic fields, and curvature corrections in generating new nontrivial black hole solutions. These results enhance our understanding of the scalarization mechanisms, providing valuable insights for future research in modified theories of gravity and developing theoretical models that can describe astrophysical black holes.

Bibliography

[1] D. D. Doneva, S. Kiorpelidi, P. G. Nedkova, E. Papantonopoulos, and S. S. Yazadjiev, "Charged Gauss-Bonnet black holes with curvature induced scalarization in the extended scalar-tensor theories," *Phys. Rev. D* **98** no. 10, (2018) 104056, arXiv:1809.00844 [gr-qc].

[2] H. Guo, S. Kiorpelidi, X.-M. Kuang, E. Papantonopoulos, B. Wang, and J.-P. Wu, "Spontaneous holographic scalarization of black holes in Einstein-scalar-Gauss-Bonnet theories," *Phys. Rev. D* **102** no. 8, (2020) 084029, arXiv:2006.10659 [hep-th].

[3] S. Kiorpelidi, T. Karakasis, G. Koutsoumbas, and E. Papantonopoulos, "Scalarization of the Reissner-Nordström black hole with higher derivative gauge field corrections," *Phys. Rev. D* **109** no. 2, (2024) 024033, arXiv:2311.10858 [gr-qc].

[4] S. Kiorpelidi, G. Koutsoumbas, A. Machattou, and E. Papantonopoulos, "Topological black holes with curvature induced scalarization in the extended scalar-tensor theories," *Phys. Rev. D* **105** no. 10, (2022) 104039, arXiv:2202.00655 [gr-qc].

[5] S. Bahamonde, V. Gakis, S. Kiorpelidi, T. Koivisto, J. Levi Said, and E. N. Saridakis, "Cosmological perturbations in modified teleparallel gravity models: Boundary term extension," *Eur. Phys. J. C* **81** no. 1, (2021) 53, arXiv:2009.02168 [gr-qc].

[6] A. Einstein, "The foundation of the general theory of relativity.," *Annalen Phys.* **49** no. 7, (1916) 769–822.

[7] E. Mach, *The Science of Mechanics: A Critical and Historical Exposition of its Principles*. Cambridge Library Collection - Physical Sciences. Cambridge University Press, 2013.

[8] A. Einstein, "On the relativity principle and the conclusions drawn from it," 1907.

[9] A. Einstein, "The Formal Foundation of the General Theory of Relativity," *Sitzungsber. Preuss. Akad. Wiss. Berlin (Math. Phys.)* **1914** (1914) 1030–1085.

[10] S. M. Carroll, *Spacetime and Geometry: An Introduction to General Relativity*. Cambridge University Press, 7, 2019.

[11] D. Hilbert, "Die Grundlagen der Physik. 1.," *Gott. Nachr.* **27** (1915) 395–407.

[12] T. P. Sotiriou, V. Faraoni, and S. Liberati, "Theory of gravitation theories: A No-progress report," *Int. J. Mod. Phys. D* **17** (2008) 399–423, arXiv:0707.2748 [gr-qc].

[13] E. Di Casola, S. Liberati, and S. Sonego, "Weak equivalence principle for self-gravitating bodies: A sieve for purely metric theories of gravity," *Phys. Rev. D* **89** no. 8, (2014) 084053, arXiv:1401.0030 [gr-qc].

[14] K. Schwarzschild, "On the gravitational field of a sphere of incompressible fluid according to Einstein's theory," *Sitzungsber. Preuss. Akad. Wiss. Berlin (Math. Phys.)* **1916** (1916) 424–434, arXiv:physics/9912033.

[15] M. D. Kruskal, "Maximal extension of Schwarzschild metric," *Phys. Rev.* **119** (1960) 1743–1745.

[16] P. Chruściel, *Elements of General Relativity*. 01, 2019.

[17] H. Reissner, "Über die Eigengravitation des elektrischen Feldes nach der Einsteinschen Theorie," *Annalen Phys.* **355** no. 9, (1916) 106–120.

[18] G. Nordström, "On the Energy of the Gravitation field in Einstein's Theory," *Koninklijke Nederlandse Akademie van Wetenschappen Proceedings Series B Physical Sciences* **20** (Jan., 1918) 1238–1245.

[19] R. Penrose, "Gravitational collapse: The role of general relativity," *Riv. Nuovo Cim.* **1** (1969) 252–276.

[20] W. Israel, "Event horizons in static electrovac space-times," *Commun. Math. Phys.* **8** (1968) 245–260.

[21] M. Heusler, *Uniqueness theorems for nonrotating holes*, p. 140{165. Cambridge Lecture Notes in Physics. Cambridge University Press, 1996.

[22] R. P. Kerr, "Gravitational field of a spinning mass as an example of algebraically special metrics," *Phys. Rev. Lett.* **11** (Sep, 1963) 237–238. https://link.aps.org/doi/10.1103/PhysRevLett.11.237.

[23] P. R. Capelo, *Astrophysical black holes*, ch. Chapter 1, pp. 1–22. https://www.worldscientific.com/doi/abs/10.1142/9789813227958_0001.

[24] Y. Cui *et al.*, "Precessing jet nozzle connecting to a spinning black hole in M87," *Nature* **621** (2023) 711–715, arXiv:2310.09015 [astro-ph.HE].

[25] E. T. Newman, R. Couch, K. Chinnapared, A. Exton, A. Prakash, and R. Torrence, "Metric of a Rotating, Charged Mass," *J. Math. Phys.* **6** (1965) 918–919.

[26] D. C. Robinson, "Uniqueness of the Kerr black hole," *Phys. Rev. Lett.* **34** (1975) 905–906.

[27] P. T. Chrusciel, J. Lopes Costa, and M. Heusler, "Stationary Black Holes: Uniqueness and Beyond," *Living Rev. Rel.* **15** (2012) 7, arXiv:1205.6112 [gr-qc].

[28] R. Ruffini and J. A. Wheeler, "Introducing the black hole," *Phys. Today* **24** no. 1, (1971) 30.

[29] J. D. Bekenstein, "Transcendence of the law of baryon-number conservation in black-hole physics," *Phys. Rev. Lett.* **28** (Feb, 1972) 452–455. https://link.aps.org/doi/10.1103/PhysRevLett.28.452.

[30] J. D. Bekenstein, "Black holes and entropy," *Phys. Rev. D* **7** (1973) 2333–2346.

[31] S. W. Hawking, "Particle Creation by Black Holes," *Commun. Math. Phys.* **43** (1975) 199–220. [Erratum: Commun.Math.Phys. 46, 206 (1976)].

[32] J. M. Bardeen, B. Carter, and S. W. Hawking, "The Four laws of black hole mechanics," *Commun. Math. Phys.* **31** (1973) 161–170.

[33] C. M. Will, "The Confrontation between General Relativity and Experiment," *Living Rev. Rel.* **17** (2014) 4, arXiv:1403.7377 [gr-qc].

[34] P. G. Roll, R. Krotkov, and R. H. Dicke, "The Equivalence of inertial and passive gravitational mass," *Annals Phys.* **26** (1964) 442–517.

[35] S. Schlamminger, K. Y. Choi, T. A. Wagner, J. H. Gundlach, and E. G. Adelberger, "Test of the equivalence principle using a rotating torsion balance," *Phys. Rev. Lett.* **100** (2008) 041101, arXiv:0712.0607 [gr-qc].

[36] A. A. Michelson and E. W. Morley, "On the Relative Motion of the Earth and the Luminiferous Ether," *Am. J. Sci.* **34** (1887) 333–345.

[37] B. Rossi and D. B. Hall, "Variation of the Rate of Decay of Mesotrons with Momentum," *Phys. Rev.* **59** (1941) 223–228.

[38] R. F. C. Vessot *et al.*, "Test of Relativistic Gravitation with a Space-Borne Hydrogen Maser," *Phys. Rev. Lett.* **45** (1980) 2081–2084.

[39] M. Fischer *et al.*, "New limits on the drift of fundamental constants from laboratory measurements," *Phys. Rev. Lett.* **92** (2004) 230802, arXiv:physics/0312086.

[40] F. W. Dyson, A. S. Eddington, and C. Davidson, "A Determination of the Deflection of Light by the Sun's Gravitational Field, from Observations Made at the Total Eclipse of May 29, 1919," *Phil. Trans. Roy. Soc. Lond. A* **220** (1920) 291–333.

[41] D. Walsh, R. F. Carswell, and R. J. Weymann, "0957 + 561 A, B - Twin quasistellar objects or gravitational lens," *Nature* **279** (1979) 381–384.

[42] A. van der Wel *et al.*, "Discovery of a Quadruple Lens in CANDELS with a Record Lens Redshift z = 1.53," *Astrophys. J. Lett.* **777** (2013) L17, arXiv:1309.2826 [astro-ph.CO].

[43] A. Einstein, "Explanation of the Perihelion Motion of Mercury from the General Theory of Relativity," *Sitzungsber. Preuss. Akad. Wiss. Berlin (Math. Phys.)* **1915** (1915) 831–839.

[44] R. S. Park, W. M. Folkner, A. S. Konopliv, J. G. Williams, D. E. Smith, and M. T. Zuber, "Precession of Mercury's Perihelion from Ranging to the MESSENGER Spacecraft," *Astron. J.* **153** no. 3, (2017) 121.

[45] C. W. F. Everitt *et al.*, "Gravity Probe B: Final Results of a Space Experiment to Test General Relativity," *Phys. Rev. Lett.* **106** (2011) 221101, arXiv:1105.3456 [gr-qc].

[46] M. A. Barstow, H. E. Bond, J. B. Holberg, M. R. Burleigh, I. Hubeny, and D. Koester, "Hubble Space Telescope spectroscopy of the Balmer lines in Sirius B," *Mon. Not. Roy. Astron. Soc.* **362** (2005) 1134–1142, arXiv:astro-ph/0506600.

[47] R. Colella, A. W. Overhauser, and S. A. Werner, "Observation of gravitationally induced quantum interference," *Phys. Rev. Lett.* **34** (1975) 1472–1474.

[48] **GRAVITY** Collaboration, R. Abuter *et al.*, "Detection of the gravitational redshift in the orbit of the star S2 near the Galactic centre massive black hole," *Astron. Astrophys.* **615** (2018) L15, arXiv:1807.09409 [astro-ph.GA].

[49] **LIGO Scientific, Virgo** Collaboration, B. P. Abbott *et al.*, "Observation of Gravitational Waves from a Binary Black Hole Merger," *Phys. Rev. Lett.* **116** no. 6, (2016) 061102, arXiv:1602.03837 [gr-qc].

[50] **LIGO Scientific, Virgo** Collaboration, B. P. Abbott *et al.*, "GWTC-1: A Gravitational-Wave Transient Catalog of Compact Binary Mergers Observed by LIGO and Virgo during the First and Second Observing Runs," *Phys. Rev. X* **9** no. 3, (2019) 031040, arXiv:1811.12907 [astro-ph.HE].

[51] **LIGO Scientific, Virgo** Collaboration, B. P. Abbott *et al.*, "GW190425: Observation of a Compact Binary Coalescence with Total Mass $\sim 3.4 M_{\odot}$," *Astrophys. J. Lett.* **892** no. 1, (2020) L3, arXiv:2001.01761 [astro-ph.HE].

[52] **LIGO Scientific, Virgo** Collaboration, R. Abbott *et al.*, "GW190412: Observation of a Binary-Black-Hole Coalescence with Asymmetric Masses," *Phys. Rev. D* **102** no. 4, (2020) 043015, arXiv:2004.08342 [astro-ph.HE].

[53] **Event Horizon Telescope** Collaboration, K. Akiyama *et al.*, "First M87 Event Horizon Telescope Results. I. The Shadow of the Supermassive Black Hole," *Astrophys. J. Lett.* **875** (2019) L1, arXiv:1906.11238 [astro-ph.GA].

[54] **Event Horizon Telescope** Collaboration, K. Akiyama *et al.*, "First M87 Event Horizon Telescope Results. II. Array and Instrumentation," *Astrophys. J. Lett.* **875** no. 1, (2019) L2, arXiv:1906.11239 [astro-ph.IM].

[55] **Event Horizon Telescope** Collaboration, K. Akiyama *et al.*, "First M87 Event Horizon Telescope Results. III. Data Processing and Calibration," *Astrophys. J. Lett.* **875** no. 1, (2019) L3, arXiv:1906.11240 [astro-ph.GA].

[56] **Event Horizon Telescope** Collaboration, K. Akiyama *et al.*, "First M87 Event Horizon Telescope Results. IV. Imaging the Central Supermassive Black Hole," *Astrophys. J. Lett.* **875** no. 1, (2019) L4, arXiv:1906.11241 [astro-ph.GA].

[57] **Event Horizon Telescope** Collaboration, K. Akiyama *et al.*, "First M87 Event Horizon Telescope Results. V. Physical Origin of the Asymmetric Ring," *Astrophys. J. Lett.* **875** no. 1, (2019) L5, arXiv:1906.11242 [astro-ph.GA].

[58] **Event Horizon Telescope** Collaboration, K. Akiyama *et al.*, "First M87 Event Horizon Telescope Results. VI. The Shadow and Mass of the Central Black Hole," *Astrophys. J. Lett.* **875** no. 1, (2019) L6, arXiv:1906.11243 [astro-ph.GA].

[59] K. G. Wilson and J. B. Kogut, "The Renormalization group and the epsilon expansion," *Phys. Rept.* **12** (1974) 75–199.

[60] A. Shomer, "A Pedagogical explanation for the non-renormalizability of gravity," arXiv:0709.3555 [hep-th].

[61] B. Zwiebach, *A first course in string theory*. Cambridge University Press, 7, 2006.

[62] E. P. Verlinde, "Emergent Gravity and the Dark Universe," *SciPost Phys.* **2** no. 3, (2017) 016, arXiv:1611.02269 [hep-th].

[63] M. Niedermaier and M. Reuter, "The Asymptotic Safety Scenario in Quantum Gravity," *Living Rev. Rel.* **9** (2006) 5–173.

[64] P. A. M. Casares, "A review on Loop Quantum Gravity," arXiv:1808.01252 [gr-qc].

[65] R. Penrose, "Gravitational collapse and space-time singularities," *Phys. Rev. Lett.* **14** (1965) 57–59.

[66] **Supernova Search Team** Collaboration, A. G. Riess *et al.*, "Observational evidence from supernovae for an accelerating universe and a cosmological constant," *Astron. J.* **116** (1998) 1009–1038, arXiv:astro-ph/9805201.

[67] **Supernova Cosmology Project** Collaboration, S. Perlmutter *et al.*, "Measurements of Ω and Λ from 42 High Redshift Supernovae," *Astrophys. J.* **517** (1999) 565–586, arXiv:astro-ph/9812133.

[68] **Planck** Collaboration, P. A. R. Ade *et al.*, "Planck 2015 results. XIII. Cosmological parameters," *Astron. Astrophys.* **594** (2016) A13, arXiv:1502.01589 [astro-ph.CO].

[69] P. J. E. Peebles and B. Ratra, "The Cosmological Constant and Dark Energy," *Rev. Mod. Phys.* **75** (2003) 559–606, arXiv:astro-ph/0207347.

[70] R. R. Caldwell, R. Dave, and P. J. Steinhardt, "Cosmological imprint of an energy component with general equation of state," *Phys. Rev. Lett.* **80** (1998) 1582–1585, arXiv:astro-ph/9708069.

[71] T. Clifton, P. G. Ferreira, A. Padilla, and C. Skordis, "Modified Gravity and Cosmology," *Phys. Rept.* **513** (2012) 1–189, arXiv:1106.2476 [astro-ph.CO].

[72] D. Lovelock, "The Einstein tensor and its generalizations," *J. Math. Phys.* **12** (1971) 498–501.

[73] D. Lovelock, "The four-dimensionality of space and the einstein tensor," *J. Math. Phys.* **13** (1972) 874–876.

[74] D. Bailin and A. Love, "KALUZA-KLEIN THEORIES," *Rept. Prog. Phys.* **50** (1987) 1087–1170.

[75] T. Mohaupt, "Introduction to string theory," *Lect. Notes Phys.* **631** (2003) 173–251, arXiv:hep-th/0207249.

[76] J. M. Ezquiaga and M. Zumalacárregui, "Dark Energy in light of Multi-Messenger Gravitational-Wave astronomy," *Front. Astron. Space Sci.* **5** (2018) 44, arXiv:1807.09241 [astro-ph.CO].

[77] E. Berti *et al.*, "Testing General Relativity with Present and Future Astrophysical Observations," *Class. Quant. Grav.* **32** (2015) 243001, arXiv:1501.07274 [gr-qc].

[78] G. R. Dvali, G. Gabadadze, and M. Porrati, "4-D gravity on a brane in 5-D Minkowski space," *Phys. Lett. B* **485** (2000) 208–214, arXiv:hep-th/0005016.

[79] A. Nicolis and R. Rattazzi, "Classical and quantum consistency of the DGP model," *JHEP* **06** (2004) 059, arXiv:hep-th/0404159.

[80] P. Horava, "Quantum Gravity at a Lifshitz Point," *Phys. Rev. D* **79** (2009) 084008, arXiv:0901.3775 [hep-th].

[81] T. Jacobson, "Einstein-aether gravity: A Status report," *PoS* **QG-PH** (2007) 020, arXiv:0801.1547 [gr-qc].

[82] S. Deser and R. P. Woodard, "Nonlocal Cosmology," *Phys. Rev. Lett.* **99** (2007) 111301, arXiv:0706.2151 [astro-ph].

[83] T. Koivisto, "Dynamics of Nonlocal Cosmology," *Phys. Rev. D* **77** (2008) 123513, arXiv:0803.3399 [gr-qc].

[84] M. Jaccard, M. Maggiore, and E. Mitsou, "Nonlocal theory of massive gravity," *Phys. Rev. D* **88** no. 4, (2013) 044033, arXiv:1305.3034 [hep-th].

[85] M. Fierz and W. Pauli, "On relativistic wave equations for particles of arbitrary spin in an electromagnetic field," *Proc. Roy. Soc. Lond. A* **173** (1939) 211–232.

[86] K. Hinterbichler, "Theoretical Aspects of Massive Gravity," *Rev. Mod. Phys.* **84** (2012) 671–710, arXiv:1105.3735 [hep-th].

[87] Y.-F. Cai, S. Capozziello, M. De Laurentis, and E. N. Saridakis, "f(T) teleparallel gravity and cosmology," *Rept. Prog. Phys.* **79** no. 10, (2016) 106901, arXiv:1511.07586 [gr-qc].

[88] S. F. Hassan and R. A. Rosen, "Bimetric Gravity from Ghost-free Massive Gravity," *JHEP* **02** (2012) 126, arXiv:1109.3515 [hep-th].

[89] K. Hinterbichler and R. A. Rosen, "Interacting Spin-2 Fields," *JHEP* **07** (2012) 047, arXiv:1203.5783 [hep-th].

[90] A. Proca, "Sur la theorie ondulatoire des electrons positifs et negatifs," *J. Phys. Radium* **7** (1936) 347–353.

[91] L. Heisenberg, "Generalization of the Proca Action," *JCAP* **05** (2014) 015, arXiv:1402.7026 [hep-th].

[92] R. Kimura, A. Naruko, and D. Yoshida, "Extended vector-tensor theories," *JCAP* **01** (2017) 002, arXiv:1608.07066 [gr-qc].

[93] C. H. Brans, "The Roots of scalar-tensor theory: An Approximate history," in *Santa Clara 2004: 1st International Workshop on Gravitation and Cosmology*. 6, 2005. arXiv:gr-qc/0506063.

[94] G. W. Horndeski, "Second-order scalar-tensor field equations in a four-dimensional space," *Int. J. Theor. Phys.* **10** (1974) 363–384.

[95] C. Brans and R. H. Dicke, "Mach's principle and a relativistic theory of gravitation," *Phys. Rev.* **124** (1961) 925–935.

[96] D. Langlois and K. Noui, "Degenerate higher derivative theories beyond Horndeski: evading the Ostrogradski instability," *JCAP* **02** (2016) 034, arXiv:1510.06930 [gr-qc].

[97] L. Heisenberg, "A systematic approach to generalisations of General Relativity and their cosmological implications," *Phys. Rept.* **796** (2019) 1–113, arXiv:1807.01725 [gr-qc].

[98] C. A. R. Herdeiro and E. Radu, "Asymptotically flat black holes with scalar hair: a review," *Int. J. Mod. Phys. D* **24** no. 09, (2015) 1542014, arXiv:1504.08209 [gr-qc].

[99] E. E. Flanagan, "The Conformal frame freedom in theories of gravitation," *Class. Quant. Grav.* **21** (2004) 3817, arXiv:gr-qc/0403063.

[100] S. W. Hawking, "Black holes in the Brans-Dicke theory of gravitation," *Commun. Math. Phys.* **25** (1972) 167–171.

[101] T. P. Sotiriou and V. Faraoni, "Black holes in scalar-tensor gravity," *Phys. Rev. Lett.* **108** (2012) 081103, arXiv:1109.6324 [gr-qc].

[102] T. Zannias, "Black holes cannot support conformal scalar hair," *J. Math. Phys.* **36** (1995) 6970–6980, arXiv:gr-qc/9409030.

[103] A. Saa, "New no scalar hair theorem for black holes," *J. Math. Phys.* **37** (1996) 2346–2351, arXiv:gr-qc/9601021.

[104] A. Saa, "Searching for nonminimally coupled scalar hairs," *Phys. Rev. D* **53** (1996) 7377–7380, arXiv:gr-qc/9602061.

[105] C. Deffayet, X. Gao, D. A. Steer, and G. Zahariade, "From k-essence to generalised Galileons," *Phys. Rev. D* **84** (2011) 064039, arXiv:1103.3260 [hep-th].

[106] T. Kobayashi, M. Yamaguchi, and J. Yokoyama, "Generalized G-inflation: Inflation with the most general second-order field equations," *Prog. Theor. Phys.* **126** (2011) 511–529, arXiv:1105.5723 [hep-th].

[107] L. Hui and A. Nicolis, "No-Hair Theorem for the Galileon," *Phys. Rev. Lett.* **110** (2013) 241104, arXiv:1202.1296 [hep-th].

[108] P. Breitenlohner, P. Forgacs, and D. Maison, "On Static spherically symmetric solutions of the Einstein Yang-Mills equations," *Commun. Math. Phys.* **163** (1994) 141–172.

[109] J. D. Bekenstein, "Novel "no-scalar-hair" theorem for black holes," *Phys. Rev. D* **51** no. 12, (1995) R6608.

[110] J. Skakala and S. Shankaranarayanan, "No minimally coupled scalar black hole hair in Lanczos-Lovelock gravity," *Class. Quant. Grav.* **31** (2014) 175005, arXiv:1402.6166 [gr-qc].

[111] T. Hertog, "Towards a Novel no-hair Theorem for Black Holes," *Phys. Rev. D* **74** (2006) 084008, arXiv:gr-qc/0608075.

[112] E. Witten, "A Simple Proof of the Positive Energy Theorem," *Commun. Math. Phys.* **80** (1981) 381.

[113] M. Heusler, "A Mass bound for spherically symmetric black hole space-times," *Class. Quant. Grav.* **12** (1995) 779–790, arXiv:gr-qc/9411054.

[114] I. Pena and D. Sudarsky, "Do collapsed boson stars result in new types of black holes?," *Class. Quant. Grav.* **14** (1997) 3131–3134.

[115] A. A. H. Graham and R. Jha, "Nonexistence of black holes with noncanonical scalar fields," *Phys. Rev. D* **89** no. 8, (2014) 084056, arXiv:1401.8203 [gr-qc]. [Erratum: Phys.Rev.D 92, 069901 (2015)].

[116] H. Dennhardt and O. Lechtenfeld, "Scalar deformations of Schwarzschild holes and their stability," *Int. J. Mod. Phys. A* **13** (1998) 741–764, arXiv:gr-qc/9612062.

[117] M. Cadoni and E. Franzin, "Asymptotically flat black holes sourced by a massless scalar field," *Phys. Rev. D* **91** no. 10, (2015) 104011, arXiv:1503.04734 [gr-qc].

[118] O. Bechmann and O. Lechtenfeld, "Exact black hole solution with selfinteracting scalar field," *Class. Quant. Grav.* **12** (1995) 1473–1482, arXiv:gr-qc/9502011.

[119] A. Anabalon, D. Astefanesei, and R. Mann, "Exact asymptotically flat charged hairy black holes with a dilaton potential," *JHEP* **10** (2013) 184, arXiv:1308.1693 [hep-th].

[120] A. Anabalon and J. Oliva, "Exact Hairy Black Holes and their Modification to the Universal Law of Gravitation," *Phys. Rev. D* **86** (2012) 107501, arXiv:1205.6012 [gr-qc].

[121] K. A. Bronnikov and G. N. Shikin, "Spherically symmetric scalar vacuum: No go theorems, black holes and solitons," *Grav. Cosmol.* **8** (2002) 107–116, arXiv:gr-qc/0109027.

[122] K. G. Zloshchastiev, "On co-existence of black holes and scalar field," *Phys. Rev. Lett.* **94** (2005) 121101, arXiv:hep-th/0408163.

[123] S. S. Gubser, "Phase transitions near black hole horizons," *Class. Quant. Grav.* **22** (2005) 5121–5144, arXiv:hep-th/0505189.

[124] B. Kleihaus, J. Kunz, E. Radu, and B. Subagyo, "Axially symmetric static scalar solitons and black holes with scalar hair," *Phys. Lett. B* **725** (2013) 489–494, arXiv:1306.4616 [gr-qc].

[125] U. Nucamendi and M. Salgado, "Scalar hairy black holes and solitons in asymptotically flat space-times," *Phys. Rev. D* **68** (2003) 044026, arXiv:gr-qc/0301062.

[126] A. Corichi, U. Nucamendi, and M. Salgado, "Scalar hairy black holes and scalarons in the isolated horizons formalism," *Phys. Rev. D* **73** (2006) 084002, arXiv:gr-qc/0504126.

[127] N. M. Bocharova, K. A. Bronnikov, and V. N. Melnikov, " ,".

[128] T. P. Sotiriou and S.-Y. Zhou, "Black hole hair in generalized scalar-tensor gravity: An explicit example," *Phys. Rev. D* **90** (2014) 124063, arXiv:1408.1698 [gr-qc].

[129] T. Torii, H. Yajima, and K.-i. Maeda, "Dilatonic black holes with Gauss-Bonnet term," *Phys. Rev. D* **55** (1997) 739–753, arXiv:gr-qc/9606034.

[130] S. O. Alexeev and M. V. Pomazanov, "Black hole solutions with dilatonic hair in higher curvature gravity," *Phys. Rev. D* **55** (1997) 2110–2118, arXiv:hep-th/9605106.

[131] P. Kanti, N. E. Mavromatos, J. Rizos, K. Tamvakis, and E. Winstanley, "Dilatonic black holes in higher curvature string gravity," *Phys. Rev. D* **54** (1996) 5049–5058, arXiv:hep-th/9511071.

[132] D. Ayzenberg and N. Yunes, "Slowly-Rotating Black Holes in Einstein-Dilaton-Gauss-Bonnet Gravity: Quadratic Order in Spin Solutions," *Phys. Rev. D* **90** (2014) 044066, arXiv:1405.2133 [gr-qc]. [Erratum: Phys.Rev.D 91, 069905 (2015)].

[133] B. Kleihaus, J. Kunz, and E. Radu, "Rotating Black Holes in Dilatonic Einstein-Gauss-Bonnet Theory," *Phys. Rev. Lett.* **106** (2011) 151104, arXiv:1101.2868 [gr-qc].

[134] G. Esposito-Farese, "Nonperturbative strong field effects in tensor - scalar gravity," in *28th Rencontres de Moriond: Perspectives in Neutrinos, Atomic Physics and Gravitation*, pp. 525–532. 1993.

[135] D. D. Doneva and S. S. Yazadjiev, "New Gauss-Bonnet Black Holes with Curvature-Induced Scalarization in Extended Scalar-Tensor Theories," *Phys. Rev. Lett.* **120** no. 13, (2018) 131103, arXiv:1711.01187 [gr-qc].

[136] H. O. Silva, J. Sakstein, L. Gualtieri, T. P. Sotiriou, and E. Berti, "Spontaneous scalarization of black holes and compact stars from a Gauss-Bonnet coupling," *Phys. Rev. Lett.* **120** no. 13, (2018) 131104, arXiv:1711.02080 [gr-qc].

[137] D. D. Doneva, F. M. Ramazanoğlu, H. O. Silva, T. P. Sotiriou, and S. S. Yazadjiev, "Spontaneous scalarization," *Rev. Mod. Phys.* **96** no. 1, (2024) 015004, arXiv:2211.01766 [gr-qc].

[138] D. D. Doneva, S. S. Yazadjiev, K. D. Kokkotas, and I. Z. Stefanov, "Quasi-normal modes, bifurcations and non-uniqueness of charged scalar-tensor black holes," *Phys. Rev. D* **82** (2010) 064030, arXiv:1007.1767 [gr-qc].

[139] J. L. Blázquez-Salcedo, D. D. Doneva, J. Kunz, and S. S. Yazadjiev, "Radial perturbations of the scalarized Einstein-Gauss-Bonnet black holes," *Phys. Rev. D* **98** no. 8, (2018) 084011, arXiv:1805.05755 [gr-qc].

[140] N. D. Birrell and P. C. W. Davies, *Quantum Fields in Curved Space*. Cambridge Monographs on Mathematical Physics. Cambridge Univ. Press, Cambridge, UK, 2, 1984.

[141] C. A. R. Herdeiro and E. Radu, "Black hole scalarization from the breakdown of scale invariance," *Phys. Rev. D* **99** no. 8, (2019) 084039, arXiv:1901.02953 [gr-qc].

[142] N. Andreou, N. Franchini, G. Ventagli, and T. P. Sotiriou, "Spontaneous scalarization in generalised scalar-tensor theory," *Phys. Rev. D* **99** no. 12, (2019) 124022, arXiv:1904.06365 [gr-qc]. [Erratum: Phys.Rev.D 101, 109903 (2020)].

[143] G. Antoniou, L. Bordin, and T. P. Sotiriou, "Compact object scalarization with general relativity as a cosmic attractor," *Phys. Rev. D* **103** no. 2, (2021) 024012, arXiv:2004.14985 [gr-qc].

[144] G. Antoniou, A. Lehébel, G. Ventagli, and T. P. Sotiriou, "Black hole scalarization with Gauss-Bonnet and Ricci scalar couplings," *Phys. Rev. D* **104** no. 4, (2021) 044002, arXiv:2105.04479 [gr-qc].

[145] G. Antoniou, C. F. B. Macedo, R. McManus, and T. P. Sotiriou, "Stable spontaneously-scalarized black holes in generalized scalar-tensor theories," *Phys. Rev. D* **106** no. 2, (2022) 024029, arXiv:2204.01684 [gr-qc].

[146] I. Z. Stefanov, S. S. Yazadjiev, and M. D. Todorov, "Scalar-tensor black holes coupled to Born-Infeld nonlinear electrodynamics," *Phys. Rev. D* **75** (2007) 084036, arXiv:0704.3784 [gr-qc].

[147] I. Z. Stefanov, S. S. Yazadjiev, and M. D. Todorov, "Phases of 4D scalar-tensor black holes coupled to Born-Infeld nonlinear electrodynamics," *Mod. Phys. Lett. A* **23** (2008) 2915–2931, arXiv:0708.4141 [gr-qc].

[148] M. Born and L. Infeld, "Foundations of the new field theory," *Proc. Roy. Soc. Lond. A* **144** no. 852, (1934) 425–451.

[149] D. Astefanesei, C. Herdeiro, A. Pombo, and E. Radu, "Einstein-Maxwell-scalar black holes: classes of solutions, dyons and extremality," *JHEP* **10** (2019) 078, arXiv:1905.08304 [hep-th].

[150] C. A. R. Herdeiro, E. Radu, N. Sanchis-Gual, and J. A. Font, "Spontaneous Scalarization of Charged Black Holes," *Phys. Rev. Lett.* **121** no. 10, (2018) 101102, arXiv:1806.05190 [gr-qc].

[151] P. G. S. Fernandes, C. A. R. Herdeiro, A. M. Pombo, E. Radu, and N. Sanchis-Gual, "Spontaneous Scalarisation of Charged Black Holes: Coupling Dependence and Dynamical Features," *Class. Quant. Grav.* **36** no. 13, (2019) 134002, arXiv:1902.05079 [gr-qc]. [Erratum: Class.Quant.Grav. 37, 049501 (2020)].

[152] P. G. S. Fernandes, C. A. R. Herdeiro, A. M. Pombo, E. Radu, and N. Sanchis-Gual, "Charged black holes with axionic-type couplings: Classes of solutions and dynamical scalarization," *Phys. Rev. D* **100** no. 8, (2019) 084045, arXiv:1908.00037 [gr-qc].

[153] J. L. Blázquez-Salcedo, C. A. R. Herdeiro, J. Kunz, A. M. Pombo, and E. Radu, "Einstein-Maxwell-scalar black holes: the hot, the cold and the bald," *Phys. Lett. B* **806** (2020) 135493, arXiv:2002.00963 [gr-qc].

[154] W. Heisenberg and H. Euler, "Consequences of Dirac's theory of positrons," *Z. Phys.* **98** no. 11-12, (1936) 714–732, arXiv:physics/0605038.

[155] P. Stehle and P. G. DeBaryshe, "Quantum Electrodynamics and the Correspondence Principle," *Phys. Rev.* **152** no. 4, (1966) 1135.

[156] R. Brito, V. Cardoso, and P. Pani, "Superradiance: New Frontiers in Black Hole Physics," *Lect. Notes Phys.* **906** (2015) pp.1–237, arXiv:1501.06570 [gr-qc].

[157] A. Dima, E. Barausse, N. Franchini, and T. P. Sotiriou, "Spin-induced black hole spontaneous scalarization," *Phys. Rev. Lett.* **125** no. 23, (2020) 231101, arXiv:2006.03095 [gr-qc].

[158] L. G. Collodel, B. Kleihaus, J. Kunz, and E. Berti, "Spinning and excited black holes in Einstein-scalar-Gauss{Bonnet theory," *Class. Quant. Grav.* **37** no. 7, (2020) 075018, arXiv:1912.05382 [gr-qc].

[159] S. Hod, "Onset of spontaneous scalarization in spinning Gauss-Bonnet black holes," *Phys. Rev. D* **102** no. 8, (2020) 084060, arXiv:2006.09399 [gr-qc].

[160] P. V. P. Cunha, C. A. R. Herdeiro, and E. Radu, "Spontaneously Scalarized Kerr Black Holes in Extended Scalar-Tensor{Gauss-Bonnet Gravity," *Phys. Rev. Lett.* **123** no. 1, (2019) 011101, arXiv:1904.09997 [gr-qc].

[161] C. A. R. Herdeiro, E. Radu, H. O. Silva, T. P. Sotiriou, and N. Yunes, "Spin-induced scalarized black holes," *Phys. Rev. Lett.* **126** no. 1, (2021) 011103, arXiv:2009.03904 [gr-qc].

[162] E. Berti, L. G. Collodel, B. Kleihaus, and J. Kunz, "Spin-induced black-hole scalarization in Einstein-scalar-Gauss-Bonnet theory," *Phys. Rev. Lett.* **126** no. 1, (2021) 011104, arXiv:2009.03905 [gr-qc].

[163] L. Annulli, C. A. R. Herdeiro, and E. Radu, "Spin-induced scalarization and magnetic fields," *Phys. Lett. B* **832** (2022) 137227, arXiv:2203.13267 [gr-qc].

[164] P. G. S. Fernandes, C. Burrage, A. Eichhorn, and T. P. Sotiriou, "Shadows and properties of spin-induced scalarized black holes with and without a Ricci coupling," *Phys. Rev. D* **109** no. 10, (2024) 104033, arXiv:2403.14596 [gr-qc].

[165] J. a. M. S. Oliveira and A. M. Pombo, "Spontaneous vectorization of electrically charged black holes," *Phys. Rev. D* **103** no. 4, (2021) 044004, arXiv:2012.07869 [gr-qc].

[166] R. R. Metsaev and A. A. Tseytlin, "Order alpha-prime (Two Loop) Equivalence of the String Equations of Motion and the Sigma Model Weyl Invariance Conditions: Dependence on the Dilaton and the Antisymmetric Tensor," *Nucl. Phys. B* **293** (1987) 385–419.

[167] D. Anninos and G. Pastras, "Thermodynamics of the Maxwell-Gauss-Bonnet anti-de Sitter Black Hole with Higher Derivative Gauge Corrections," *JHEP* **07** (2009) 030, arXiv:0807.3478 [hep-th].

[168] T. P. Sotiriou and S.-Y. Zhou, "Black hole hair in generalized scalar-tensor gravity," *Phys. Rev. Lett.* **112** (2014) 251102, arXiv:1312.3622 [gr-qc].

[169] E. Babichev and C. Charmousis, "Dressing a black hole with a time-dependent Galileon," *JHEP* **08** (2014) 106, arXiv:1312.3204 [gr-qc].

[170] R. Benkel, T. P. Sotiriou, and H. Witek, "Black hole hair formation in shift-symmetric generalised scalar-tensor gravity," *Class. Quant. Grav.* **34** no. 6, (2017) 064001, arXiv:1610.09168 [gr-qc].

[171] R. Benkel, T. P. Sotiriou, and H. Witek, "Dynamical scalar hair formation around a Schwarzschild black hole," *Phys. Rev. D* **94** no. 12, (2016) 121503, arXiv:1612.08184 [gr-qc].

[172] P. Kanti, N. E. Mavromatos, J. Rizos, K. Tamvakis, and E. Winstanley, "Dilatonic black holes in higher curvature string gravity. 2: Linear stability," *Phys. Rev. D* **57** (1998) 6255–6264, arXiv:hep-th/9703192.

[173] B. Kleihaus, J. Kunz, S. Mojica, and E. Radu, "Spinning black holes in Einstein{Gauss-Bonnet{dilaton theory: Nonperturbative solutions," *Phys. Rev. D* **93** no. 4, (2016) 044047, arXiv:1511.05513 [gr-qc].

[174] G. Antoniou, A. Bakopoulos, and P. Kanti, "Evasion of No-Hair Theorems and Novel Black-Hole Solutions in Gauss-Bonnet Theories," *Phys. Rev. Lett.* **120** no. 13, (2018) 131102, arXiv:1711.03390 [hep-th].

[175] A. Bakopoulos, G. Antoniou, and P. Kanti, "Novel Black-Hole Solutions in Einstein-Scalar-Gauss-Bonnet Theories with a Cosmological Constant," *Phys. Rev. D* **99** no. 6, (2019) 064003, arXiv:1812.06941 [hep-th].

[176] W. F. Buell and B. A. Shadwick, "Potentials and bound states," *American Journal of Physics* **63** no. 3, (03, 1995) 256–258. https://doi.org/10.1119/1.17935.

[177] G. Antoniou, A. Bakopoulos, and P. Kanti, "Black-Hole Solutions with Scalar Hair in Einstein-Scalar-Gauss-Bonnet Theories," *Phys. Rev. D* **97** no. 8, (2018) 084037, arXiv:1711.07431 [hep-th].

[178] R. M. Wald, "Black hole entropy is the Noether charge," *Phys. Rev. D* **48** no. 8, (1993) R3427–R3431, arXiv:gr-qc/9307038.

[179] V. Iyer and R. M. Wald, "Some properties of Noether charge and a proposal for dynamical black hole entropy," *Phys. Rev. D* **50** (1994) 846–864, arXiv:gr-qc/9403028.

[180] J. W. York, Jr., "Black Hole in Thermal Equilibrium With a Scalar Field: The Back Reaction," *Phys. Rev. D* **31** (1985) 775.

[181] G. W. Gibbons and R. E. Kallosh, "Topology, entropy and Witten index of dilaton black holes," *Phys. Rev. D* **51** (1995) 2839–2862, arXiv:hep-th/9407118.

[182] M. Natsuume, "Higher order correction to the GHS string black hole," *Phys. Rev. D* **50** (1994) 3949–3953, arXiv:hep-th/9406079.

[183] Y. Kats, L. Motl, and M. Padi, "Higher-order corrections to mass-charge relation of extremal black holes," *JHEP* **12** (2007) 068, arXiv:hep-th/0606100.

[184] Y. S. Myung and D.-C. Zou, "Instability of Reissner{Nordström black hole in Einstein-Maxwell-scalar theory," *Eur. Phys. J. C* **79** no. 3, (2019) 273, arXiv:1808.02609 [gr-qc].

[185] E. Poisson, *A Relativist's Toolkit: The Mathematics of Black-Hole Mechanics*. Cambridge University Press, 12, 2009.

[186] D. Garfinkle, G. T. Horowitz, and A. Strominger, "Charged black holes in string theory," *Phys. Rev. D* **43** (1991) 3140. [Erratum: Phys.Rev.D 45, 3888 (1992)].

[187] E.-A. Kontou and K. Sanders, "Energy conditions in general relativity and quantum field theory," *Class. Quant. Grav.* **37** no. 19, (2020) 193001, arXiv:2003.01815 [gr-qc].

[188] M. S. Morris and K. S. Thorne, "Wormholes in space-time and their use for interstellar travel: A tool for teaching general relativity," *Am. J. Phys.* **56** (1988) 395–412.

[189] P. Dorlis, N. E. Mavromatos, and S.-N. Vlachos, "Bypassing Bekenstein's no-scalar-hair theorem without violating the energy conditions," *Phys. Rev. D* **108** no. 6, (2023) 064004, arXiv:2305.18031 [gr-qc].

[190] C. R. Stephens, G. 't Hooft, and B. F. Whiting, "Black hole evaporation without information loss," *Class. Quant. Grav.* **11** (1994) 621–648, arXiv:gr-qc/9310006.

[191] L. Susskind, "Strings, black holes and Lorentz contraction," *Phys. Rev. D* **49** (1994) 6606–6611, arXiv:hep-th/9308139.

[192] L. Susskind, "The World as a hologram," *J. Math. Phys.* **36** (1995) 6377–6396, arXiv:hep-th/9409089.

[193] J. M. Maldacena, "The Large N limit of superconformal field theories and supergravity," *Adv. Theor. Math. Phys.* **2** (1998) 231–252, arXiv:hep-th/9711200.

[194] S. A. Hartnoll, "Lectures on holographic methods for condensed matter physics," *Class. Quant. Grav.* **26** (2009) 224002, arXiv:0903.3246 [hep-th].

[195] C. P. Herzog, "Lectures on Holographic Superfluidity and Superconductivity," *J. Phys. A* **42** (2009) 343001, arXiv:0904.1975 [hep-th].

[196] J. McGreevy, "Holographic duality with a view toward many-body physics," *Adv. High Energy Phys.* **2010** (2010) 723105, arXiv:0909.0518 [hep-th].

[197] G. T. Horowitz, "Introduction to Holographic Superconductors," *Lect. Notes Phys.* **828** (2011) 313–347, arXiv:1002.1722 [hep-th].

[198] S. Sachdev, "Condensed Matter and AdS/CFT," *Lect. Notes Phys.* **828** (2011) 273–311, arXiv:1002.2947 [hep-th].

[199] P. Breitenlohner and D. Z. Freedman, "Positive Energy in anti-De Sitter Backgrounds and Gauged Extended Supergravity," *Phys. Lett. B* **115** (1982) 197–201.

[200] S. A. Hartnoll, C. P. Herzog, and G. T. Horowitz, "Holographic Superconductors," *JHEP* **12** (2008) 015, arXiv:0810.1563 [hep-th].

[201] S. S. Gubser, "Breaking an Abelian gauge symmetry near a black hole horizon," *Phys. Rev. D* **78** (2008) 065034, arXiv:0801.2977 [hep-th].

[202] S. A. Hartnoll, C. P. Herzog, and G. T. Horowitz, "Building a Holographic Superconductor," *Phys. Rev. Lett.* **101** (2008) 031601, arXiv:0803.3295 [hep-th].

[203] S. S. Gubser and S. S. Pufu, "The Gravity dual of a p-wave superconductor," *JHEP* **11** (2008) 033, arXiv:0805.2960 [hep-th].

[204] M. M. Roberts and S. A. Hartnoll, "Pseudogap and time reversal breaking in a holographic superconductor," *JHEP* **08** (2008) 035, arXiv:0805.3898 [hep-th].

[205] J.-W. Chen, Y.-J. Kao, D. Maity, W.-Y. Wen, and C.-P. Yeh, "Towards A Holographic Model of D-Wave Superconductors," *Phys. Rev. D* **81** (2010) 106008, arXiv:1003.2991 [hep-th].

[206] C. P. Herzog, "An Analytic Holographic Superconductor," *Phys. Rev. D* **81** (2010) 126009, arXiv:1003.3278 [hep-th].

[207] F. Benini, C. P. Herzog, and A. Yarom, "Holographic Fermi arcs and a d-wave gap," *Phys. Lett. B* **701** (2011) 626–629, arXiv:1006.0731 [hep-th].

[208] E. Witten, "Anti-de Sitter space, thermal phase transition, and confinement in gauge theories," *Adv. Theor. Math. Phys.* **2** (1998) 505–532, arXiv:hep-th/9803131.

[209] P. Breitenlohner and D. Z. Freedman, "Stability in Gauged Extended Supergravity," *Annals Phys.* **144** (1982) 249.

[210] T. Jacobson, G. Kang, and R. C. Myers, "Black hole entropy in higher curvature gravity," in *16th Annual MRST (Montreal-Rochester-Syracuse-Toronto) Meeting on High-energy Physics: What Next? Exploring the Future of High-energy Physics*. 5, 1994. arXiv:gr-qc/9502009.

[211] S. Ryu and T. Takayanagi, "Holographic derivation of entanglement entropy from AdS/CFT," *Phys. Rev. Lett.* **96** (2006) 181602, arXiv:hep-th/0603001.

[212] X. Dong, "Holographic Entanglement Entropy for General Higher Derivative Gravity," *JHEP* **01** (2014) 044, arXiv:1310.5713 [hep-th].

[213] Q. Pan, B. Wang, E. Papantonopoulos, J. Oliveira, and A. B. Pavan, "Holographic Superconductors with various condensates in Einstein-Gauss-Bonnet gravity," *Phys. Rev. D* **81** (2010) 106007, arXiv:0912.2475 [hep-th].

[214] R. Gregory, S. Kanno, and J. Soda, "Holographic Superconductors with Higher Curvature Corrections," *JHEP* **10** (2009) 010, arXiv:0907.3203 [hep-th].

[215] H.-F. Li, R.-G. Cai, and H.-Q. Zhang, "Analytical Studies on Holographic Superconductors in Gauss-Bonnet Gravity," *JHEP* **04** (2011) 028, arXiv:1103.2833 [hep-th].

[216] X.-M. Kuang, W.-J. Li, and Y. Ling, "Holographic Superconductors in Quasi-topological Gravity," *JHEP* **12** (2010) 069, arXiv:1008.4066 [hep-th].